Radiometer calibration and retrieval algorithms for passive remote sensing of the atmosphere

Pleijers, M.J.H.

Award date:
1997

Eindhoven University of Technology
Faculty of Electrical Engineering
Division of Telecommunication Technology and Electromagnetics

Radiometer Calibration and Retrieval Algorithms for Passive Remote Sensing of the Atmosphere

by M.J.H Pleijers

Report of graduation work
Performed from November 1996 to August 1997

Professor : prof.dr.ir. G. Brussaard
Supervisors : drs. S.C.H.M. Jongen and dr.ir. M.H.A.J. Herben

Abstract

Microwave radiometers are widely used for the passive remote sensing of the atmosphere. The Radiocommunications Group of the Division of Telecommunication Technology and Electromagnetics possesses two radiometer systems for remote sensing applications. One of these systems, the RESCOM radiometer, was borrowed from ESA–ESTEC and has been used for the CLARA (CLouds And RAdiation) measurement campaigns. The other one, the TUE radiometer, has been designed at the Eindhoven University of Technology.

The TUE radiometer 29.8 GHz channel has been calibrated with a hot and a cold load. The behaviour of this Dicke–type radiometer is assumed to be linear over its full range, but that has never been tested before. In this report the linearity of the TUE radiometer has been tested, using the data of the 31.7 GHz channel of the RESCOM radiometer. Linear regression lines have been used in order to find a transformation from brightness temperatures measured with the TUE radiometer to brightness temperatures measured with the RESCOM radiometer. The analysis showed that the assumption that the behaviour of the radiometer was linear, was correct. During the data analysis the data files of the RESCOM radiometer turned out to be corrupted. Before the data files could be used, they first had to be restored.

For the retrieval of the integrated water vapor amount V and the integrated liquid water amount L of the atmosphere, the Matched Atmosphere Algorithm has been designed. The version of the algorithm, now in use, is a version based on a look–up structure. This algorithm uses the Microwave Propagation Model of H.J. Liebe, as a model for the propagation of microwave radiation in the atmosphere. This model has been extended with the part describing the attenuation due to rain. For the retrieval of V and L, the brightness temperatures measured with the 21.3 GHz channel and the 31.7 GHz channel of the RESCOM radiometer are used.

The data obtained during the CLARA measurement campaigns showed that during periods of clear sky, the retrieved values of liquid water appeared to be negative. This however is physically impossible. There are various possible causes for this problem. One possible cause is the accuracy of the RESCOM radiometer. Variation of the brightness temperatures within the accuracy range of the radiometer showed that the occurrence of negative L–values could not be explained solely by the variations within the accuracy range. The amounts by which the brightness temperatures had to be changed were larger than the accuracy range.

Another possible cause was the inaccuracy of the extrapolation procedure used in the retrieval algorithm. For the extrapolation of V and L, the three nearest points in the look–up table that define a plane, are calculated and the plane is used for the extrapolation. A new extrapolation procedure has been designed that is based on a square fit of the points in the reduced look–up table representing thin clouds. With this new extrapolation procedure the retrieval of L still remains negative but is less negative than the retrieval with the three nearest points.

Acknowledgements

First of all, I would like to thank my parents and my sister for their moral support. Next, I would like to thank my supervisors Suzanne Jongen and Mat Herben and professor Brussaard who made it possible for me to graduate. I also want to thank Pol v.d. Coevering for his help with the conversion of the data from the TUE radiometer. Last but not least I would like to thank all members of the radiocommunications group for the interesting discussions about type setting in LaTeX and the exciting games of darts and table tennis.

Moeilijke bergen kunnen soms makkelijk en makkelijke bergen kunnen soms moeilijk zijn

On a postcard from Alexandra Smeets to Bernhard, Prince of the Netherlands and patron of the expedition, during the SONY ON TOP All over the World Expedition on the occasion of the 25th anniversary of the Valkenburgse Alpen Vrung in 1992.

Contents

List of Figures

List of Tables

Chapter 1

General Introduction

Radiometers are very useful for the remote sensing of the earth's atmosphere. They are used for the continuous observation of integrated amounts of water vapor (V) and liquid water content (L) in the atmosphere.

1.1 This Graduation Project

My graduation work is a part of the Awater–project. This AWater–Project is a cooperation between Eindhoven University of Technology and Delft University of Technology. Their aim is to develop a method to measure water content, particle size and concentration of clouds with radar and radiometer.

For Eindhoven University of Technology this aim consists of:

- Development and validation of algorithms to calculate atmospheric water content;
- Retrieval of the system parameters of a payable measurement instrument for cloud research.

For Delft University of Technology this aim consists of:

- Development of a method to calculate water content, particle size and concentration of clouds and light rain from radar measurements.

For this purposes, the Eindhoven University of Technology uses the RESCOM radiometer at frequencies of 21.3, 23.8, 31.7, 51.3, 53.9 and 54.9 GHz. Delft University uses their weather radar at 3.315 GHz.

Figure 1.1 shows why the frequencies in the region of 20 and 30 GHz are chosen. Near 22 GHz an absorption peak of water vapor is located, which gives us the opportunity to measure attenuation contributions of water vapor. With the channel in the 30 GHz region it is possible to determine the effects of liquid water in the atmosphere, because this is a window where the attenuation due to water vapor is low compared to 20 GHz region and the contribution of oxygen is still low. The 50 GHz region cannot be used for the retrieval of water vapor or liquid water because both frequencies are located in the oxygen band (50 to 70 GHz). The zenithal attenuation is very high and influences of water vapor and liquid water are overshadowed by

oxygen attenuation. This frequency region however is very well suited for the determination of temperature profiles. In further stages of the Awater project the results of the 50 GHz measurements will be used to create realistic temperature profiles.

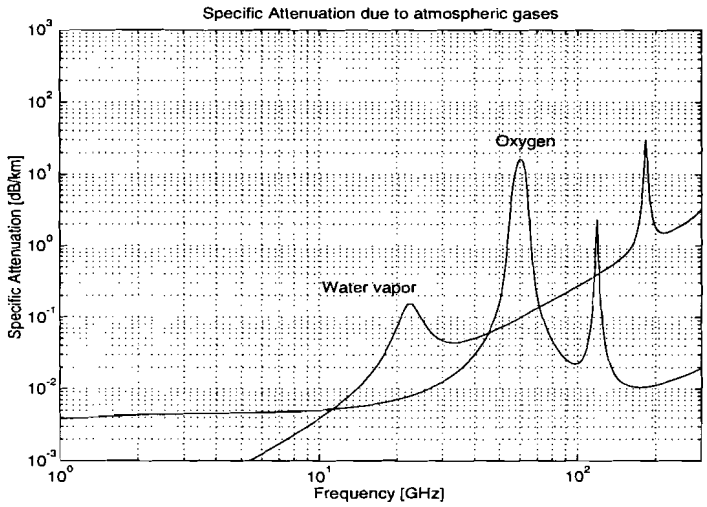

Figure 1.1: Specific attenuation due the presence of water vapor and oxygen.

At the satellite ground station of the Eindhoven University of Technology an other radiometer is stationed, called the TUE radiometer. This radiometer has been designed for an extensive propagation measurement campaign with the Olympus satellite and uses channels at 12.7, 20 and 29.8 GHz. This campaign included the use of radiometers for the comparative analysis of attenuation and noise radiation. This measurement campaign stopped when the Olympus satellite was seriously damaged. The radiometer now is going to be used for atmospheric measurements within the AWater–project too.

Part of this radiometer, the 29.8 GHz channel, has been calibrated with both a hot and cold load. The behaviour between those calibration points is assumed to be linear, but has never been checked yet. The availability of the RESCOM radiometer for the Awater–project makes it possible to use it for the calibration of TUE radiometer. Both radiometers are used in simultaneous measurements during lang periods of time. The data from these measurements are used of the calibration.

The Eindhoven University of Technology participates with the Awater–project in the CLARA–Project [1]. The representation of clouds and their impact on radiative transfer remains one of the greatest sources of uncertainty in present day climate models. To improve this representation, better parameterizations of clouds are needed, both of the macrophysics and dynamics (cloud cover, cloud structure and turbulence) and of the microphysics (droplet spectra, distinction between ice and water, role of condensation nuclei and precipitation formation). In addition, the relation between the micro- and macro-properties of clouds and radiative transfer has to be clarified.

The CLARA project (CLouds And RAdiation) focuses on microphysics, their relation with macro-properties of clouds and their importance for routine observations of clouds by satellite and ground-based remote sensing. The information of the field campaigns will be used to improve routine retrieval methods and will also serve to test detailed models for clouds and

radiative transfer. These case studies will further serve as a validation for parameterizations, that will be included in general circulation models.

Anthropogenic aerosol particles serve as extra cloud condensation nuclei. This results in clouds with a larger number of droplets for a given liquid water content and thus a higher albedo. Measurements in the ECN cloud chamber revealed that the number of cloud droplets in "polluted" air is higher by a factor of four compared to that in relatively clean air. The CLARA project offers the means to check if the cloud chamber results can indeed be extrapolated to the actual atmosphere.

The algorithms that are used to derive physical parameters from the measurements are based on several crude assumptions about the micro-physical properties of the clouds and the relation between these properties and the measured (macro-physical) properties. This project offers the opportunity for validation of the different remote sensing techniques with in situ measurements.

In the CLARA project the following parties and instruments are involved:

KNMI	:	Infrared Radiometer: 9.6–11.5 μm
		Radiosondes
DUT	:	Atmospheric Research Radar: 3.315 GHz
		Doppler Sodar: Wind Temperature Inversions
		Meteostation: Temperature, Relative Humidity, Wind
RIVM	:	Lidar: 1064 nm, 532 nm
ESTEC	:	Lidar: 906 nm
ECN	:	FSSP–100: Forward Scattering Spectrometer Probe
		SMPS
EUT	:	20/30/50 GHz Radiometer
RAL	:	ATSR (Along Track Scanning Radiometer)
Other Satellites	:	AVHRR, Meteosat

The Role of the Awater–project in the CLARA–project is:

- Validation of V and L retrieval;
- Improvement of the knowledge of microwave transport in clouds.

The second part of my graduation work deals with the extension and refinement of the Matched Atmosphere Algorithm. This algorithm is used for the retrieval of V and L. For the description of the propagation of microwaves in the atmosphere the MPM model of Liebe is used. During the CLARA measurement campaigns negative values for the cloud liquid water content were detected. The question is how much the brightness temperatures at 21.3 and 31.7 GHz have to be corrected in order to eliminate this negative values. It is even more interesting to see whether this correction factor remains the same during all CLARA periods. Also is examined whether these corrections are located within the accuracy of the radiometer.

In the version of MPM used during the CLARA campaigns, the contribution of rain in the attenuation has not been implemented yet. Now a procedure has been designed for this rain contribution.

During the CLARA periods it turned out that our implementation of the matched atmosphere algorithm has problems during periods with multiple cloud layers. In order to reduce these problems two methods are evaluated. For these methods data of radar or lidar are required.

The version of the Matched Atmosphere Algorithm that is used during all our experiments used look-up tables for the retrieval of liquid water content and water vapor content. Interpolation and extrapolation together with the look-up tables determine the values of V and L. The availability of the latest MATLAB version, version 5.0, makes it possible to use new interpolation and extrapolation techniques for a better determination of both V and L. Besides these new inter- and extrapolation techniques the new MATLAB version gives us the opportunity to create new look up tables with more than two input parameters. In the old version only two–dimensional arrays were possible.

1.2 Organisation of the Report

Chapter Two describes the radiometer as a measurement instrument. Two types of radiometers are discussed, a Dicke radiometer (TUE radiometer) and a noise injection radiometer (RESCOM radiometer). Furthermore the calibration of both radiometers is described.

Chapter Three deals with the calibration of the TUE radiometer with the RESCOM Radiometer. The definition of the problem and the analysis methods are discussed first. Then the data selection and the problems that arose during the data processing are described. Finally the results and conclusions are presented.

In Chapter Four some principles of radiometry are presented. The most important principles and tools are introduced. A description of Liebe's Microwave Propagation Model and the Matched Atmosphere Algorithm are part of this chapter.

Chapter Five deals with the problem of the retrieval of negative L–values. There are two possible causes for the negative L–values. One of them, the accuracy of the RESCOM Radiometer has been evaluated in this chapter. The other possible cause is discussed in Chapter Six

Chapter Six describes the refinements and extensions of both the MPM model and the Matched Atmosphere Algorithm. First the implementation of rain in the MPM model is briefly discussed. Secondly a new extrapolation method is introduced in order to improve the accuracy of the Matched Atmosphere Algorithm. The accuracy of the Matched Atmosphere Algorithm is the second possible cause of negative L–values.

Chapter Seven finally contains the general conclusions and recommendations.

Chapter 2

Radiometers

2.1 The Radiometer as a Measurement Instrument

A radiometer is an instrument that measures the radiation emitted and reflected from objects in the universe. Every object in the universe emits and absorbs radiation. The typical radiometer uses the heterodyne principle [2], where both the technique and terminology date from the early days of radio.The simplest version of a heterodyne radiometer is a total power radiometer.

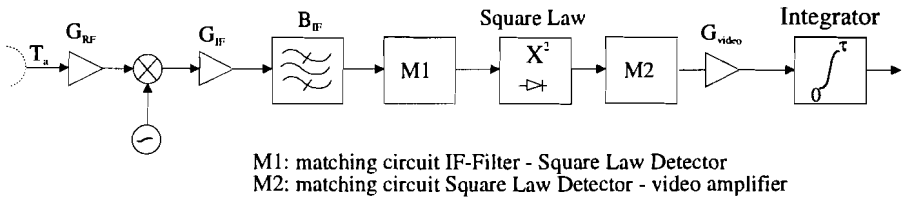

Figure 2.1: Layout of a Total Power Radiometer.

The radio-frequency or RF signal is translated to a different and usually lower frequency before it is detected. A RF signal at some frequency incident on the antenna is coupled by that antenna into a transmission line, the function of which is to carry the RF signal to and from the various elements of the circuit. Signals at microwave frequencies are often difficult or impossible to deal with directly, whereas a signal that has been downconverted to a sufficiently Intermediate Frequency, IF, can be handled with various techniques. After amplification and filtering, the power of the IF signal is measured with a square law detector. This element is typically a diode working in its $i = v^2$ range and produces an output voltage that is proportional to the input power. The resulting output voltage is given by

$$V_{out} = cBG\,(T_a + T_{rec}) \tag{2.1}$$

with B the bandwidth of the pre–detection filter, G the total gain of the receiver and c is proportionality constant which includes the voltage sensitivity of the detector diode. If absolute accuracy is concerned, the total power radiometer cannot be regarded generally as sufficient stable to satisfy reasonable requirements of absolute accuracy. This due to the fact that no extra countermeasures have been incorporated in order to overcome the problem of gain and system noise–instabilities.

In our experiments we use both the TUE radiometer and the RESCOM radiometer. These are both different types of radiometers. The 29.8 GHz TUE radiometer is a Dicke type radiometer. The RESCOM radiometer is a noise–injection radiometer. Both radiometer types are heterodyne radiometers, based on the total power radiometer The following subsections describe how these two types of radiometers work.

2.1.1 Dicke Radiometer

The Dicke radiometer [3] is an extension of a total power radiometer. The total power radiometer has stability problems. These problems are partly solved by the Dicke radiometer. The Dicke radiometer is basically a total power radiometer with the addition of a microwave switch, a load at a well-defined temperature and a synchronous detector between the square law detector and the integrator. The receiver monitors the input signal for only half the measuring time and during the other half, it monitors the reference noise temperature of the load. If the switch is operated at a rate higher than the highest frequency of gain fluctuations, the gain can be considered to be constant during one switch period. Figure 2.2 shows the layout of the essential elements of a Dicke radiometer. The input of the radiometer is switched

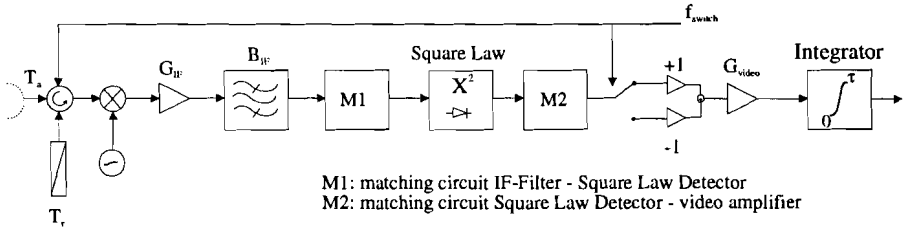

Figure 2.2: Layout of a Dicke Radiometer.

with a frequency f_{switch} to the antenna noise temperature and the reference noise temperature. When f_{switch} is so rapid that G, T_a and T_{rec} can be considered to be constant, V_{out} can be given as

$$V_{out1} = \begin{cases} c \cdot B\,(T_a + T_{rec}) \cdot G & \text{during the first half period of } f_{switch} \\ c \cdot B\,(T_r + T_{rec}) \cdot G & \text{during the second half period} \end{cases} \tag{2.2}$$

If $1/f_{switch} << \tau$, the integration constant, the output of the integrator is

$$V_{out} = c \cdot B\,(T_a - T_r)\,G \tag{2.3}$$

Comparing equation 2.1 and 2.3 shows that T_{rec} has been eliminated and as long as $T_a - T_r$ is significantly less than $T_a + T_{rec}$, the effect of any gain instabilities has been reduced. That results in a better immunity to instabilities. The penalty paid for the improvement of stability is an increase in the ideal sensitivity.

2.1.2 Noise–Injection Radiometer

Figure 2.3 shows the block diagram of a noise–injection radiometer [3].

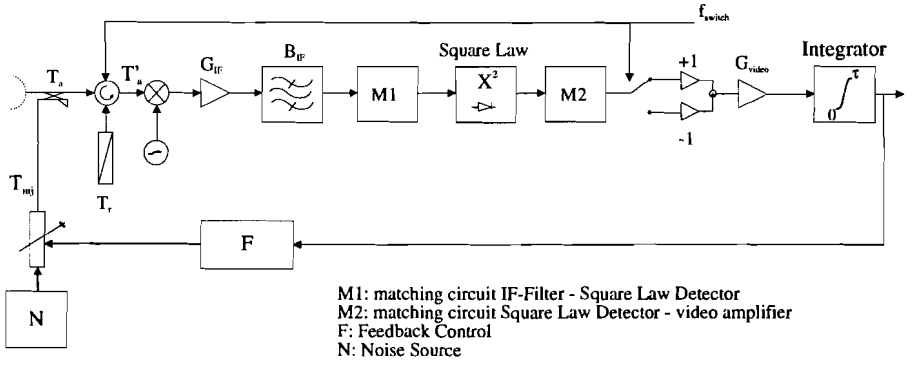

Figure 2.3: Layout of a noise–injection radiometer.

It is capable of eliminating the uncertaincies introduced by T_{rec} and G variations, since it includes the components that are subject to instabilities in a feedback loop, which continuously adjusts the reference noise temperature to the input noise temperature. This leads to

$$V_{out} = c\left(T'_a - T_r\right) G = 0 \qquad \text{if } T'_a = T_r \tag{2.4}$$

with $T'_a = T_a + T_{inj}$. So, a knowledge of T_{inj} and T_r gives sufficient information for determining T_a. The accuracy of T_a will depend only on the accuracy of T_{inj} and T_r and is independent of the radiometer gain and receiver noise fluctuations. The absolute accuracy of the noise-injection radiometer seems to be about the same as for the Dicke radiometer, although the noise-injection radiometer is sometimes reported to have a better accuracy [3].

2.2 Calibration of Radiometers

In order to translate the output voltages of the radiometers into brightness temperatures a calibration principle has to be followed. This procedure can also be used to compensate for undesired behaviour of the radiometer itself. Two calibration procedures are outlined in this section.

2.2.1 Calibration with Hot and Cold Load of the TUE Radiometer

For the calibration of radiometers with standard noise sources [4], the exact brightness temperatures of these standards must be known. An often–used noise source is a matched load, cooled with liquid nitrogen (T= 77.36 K). If the relationship between the detected receiver output voltage and the measured noise is linear, only one further calibration temperature is required. For a Dicke radiometer, like our TUE radiometer, this temperature is readily available, since this is the load that is looked at every half period. The reference plane of this load and a load in front of the antenna is different and therefore a translation should be made. Another way to solve these problems is to place a second load in front of the antenna that is at ambient temperature. The first calibration point is called the cold load, the second the hot load.

For the cold load calibration, the aperture of the antenna is placed directly over a box containing microwave absorbing material. The porous absorbing material is saturated with liquid oxygen. It is characterized by a very small reflection coefficient and therefore acts like a black body with brightness temperature equal to its physical temperature.

For the hot load we use the same principle but the nitrogen is omitted. If the absorber still acts like a black body, the brightness temperature is equal to the ambient temperature.

If and only if the radiometer is linear, then we can determine the antenna temperature T_a for a target at an unknown temperature (Figure 2.4) as

$$T_a = c(V - V_0) \tag{2.5}$$

Where V_0 is the voltage offset due to the receiver temperature, and the radiometer constant c is determined as

$$c = \frac{T_{hot} - T_{cold}}{V_{hot} - V_{cold}} \tag{2.6}$$

where the voltages V_{hot} and V_{cold} are the measured output voltages for the respective T_{hot} and T_{cold} loads.

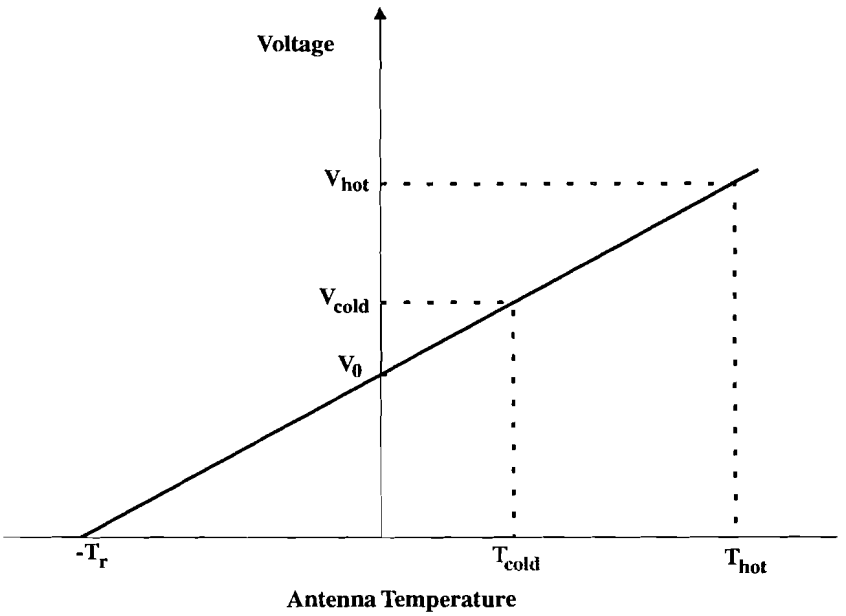

Figure 2.4: Calibration of antenna temperature using a hot and cold load.

The calibration coefficient is given by the measured slope, and the voltage intercept for zero antenna temperature determines the receiver temperature T_r.

2.2.2 Calibration of the RESCOM Radiometer

The RESCOM radiometer also has been calibrated with a cold load. In this case a calibrated cryogenically cooled waveguide load is used for the basic calibration. The purpose of this basic calibration of the radiometer receiver is to adjust the level of the noise pulses to be injected via the coupler into the input waveguide of the receiver front end. There is a linear relation between the number of injected noise pulses and the measured brightness temperature. The maximum brightness temperature that can be measured with the radiometer is 313 K. The maximum number of pulses that can be injected during an integration time is 2048. This means that each injected noise pulse represents 313/2048 = 0.153 K.

In the RESCOM radiometer another calibration is available Within the controller software of the RESCOM radiometer [5], a semi-automatic calibration procedure is available. This calibration procedure uses tip–curve measurements. This measurement under clear sky conditions is the most precise method of overall system calibration. The feed assembly and the antenna reflector loss estimates shall be adjusted initially in this way, and likewise periodic checks of system calibration can be made.

Tip curve calibration is based on the assumption that, under clear sky conditions, the atmosphere is homogeneous stratified. The attenuation of a satellite signal will follow a secant law, since the pathlength through the atmosphere varies in this way.
therefore

$$A = \frac{A_z}{\sin\theta} \tag{2.7}$$

with A_z the attenuation at $\theta = 90°$ and θ the elevation of the path.

By plotting a versus $1/\sin\theta$, a straight line is obtained which intersects the A–axis at zero. If the calibration is not correct, the intersection will differ from zero. This method cannot be used in the oxygen absorption band from 52 to 68 GHz, where the absorption even in the lower part of the atmosphere is so high that the assumption does not hold.

For low A_z–values, the sky noise temperature instead of attenuation may be used, since

$$T_s \backsimeq T_{bg} + \frac{T_z - T_{bg}}{\sin\theta} \tag{2.8}$$

where T_z is T_s at $\theta = 90°$ and $T_{bg} = 2.7K$.

Then by plotting T_s versus $1/\sin\theta$, the points will lie on a straight line intersecting the T_s–line at 2.7 K, if the calibration is correct (figure 2.5).

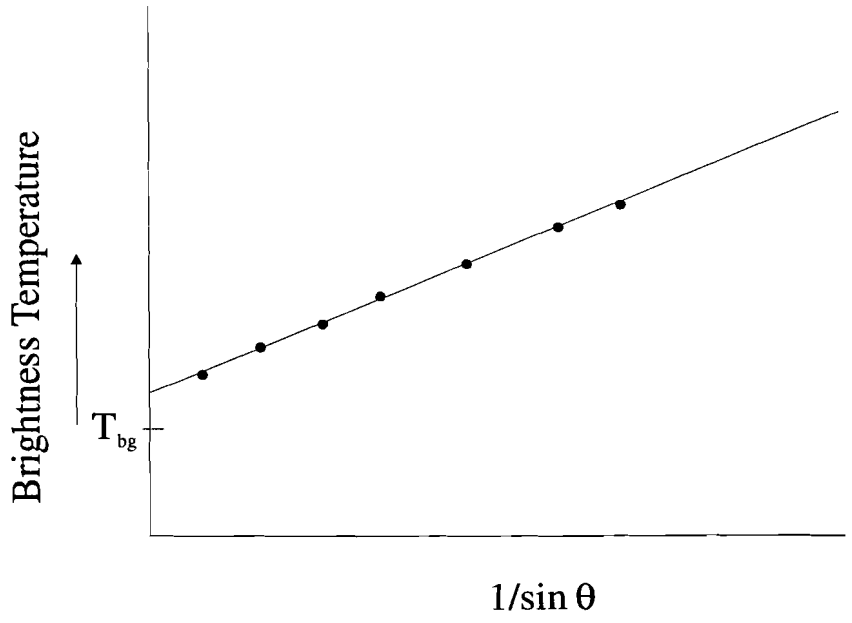

Figure 2.5: Calibration of antenna temperature with a tip–curve calibration.

A large spreading of the points may indicate that suitable conditions have not been existed during the measurement. If the results of a tip–curve measurement have been deemed valid

and the intersection deviates from the ideal value it must be concluded that a change in system calibration has occurred, and that a recalibration therefore is required.

A change might be due to either a change in the loss/reflection characteristics of horn–input waveguide circuits, or more likely a change in level of injected noise. Which of these causes is true in an actual situation cannot immediately be determined, but in any case the recalibration can be obtained by adjusting the loss factor L_h in the SETUPS file.

If T_s is plotted the factor of correction is found as

$$1 + 0.0035(T(0) - 2.7) \tag{2.9}$$

where $T(0)$ is the actual intersection value.

If A is plotted the correction factor is

$$10^{\left(\frac{A(0)}{10}\right)} \tag{2.10}$$

The relevant L_h factor found in the SETUPS file is multiplied by the correction factor and the new value is entered in the file. This correction factor means that the linear relation between the number of injected noise pulses and the brightness temperature is rotated around the reference point, $T_b = 313$ and 0 injected noise pulses. This is shown in figure 2.6.

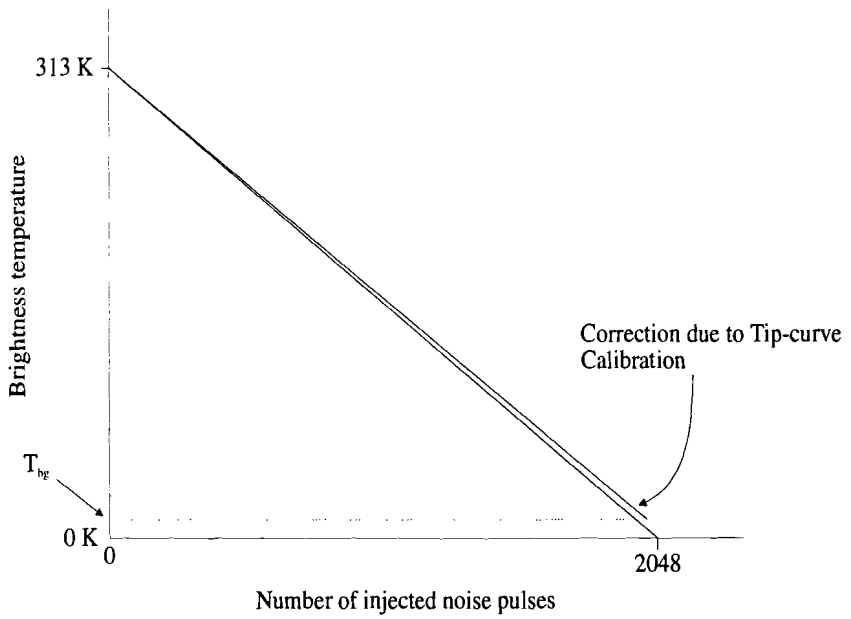

Figure 2.6: Effect of the correction factor calculated from the tip–curve calibration.

By careful evaluation of the tip–curve measured under stable and favourable conditions a system calibration accuracy of 1 K should be obtainable. However, it is required that not only T_s, but also the elevation is measured correctly. An offset in the measured angle, e.g. due to incorrect pointing alignment, will give the best fit line an erroneous slope and intersection. Especially with low elevation angle, the accuracy of the elevation angle is very important. An offset of 1° then could cause an error of 1.5 K. Therefore an absolute alignment better than 0.5° must be maintained [5].

Chapter 3

Calibration of the TUE Radiometer with the RESCOM Radiometer

3.1 Problem Definition

At the Eindhoven University of Technology an analog radiometer, called TUE radiometer, has been designed for an extensive propagation measurement campaign with the Olympus satellite.

The TUE radiometer has 3 channels measuring at the frequencies 12.7, 20 and 29.8 GHz. The advantage of the TUE radiometer is that it has an analog output, so that the sample rate can be varied. On the other hand the 30 GHz channel has not been accurately calibrated yet. Part of the radiometer system was calibrated with a hot and a cold load, but linearity has not been checked yet.

For this linearity check we will use the RESCOM radiometer. When a tip–curve calibration of the RESCOM radiometer has been performed, the RESCOM radiometer will be linear on its full range. The RESCOM 20/30/50 GHz radiometer measures at the frequencies 21.3, 23.8, 31.7, 51.25, 53.85 and 54.85 GHz.

Both radiometers have the following specifications:

Property	**RESCOM Radiometer**	**TUE Radiometer**
Beamwidth 3 dB	$1.9° \pm 0.1°$	3.7°
Beamwidth 10 dB	$4.1° \pm 0.2°$	6.3°
Beam efficiency, at aperture	96% min. at 5° from axis	
Beam axis alignment	0.2° max. deviation	
Integration time	1 sec	1 sec
Sample rate	1 sample/sec	3 samples/sec

Table 3.1: Relevant Specifications of both radiometers

In order to be able to use the TUE radiometer for atmospheric measurements, our aim is to check linearity of the 29.8 GHz channel of the TUE radiometer with the 31.7 GHz channel of the RESCOM radiometer. These channels are chosen because their frequencies are located close to eachother. Therefore, it is not necessary to introduce a lot of theory. When only less

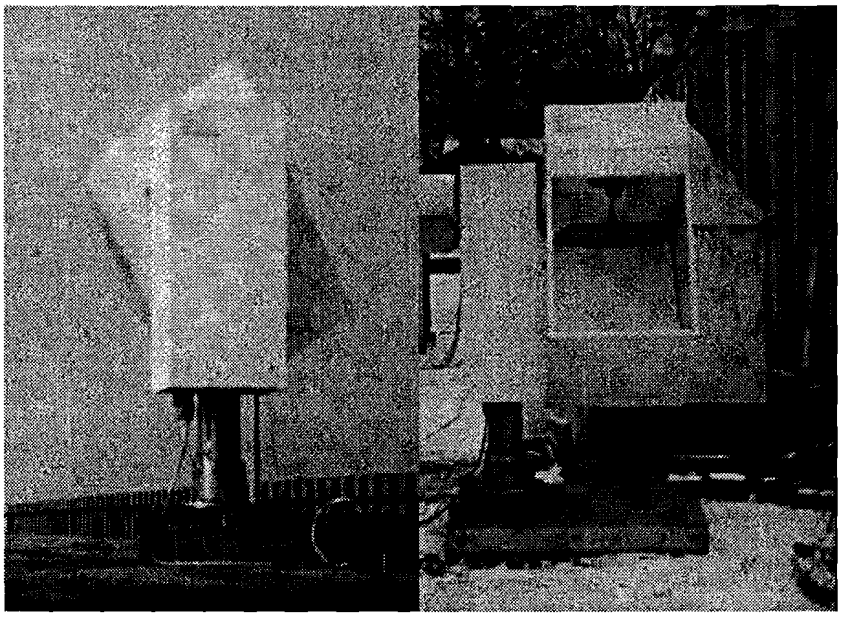

Figure 3.1: RESCOM Radiometer.

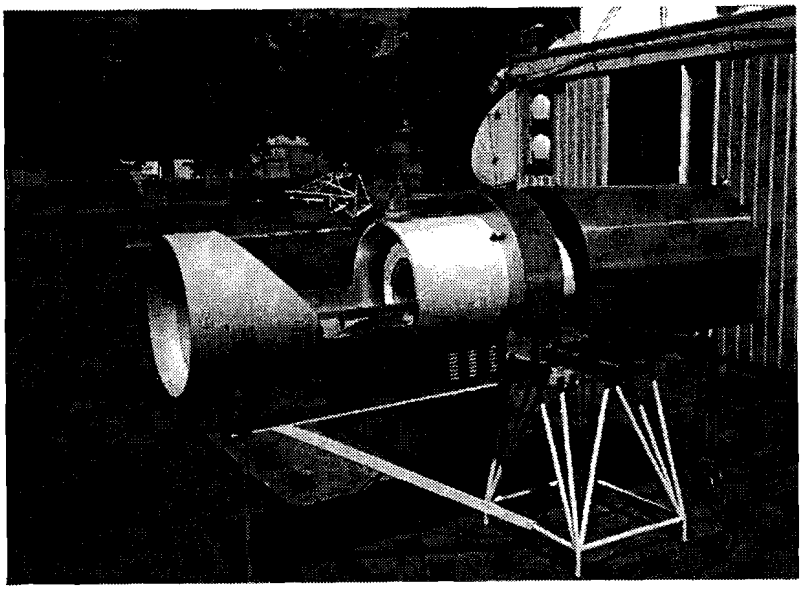

Figure 3.2: TUE Radiometer.

theory is introduced, also the possibility of introducing errors is reduced.

The RESCOM radiometer has a built-in procedure for tip-curve calibration.When the tip–curve calibration took place under stable and favourable conditions, a system calibration accuracy of 1K should be obtainable. At one moment both radiometers were synchronized and from this moment on both radiometers have been measuring during clear sky periods, cloudy periods and periods with precipitation. During this experiment two properties of the data will be checked. First is investigated whether there exist a linear relationship between the data of the RESCOM radiometer and the TUE radiometer. The correlation coefficient between both measurements is an indication for this linearity. Secondly regression lines are calculated in order to transform TUE brightness temperatures into RESCOM brightness temperatures. Figure 3.3 shows the measurement equipment. The attenuation, and thus the

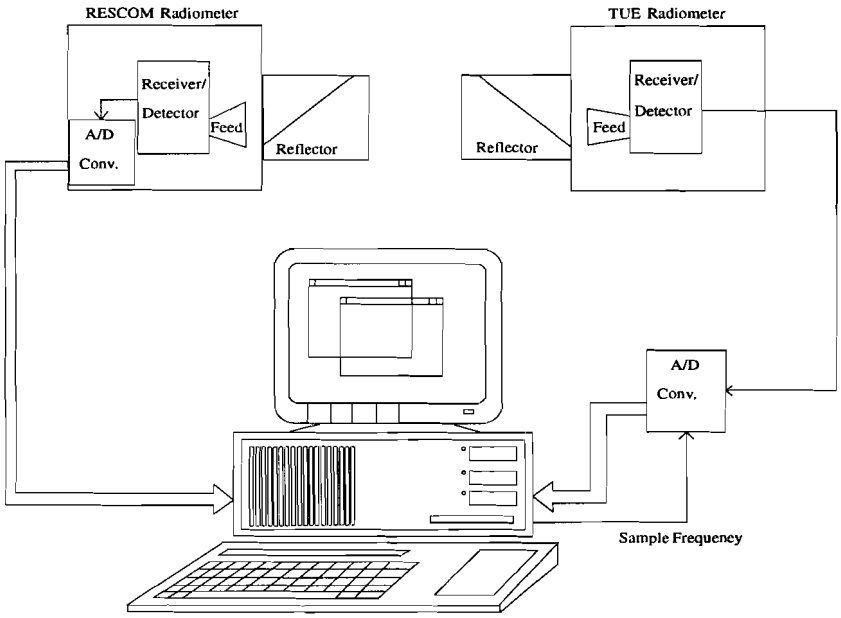

Figure 3.3: Measurement equipment.

brightness temperature in the atmosphere depends on its contents, the amount of rain, but also the frequency that is used. Figures 1.1 and 3.4 show this frequency effect for gaseous and rain attenuation respectively.

As one can see, only a slight difference in frequency can cause a large difference in attenuation and brightness temperature. Therefore, the effects of the slight difference between the frequency of the RESCOM and TUE radiometer should be determined.

With Liebe's MPM [6], it is possible to calculate this difference caused by the frequency difference. This has been done as follows: In the first place a set of atmospheres has been generated by varying both R and H_{base}. The rain rate varied from 0 to 200 mm/h, with a stepsize of 10 mm/h. H_{base} varied from 0 to 2.3 km, with a stepsize of 100 m. For this set of atmospheres T_b at 29.8 GHz (TUE) and 31.7 GHz (RESCOM) have been calculated, using MPM. In the implementation of MPM made by H. Hollander [7] the contribution of rain has not been specified. I included the rain contributions in a new version of MPM. How this was done will be described in Chapter Six.

In order to exclude the effects caused by changing the other groundlevel values, ground

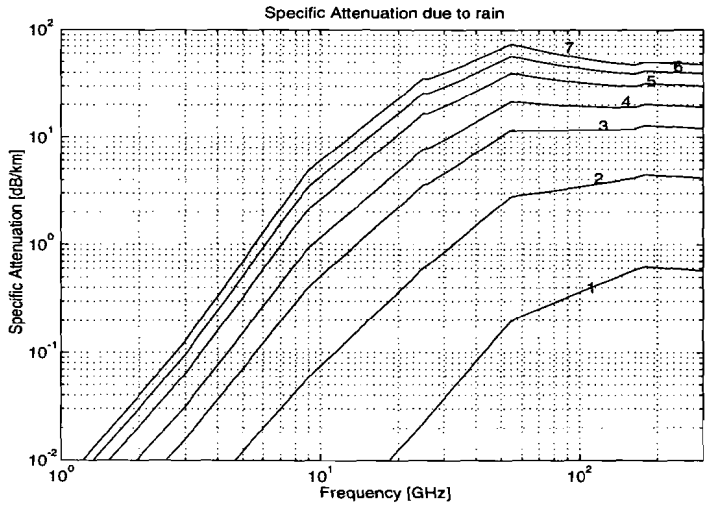

Figure 3.4: Specific attenuation due to rain; with rainrates specified as 1: 0.25 mm/h, 2: 5 mm/h, 3: 25 mm/h, 4: 50 mm/h, 5: 100 mm/h, 6: 150 mm/h, 7: 200 mm/h.

temperature T_s, ground pressure P_s and ground relative humidity RH_s, the above mentioned experiment was repeated with several groundlevel configurations.

In order to find out what the influence of measuring at a different frequency is, the calculated brightness temperatures at 29.8 GHz and 31.7 GHz are plotted as pairs in a figure It looks like all these points lie on a straight line. In fact their location can be described with a higher order function, but the parameters accompanying the second order and higher order terms are very small compared to the linear and constant term parameters. Because of the very small contribution of the higher order terms, the points are fitted by a linear regression line. The least squares method of Gauss [8] is used to find the regression lines.

For the various groundlevel configurations the following regression lines have been found:

Groundlevel [T_s P_s RH_s R]	Regression Line
[15 101.3 60 R]	$T_{TUE} = -10.5956 + 1.0312 \cdot T_{RESCOM}$
[5 101.3 60 R]	$T_{TUE} = -9.9973 + 1.0301 \cdot T_{RESCOM}$
[25 101.3 60 R]	$T_{TUE} = -13.6258 + 1.0439 \cdot T_{RESCOM}$
[5 98.3 60 R]	$T_{TUE} = -9.7243 + 1.0298 \cdot T_{RESCOM}$
[40 104.3 100 R]	$T_{TUE} = -16.5956 + 1.0501 \cdot T_{RESCOM}$

Table 3.2: Regression lines for frequency difference compensation.

The slope of the regression lines does not vary very much. For the frequency compensation an average regression line is calculated. With this average regression line a conversion from RESCOM radiometer brightness temperature to RESCOM reference brightness temperature has been made. This reference brightness temperature will be used for the linearity check of the TUE radiometer.

$$T_{RESCOM_{ref}} = -12.1077 + 1.0370 \cdot T_{RESCOM} \quad [K] \tag{3.1}$$

Figure 3.5 shows the locations of the (RESCOM,TUE)–pairs for the groundlevel configuration [15 101.3 60 R], together with the linear regression line.

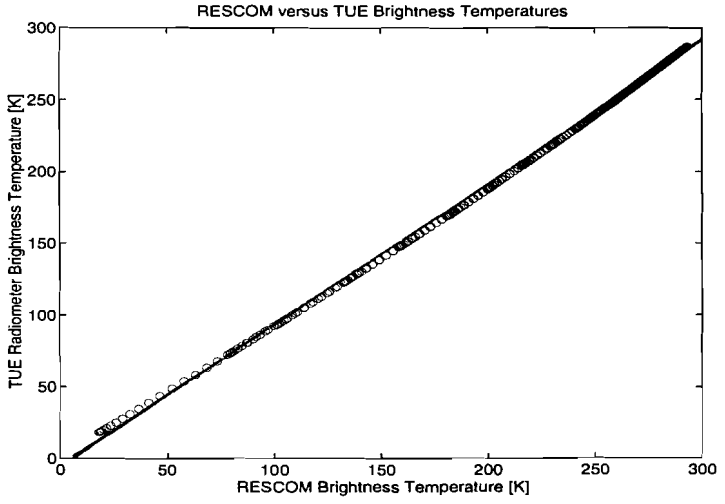

Figure 3.5: RESCOM versus TUE radiometer brightness temperatures for a groundlevel configuration [15 101.3 60 R].

3.2 Analysis Methods

3.2.1 Correlation

The analysis of the data is based on statistical methods. In order to understand the methods used for the data analysis, first an overview of the statistical parameters needed for the analysis is given.

Definition 1 *For a stochastic variable* $\underline{x}$ *its mean or expected value is called* $\mu_{\underline{x}}$

Definition 2 *The variance* $\sigma^2_{\underline{x}}$ *is defined as*

$$\sigma^2_{\underline{x}} = \mu_{(\underline{x}-\mu_{\underline{x}})^2} = \mu_{\underline{x}^2} - (\mu_x)^2$$

The standard deviation is defined as the square root of the variance and is symbolized as $\sigma_{\underline{x}}$.

Suppose we have two stochastic variables called $\underline{x}$ and $\underline{y}$, then the covariance between those variables can be defined as

The covariance between $\underline{x}$ and $\underline{y}$ symbolized as $cov(\underline{x}, \underline{y})$ is defined as

Definition 3

$$cov(\underline{x}, \underline{y}) = \mu_{(\underline{x}-\mu_{\underline{x}})(\underline{y}-\mu_{\underline{y}})} = \mu_{\underline{x}\underline{y}} - \mu_{\underline{x}}\mu_{\underline{y}}$$

With the covariance and the standard deviation of both stochastic variables now the correlation coefficient can be calculated as

Definition 4 *The correlation coefficient* $\rho(\underline{x}, \underline{y})$ *can be defined as*

$$\rho(\underline{x}, \underline{y}) = \frac{cov(\underline{x}, \underline{y})}{\sigma_{\underline{x}}\sigma_{\underline{y}}}$$

Covariance and correlation coefficient determine the dependency between the two stochastic variables. When $\rho(\underline{x}, \underline{y}) \approx 1$, that is when $cov(\underline{x}, \underline{y}) \approx \sigma_{\underline{x}}\sigma_{\underline{y}}$, then large values for $\underline{x}$ go together with large values of $\underline{y}$ and low values of $\underline{x}$ go together with low values of $\underline{y}$. This is exactly what we want to achieve.

3.2.2 Synchronisation Control

Although we assume that, when we open the data files of both the RESCOM and TUE radiometer, they start at 0:00.00, still synchronisation differences may occur. These synchronisation differences, caused by clock differences in both registration computers, could be several seconds. These synchronisation differences are not caused by sampling the analog TUE radiometer, because an average over one second is calculated. Synchronisation problems also occur when both radiometers do not look in the zenith direction. If one of the radiometers does not look in the zenith direction, a cloud will be detected by that radiometer earlier or later than by the other radiometer. Whether this synchronisation differences occur, can be detected by shifting one data file relative to the other(Figure 3.6). If after this shift the correlation coefficient improves, a synchronisation difference has been detected. The shifted data file then will be used for further analyses.

3.2.3 Linear Regression Lines

In regression analysis there are two variables. The first one, the TUE_{ref} radiometer data, is called $\underline{x}$, and is an independent variable. The other, the dependent variable $\underline{y}$, is the data of TUE radiometer. We are interested in the dependence of $\underline{y}$ on $\underline{x}$.

First n values $\underline{x}_1, \underline{x}_2, \ldots, \underline{x}_n$ of $\underline{x}$ are selected, and then the corresponding $\underline{y}$–values are observed, so that a sample of the form $(\underline{x}_1, \underline{y}_1), \ldots, (\underline{x}_n, \underline{y}_n)$ will be obtained.

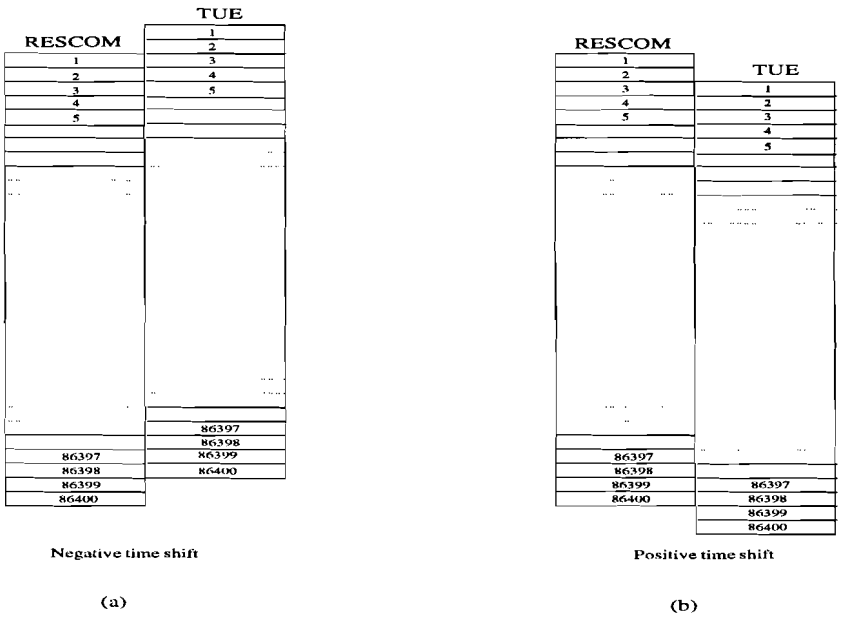

Figure 3.6: Time shifts (a) Negative time shift; (b) Positive time shift.

In regression analysis the mean μ of $\underline{y}$ is assumed to depend on $\underline{x}$, that is, it is a function $\mu = \mu(\underline{x})$ in the ordinary sense. The curve of $\mu(\underline{x})$ is called the regression curve of $\underline{y}$ on $\underline{x}$. The simplest case, when $\mu(\underline{x})$ is a linear function, will be used in a first attempt to fit the data of the TUE radiometer on the TUE_{ref} data. The sample values will be plotted as n points in the xy-plane. If the points are scattered, fitting "by eye" becomes unreliable, and a mathematical method for fitting lines that yields a unique result depending only on the points, is needed.

During periods in which the circumstances of the atmosphere do not vary very much, all data points are located in a cluster, close to each other. This happens for example during clear sky periods. The influences of data points that are not located in such a cluster, are attenuated by the large number of points in the cluster. This means that the linear fit is not optimal for the points not located in a such a cluster. A solution of this problem is the reduction of the point density, where the point density is the number of points in a block of some size. In our case TUE_{ref} is divided in blocks with a size of 5 K. In each block the data points are divided in groups of 50 data points. For each complete group of 50 points, the average is calculated, the average is stored, and the 50 points are removed from the data file. When a group does not contain 50 points, it will remain unchanged. By this procedure the point density of blocks containing clusters of data points is reduced, and therefore the contributions of points outside the clusters are much larger.

A widely used procedure is the **Method of Least Squares** by Gauss [8]. In this situation it may be formulated as

Definition 5 *The straight line should be fitted through the given points so that the sum of the squares of the distances of those points from the straight line is minimum, where the distance is measured in the vertical direction (the y-direction).*

Assumption 1 *The $\underline{x}$-values $\underline{x}_1, \ldots, \underline{x}_n$ of the sample $(\underline{x}_1, \underline{y}_1), \ldots, (\underline{x}_n, \underline{y}_n)$ are not all equal.*

Consider a sample $(\underline{x}_1, \underline{y}_1), \ldots, (\underline{x}_n, \underline{y}_n)$ of size n. The vertical distance of sample value $(\underline{x}_j, \underline{y}_j)$ from a straight line $y = a + bx$ is $|\underline{y}_j - a - b\underline{x}_j|$. The sum of the squares of these distances then becomes

$$q = \sum_{j=1}^{n} \left(\underline{y}_j - a - b\underline{x}_j\right)^2 \tag{3.2}$$

In the method of least squares the a and b are chosen such that they minimize q. q depends on a and b and a necessary condition for q to be minimum is

$$\frac{\partial q}{\partial a} = 0 \quad \text{and} \quad \frac{\partial q}{\partial b} = 0 \tag{3.3}$$

From this condition we obtain

$$\underline{y} - \overline{\underline{y}} = b\,(\underline{x} - \overline{\underline{x}}) \tag{3.4}$$

where

$$\overline{\underline{x}} = \tfrac{1}{n}\,(\underline{x}_1 + \cdots + \underline{x}_n) \quad \text{and} \quad \overline{\underline{y}} = \tfrac{1}{n}\left(\underline{y}_1 + \cdots + \underline{y}_n\right) \tag{3.5}$$

The straight line Equation 3.4 is called the **regression line** of the $\underline{y}$-values of the sample on the $\underline{x}$-values of the sample. Its slope b is called the **regression coefficient** of $\underline{y}$ on $\underline{x}$, and it will be shown that

$$b = \frac{S_{xy}}{S_1^2} \tag{3.6}$$

where

$$S_1^2 = \frac{1}{n-1}\sum_{j=1}^{n}\left(\underline{x}_j - \overline{\underline{x}}\right)^2 = \frac{1}{n-1}\left[\sum_{j=1}^{n}\underline{x}_j^2 - \frac{1}{n}\left(\sum_{j=1}^{n}\underline{x}_j\right)^2\right] \tag{3.7}$$

and

$$S_{xy} = \frac{1}{n-1}\sum_{j=1}^{n}\left(\underline{x}_j - \overline{\underline{x}}\right)\left(\underline{y}_j - \overline{\underline{y}}\right) = \frac{1}{n-1}\left[\sum_{j=1}^{n}\underline{x}_j\underline{y}_j - \frac{1}{n}\left(\sum_{i=1}^{n}\underline{x}_i\right)\left(\sum_{i=1}^{n}\underline{y}_i\right)\right] \tag{3.8}$$

S_1^2 is called the **variance** and S_{xy} is called the **covariance** of the sample. Obviously, the regression line Equation 3.4 passes through the point $(\overline{x}, \overline{y})$. Using Equation 3.2 and 3.3 to derive Equation 3.4 we find

$$\frac{\partial q}{\partial a} = -2\sum_{j=1}^{n}\left(\underline{y}_j - a - b\underline{x}_j\right) = 0$$

$$\frac{\partial q}{\partial b} = -2\sum_{j=1}^{n}\underline{x}_j\left(\underline{y}_j - a - b\underline{x}_j\right) = 0$$

Thus

$$na + b\sum_{j=1}^{n} \underline{x}_j = \sum_{j=1}^{n} \underline{y}_j$$
$$a\sum_{j=1}^{n} \underline{x}_j + b\sum_{j=1}^{n} \underline{x}_j^2 = \sum_{j=1}^{n} \underline{x}_j \underline{y}_j$$

Because of Assumption 1, the determinant

$$n\sum_{j=1}^{n} \underline{x}_j^2 - \left(\sum_{j=1}^{n} \underline{x}_j\right)^2 = n(n-1)s_1^2$$

of this system of linear equations is not zero, and the system has a unique solution:

$$a = \overline{\underline{y}} - b\overline{\underline{x}} \quad \text{and} \quad b = \frac{n\sum_{j=1}^{n} \underline{x}_j \underline{y}_j - \sum_{i=1}^{n} \underline{x}_i \sum_{i=1}^{n} \underline{y}_i}{n(n-1)s_1^2} \tag{3.9}$$

This yields Equation 3.4.

Matrix Calculation Method

The method of least squares can also be implemented in a matrix structure. The TUE_{ref} data and the TUE radiometer data are stored in a n x 2 matrix. Each column represents the data of a radiometer. The first column, x, represents the TUE_{ref} data and the second column, y, represents the data of the TUE radiometer. Each row represents a (x, y)-pair from the sample. There are n such pairs in the sample which results in a n x 2 matrix $\mathcal{A}$.

$$\mathcal{A} = \begin{pmatrix} \underline{x}_1 & \underline{y}_1 \\ \vdots & \vdots \\ \underline{x}_n & \underline{y}_n \end{pmatrix} \tag{3.10}$$

First the mean per column has to be calculated using Equation 3.5. The results are stored in a row vector $\vec{\mu} = (\overline{\underline{x}}\ \overline{\underline{y}})$.

For the calculation of the variance as well as the covariance, the difference between the sample values $\underline{x}_j$ and $\underline{y}_j$ and their means $\overline{\underline{x}}$ and $\overline{\underline{y}}$, is needed. This results in an matrix $\mathcal{A}_d$

$$\mathcal{A}_d = \mathcal{A} - \mathcal{O} \cdot \vec{\mu} \tag{3.11}$$

where $\mathcal{O}$ is a n x 1 matrix filled with ones.

$$\mathcal{A}_d = \begin{pmatrix} \underline{x}_1 - \overline{\underline{x}} & \underline{y}_1 - \overline{\underline{y}} \\ \vdots & \vdots \\ \underline{x}_n - \overline{\underline{x}} & \underline{y}_n - \overline{\underline{y}} \end{pmatrix} \tag{3.12}$$

In Equations 3.7 and 3.8 $(\underline{x}_j - \overline{\underline{x}})^2$ and $(\underline{x}_j - \overline{\underline{x}})(\underline{y}_j - \overline{\underline{y}})$ are required. Furthermore all terms

have to be divided by $n-1$. This can be obtained with

$$COV = \frac{\mathcal{A}_d^T \cdot \mathcal{A}_d}{n-1} \tag{3.13}$$

$$= \frac{1}{n-1} \cdot \begin{pmatrix} \underline{x}_1 - \overline{\underline{x}} & \cdots & \underline{x}_n - \overline{\underline{x}} \\ \underline{y}_1 - \overline{\underline{y}} & \cdots & \underline{y}_n - \overline{\underline{y}} \end{pmatrix} \cdot \begin{pmatrix} \underline{x}_1 - \overline{\underline{x}} & \underline{y}_1 - \overline{\underline{y}} \\ \vdots & \vdots \\ \underline{x}_n - \overline{\underline{x}} & \underline{y}_n - \overline{\underline{y}} \end{pmatrix} \tag{3.14}$$

$$= \begin{pmatrix} S_1^2 & S_{xy} \\ S_{xy} & S_2^2 \end{pmatrix} \tag{3.15}$$

Now all parameters necessary to calculate the coefficients of the regression line have been determined.

MATLAB [9] also uses the matrix method and has a built-in function called **cov**, which calcutates the covariance matrix.

3.2.4 Confidence Levels

In the previous subsection we calculated a linear regression function with slope b. This b however is only the maximum likelihood estimate of the slope β. Because we use a population of samples, we cannot draw conclusions about the population that are 100% certain. Therefore we modify the problem as

Choose a probability γ close to 1. Then determine two quantities Θ_1 and Θ_2 such that the probability that Θ_1 and Θ_2 include the exact unknown value of the parameter β is equal to γ.

Numerical values of those two quantities should be computed from the given samples. Those sample values may be regarded as observed values of the random variables. Then Θ_1 and Θ_2 are functions of this random variables and therefore random variables, too. Thus our requirement may be written as:

$$P(\Theta_1 \leqq \beta \leqq \Theta_2) = \gamma \tag{3.16}$$

If we know such functions Θ_1 and Θ_2 and a sample is given, we may compute a numerical value θ_1 of Θ_1 and a numerical value θ_2 of Θ_2. The interval with endpoints θ_1 and θ_2 is called the **confidence interval**, and γ is called the **confidence level**. The choice of γ is not a mathematical question, but must be answered from the viewpoint of the application. Raising the confidence level results in longer confidence intervals. In the data analysis the confidence intervals are calculated for $\gamma = 0.9, 0.95, 0.98, 0.99$ and 0.999. The remaining part of this subsection contains the deviation of the confidence interval in our situation.

Consider the following two assumptions:

Assumption 2 *For each fixed $\underline{x}$ the random variable $\underline{y}$ is normal with mean $\mu(\underline{x}) = \alpha + \beta\underline{x}$ and variance σ^2, where the latter is independent of $\underline{x}$.*

Assumption 3 *The n performances of the experiment by which the sample $(\underline{x}_1, y_1), \ldots, (\underline{x}_n, \underline{y}_n)$ has been obtained, are independent.*

β in Assumption 2 is called the regression coefficient of the population, because it can be shown that under Assumption 1–3 the maximum likelihood estimate of β is the sample regression coefficient b in Equation 3.6.

Under Assumptions 1–3 a confidence interval for β can be obtained, using the following procedure:

1. Choose confidence level γ
2. Determine the solution c of the equation

$$F(c) = \frac{1}{2}(1+\gamma) \tag{3.17}$$

from the table of the t–distribution with $n-2$ degrees of freedom (Appendix A).

3. Using a sample $(x_1, y_1), \ldots, (x_n, y_n)$, compute $(n-1)S_1^2$ from Equation 3.7, $(n-1)S_{xy}$ from Equation 3.8 and b from Equation 3.6

$$(n-1)S_2^2 = \sum_{j=1}^{n} y_j^2 - \frac{1}{n}\left(\sum_{j=1}^{n} y_j\right)^2 \tag{3.18}$$

and

$$q_0 = (n-1)(S_2^2 - b^2 S_1^2) \tag{3.19}$$

4. Compute

$$k = c\sqrt{\frac{q_0}{(n-2)(n-1)S_1^2}} \tag{3.20}$$

The confidence interval is

$$CONF = \{b - k \leq \beta \leq b + k\} \tag{3.21}$$

3.3 Data Selection

Our objective is to come to a judgment about the stability of the TUE radiometer. Therefore short term variations as well as long term variations should be investigated. Because precipitation, in particular rain, has an enormous influence on the attenuation, or brightness temperature of the atmosphere, both periods with and without rain are distinguished. For each month that is considered, three days with and three days without precipitation are selected. The short term variations are investigated by comparing the daily variations, the long term variations on the other hand are evaluated by comparing the monthly variations.

In 1996 there were three measurement campaigns for the CLARA–project. During those three campaigns, the RESCOM radiometer was stationed on top of the building of the Faculty of Electrical Engineering at Delft University of Technology. During these measurement campaigns the TUE radiometer was still stationed at the satellite groundstation of the Eindhoven University of Technology. Due to this site diversity, the data measured during these campaigns with both radiometers cannot be compared for calibration purposes. The periods that this site diversity exists, are the measurement periods of the campaign and the transportation periods from and to Delft. These measurement campaigns were:

1. First campaign: 15 April 1996 till 27 April 1996;

2. Second campaign: 19 August 1996 till 4 September 1996; and

3. Third campaign: 18 November 1996 till 11 December 1996

Furthermore it is necessary to know that the data of the selected days are correct. This means that no disturbances are allowed, like the blockage of the antenna, maintenance or errors. In the logbooks of both radiometers this has to be checked. Interruption of the RESCOM radiometer can also be detected by checking the datafiles. When no interruption occurred, all the data of one day are stored in one file. In case of an interruption the data file is closed and a new data file is generated. So RESCOM data are free of errors when only one data file per day occurs.

These selection criteria result in the following selection of days:
In August no days can be found with rain. Days from August, 1, 1996 to August, 19, 1996

Month	Days without rain	Days with rain
May 1996	May, 9, 1996	May, 16, 1996
	May, 10, 1996	May, 21, 1996
	May, 11, 1996	May, 22, 1996
June 1996	June, 25, 1996	June, 8, 1996
	June, 26, 1996	June, 28, 1996
	June, 27, 1996	June, 29, 1996
July 1996	July, 8, 1996	July, 2, 1996
	July, 11, 1996	July, 3, 1996
	July, 12, 1996	July, 4, 1996
August 1996	August, 1, 1996	
	August, 3, 1996	
	August, 4, 1996	

Table 3.3: Days selected for the linearity check.

contain no suitable data files with rain. After August, 19 the second CLARA campaign is running, so there is again a site difference.

3.4 Problems with Data Comparison

The data of both radiometers are collected on two separate systems. The data of the TUE radiometer is collected on a UNIX system, while the data of the RESCOM radiometer is collected on a PC with a program running under MS-DOS. The data files of both radiometers are then converted to standard ASCII files.

The TUE radiometer data file is a file with one column of data, representing the 30 GHz brightness temperatures.

The RESCOM radiometer data file (ASCII) contains three lines for each second. Each line contains the information of the measurement time and the brightness temperature of the specific channel at that moment. This file is converted in MATLAB to an ASCII file containing one line for each measurement second and four columns, representing 31.7 GHz, 23.8 GHz and 21,3 GHz brightness temperatures and measurement time in decimal representation. This means that for example 3.5 represents 3:30.00 and 9.9605556 represents 9:41.26.

While inspecting and comparing the data of the TUE and RESCOM radiometer, we discovered that the converted RESCOM files were larger than the TUE files. This was strange, because both radiometers use a sample rate of one sample a second.

The RESCOM files contained 86423, 86424 or 86425 data points each day, where as this should be $24 \cdot 60 \cdot 60 = 86400$. This would mean that there are 23, 24 or 25 points too much.

Doubles

Our first thought was that, when there are 23, 24 or 25 points to much, during 23, 24 or 25 seconds two samples a second have been made. It also seemed that this error occurred once every hour. In order to test this possibility a program in MATLAB has been written, that detected whether a time period occurred twice in an ASCII file and that time period is written to a file. An example of such a file, for June, 11, 1996, can be found in appendix D.

We see that more than 23, 24 or 25 double time periods occurred. On 11 June 1996 there were 34 double time periods, every hour at least one (except for the period 16.00:00 – 16.59:59). During 11 hours two double periods occurred, which explained the 34 errors. Being a double only meant that the measurement time of two successive data points were the same, the brightness temperature of both these points were not necessarily the same.

We still could not explain the fact that we found 11 double periods more than the number of doubles we expected from the overflow of data points. Therefore we developed another test.

3.4.1 Gaps

The ASCII data file also has been checked on time jumps larger than 1 second. Eleven of these time jumps larger than 1 second occurred on June, 11, 1996. They were all jumps of two seconds. I will call them gaps.

When in an hour two doubles occurred and a gap, the gap was located between both doubles, but not exactly in between. In order to define a relation between the number of doubles and the number of gaps, the following variables will be introduced:

- d : number of doubles
- g : number of gaps
- l : number of lines in the data file after conversion in MATLAB

The following relation (invariant in the loop [10]) holds

$$l - 86400 = d - g \tag{3.22}$$

3.4.2 DCF-clock

One possible explanation could be that these problems are caused by the DCF-clock of the 20/30 GHz RESCOM radiometer part and the 50 GHz RESCOM radiometer part.The DCF-clock is used to synchronize the computer clocks of both radiometer parts. They are only synchronized at the start of the measurement program rad.exe. This synchronization procedure could explain an error, but does not explain the occurrence of an error each hour or twice an hour.

In order to exclude the influence of the DCF-clock, the clock was disconnected from Friday 11 April 1997 to Monday 14 April 1997, and the data of 12 and 13 April 1997 have been analysed. Although the DCF-clock was disconnected the errors still occurred, so we may conclude they were not caused by the use of the DCF-clock.

3.4.3 Correction of the data files

In order to make the ASCII files suitable for the calibration procedure of the TUE radiometer, the ASCII files were corrected. I will describe how this was done.

One double in an hour

When there is only one double period in an hour the following procedure is used:

1. Calculate the mean of both brightness temperatures for a double time period;
2. Replace the brightness temperature of the first element of a double by the mean;
3. Delete the second element of a double from the data file.

In formula:

$$l \longrightarrow l - 1 \tag{3.23}$$
$$d \longrightarrow d - 1 \tag{3.24}$$

Combination of Double–Gap–Double in an hour

When a combination of a double–gap–double occurs in an hour, the gap is located between the two doubles, but not exactly between the two doubles. The correction of this problem is complexer than just cancelling a single double. The following procedure will be used:

1. Find the second element of the first double.
2. Increase the time for that element and for all following measurement periods up to and including the beginning of the gap with one second.
3. Cancel the second double using de procedure described in the previous section.

Figure 3.7 gives a graphical representation of the first two steps in the procedure.

The complete procedure results in

$$l \longrightarrow l - 1 \tag{3.25}$$
$$d \longrightarrow d - 2 \tag{3.26}$$
$$g \longrightarrow g - 1 \tag{3.27}$$

Combination of two Doubles in an hour without a Gap

The situation with two doubles within an hour, and no gap in the same hour is very simple to correct. The procedure described in section 5.1 is used twice. This results in:

$$l \longrightarrow l - 2 \tag{3.28}$$
$$d \longrightarrow d - 2 \tag{3.29}$$

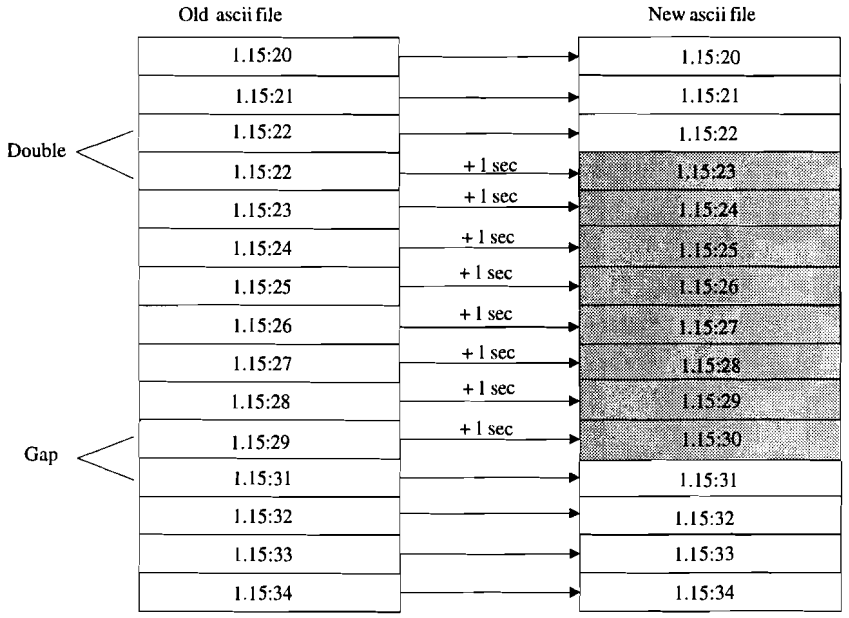

Figure 3.7: Cancelling a Double–Gap combination .

Total Program

The total program works with a loop-structure that will be executed for each hour of the day. Each execution step, one of the situations described in this section occurs. Each time a procedure is used and the values of l, d and g are updated [10]. These values remain the same or decrease. At the end of the loop, when the whole file is corrected, l will have the value 86400 and d and g have the value 0, and relation 4.1 still holds, namely

$$0 = 0$$

3.5 Results

In this section the results of the analysis of the data of the RESCOM and TUE radiometer are presented. The results of days without and with rain are separated in two subsections.

3.5.1 No Rain Involved

Linearity Check by Correlation

For the days without rain the following correlation coefficients are found (Table 3.4):

Day	Correlation Coefficient
May, 9, 1996	0.958
May, 10, 1996	0.986
May, 11, 1996	0.986
June, 25, 1996	0.975
June, 26, 1996	0.906
June, 27, 1996	0.998
July, 8, 1996	0.960
July, 11, 1996	0.798
July, 12, 1996	0.756
August, 1, 1996	0.822
August, 3, 1996	0.822
August, 4, 1996	0.857

Table 3.4: Correlation Coefficients for days without rain.

For the days in May and June together with the first day of July the correlation coefficient is very high and varies between 0.906 and 0.998. The last day of July and the first two days in August the correlation is significantly lower than the days in May and June. For these measurement days the mean correlation coefficient is 0.902 with a standard deviation of 0.0827.

In table 3.5 the mean and standard deviation per month are calculated. The sudden decreasement of the correlation coefficient in July results in a high standard deviation in that month.

Month	$\mu_{corr.coeff.}$	$\sigma_{corr.coeff.}$
May	0.9767	0.0132
June	0.9597	0.0391
July	0.8380	0.0880
August	0.8337	0.0165

Table 3.5: Mean and standard deviation per month of correlation coefficients for days without rain.

Synchronisation

Figure 3.8 shows the effect of the time shift on the correlation coefficient. A time shift of -2 or -1 seconds will increase the correlation coefficient but this increasement only takes place in the fourth decimal. Other time shifts decrease the correlation coefficient. We may conclude

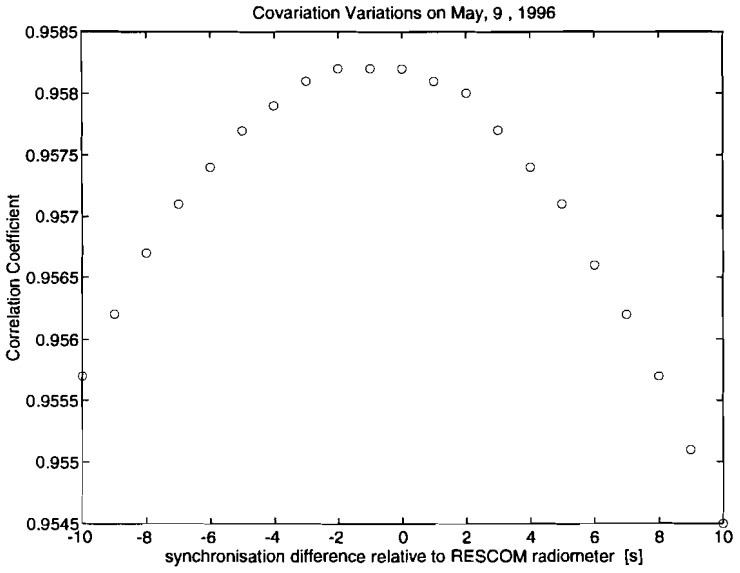

Figure 3.8: Correlation Variations due to data file shifting on May, 9, 1996.

that it is not necessary to shift one of the data files relative to each other, because it only results in a slight increasement of the correlation coefficient. Also for the other days without rain it is not necessary to shift one of the datafiles.

Regression Lines for Brightness Temperature Translations

With the least squares method of Gauss described in the beginning of this chapter the following regression lines are found, taking into account the frequency difference between the two radiometers and the point density reduction (Table 3.6).

Day	Regression Lines
May, 9, 1996	$T_{TUE} = -6.1112 + 0.9484 \cdot T_{RESCOM_{ref}}$
May, 10, 1996	$T_{TUE} = -6.1492 + 0.9980 \cdot T_{RESCOM_{ref}}$
May, 11, 1996	$T_{TUE} = -4.0593 + 0.9409 \cdot T_{RESCOM_{ref}}$
June, 25, 1996	$T_{TUE} = 0.0082 + 0.9101 \cdot T_{RESCOM_{ref}}$
June, 26, 1996	$T_{TUE} = -3.4873 + 0.9792 \cdot T_{RESCOM_{ref}}$
June, 27, 1996	$T_{TUE} = -2.2599 + 0.9544 \cdot T_{RESCOM_{ref}}$
July, 8, 1996	$T_{TUE} = -4.1732 + 0.9889 \cdot T_{RESCOM_{ref}}$
July, 11, 1996	$T_{TUE} = 2.4839 + 0.8606 \cdot T_{RESCOM_{ref}}$
July, 12, 1996	$T_{TUE} = 0.7693 + 0.8751 \cdot T_{RESCOM_{ref}}$
August, 1, 1996	$T_{TUE} = 1.4914 + 0.8466 \cdot T_{RESCOM_{ref}}$
August, 3, 1996	$T_{TUE} = -2.1879 + 0.8752 \cdot T_{RESCOM_{ref}}$
August, 4, 1996	$T_{TUE} = -2.3186 + 0.8661 \cdot T_{RESCOM_{ref}}$

Table 3.6: Regression Lines for days without rain.

For the days with the high correlation coefficient the slope of the regression line varies from 0.8466 to 0.9980, while the constant factor varies from -6.1492 and 2.4839. For the days with the lower correlation coeffficient the slope of the regression line is lower, but the constant factor is higher. It is typical that for the last two days in July and all the days in August, the correlation coefficient is much lower than the other days. For both the constant factor and the slope, the mean and standard deviation are calculated. For these measurement days the mean for the constant factor is -2.1662 with standard deviation 2.7259. The mean for the slope is 0.9203 with standard deviation 0.0522.

Month	$\mu_{constant}$	$\sigma_{constant}$	μ_{slope}	σ_{slope}
May	-5.4399	0.9764	0.9624	0.0253
June	-1.9130	1.4480	0.9479	0.0286
July	-0.3067	2.8222	0.9082	0.0574
August	-1.0050	1.7661	0.8626	0.0119

Table 3.7: Mean and standard deviation per month for constant factor and slope for days with rain.

Table 3.7 shows the means and standard deviations of the constant factor and slope of the regression lines for days without rain.

Figure 3.9 shows the regression lines together with the average of one minute data for May, 9, 1996 and May, 10, 1996.

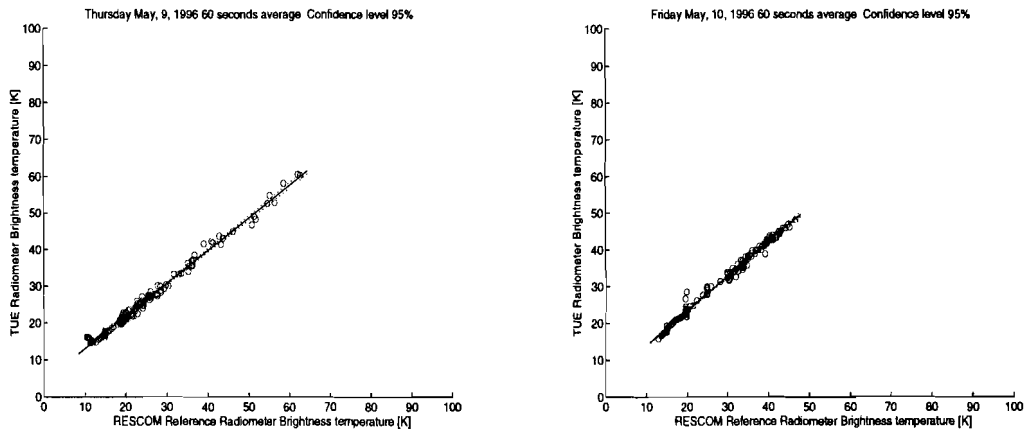

(a) (b)

Figure 3.9: Regression Lines together with one minute average data: (a) May, 9, 1996; (b) May, 10, 1996.

Confidence Levels

Table 3.8 shows the confidence intervals for several confidence levels.

Day	$\gamma = 0.9$		$\gamma = 0.95$		$\gamma = 0.98$		$\gamma = 0.99$		$\gamma = 0.999$	
	$b-k$	$b+k$	$b-k$	$b+k$	$b-k$	$b+k$	$b-k$	$b+k$	$b-k$	$b+k$
May, 9, 1996	0.9376	0.9593	0.9355	0.9614	0.9331	0.9638	0.9314	0.9654	0.9281	0.9688
May, 10, 1996	0.9861	1.0099	0.9839	1.0121	0.9813	1.0147	0.9795	1.0165	0.9766	1.0202
May, 11, 1996	0.9332	0.9486	0.9318	0.9500	0.9301	0.9517	0.9289	0.9529	0.9266	0.9552
June, 25, 1996	0.8963	0.9239	0.8937	0.9265	0.8906	0.9296	0.8885	0.9317	0.8842	0.9360
June, 26, 1996	0.9638	0.9947	0.9609	0.9976	0.9574	1.0010	0.9551	1.0034	0.9503	1.0081
June, 27, 1996	0.9493	0.9596	0.9484	0.9605	0.9472	0.9617	0.9465	0.9624	0.9459	0.9630
July, 8, 1996	0.9725	1.0053	0.9694	1.0084	0.9657	1.0121	0.9632	1.0146	0.9581	1.0197
July, 11, 1996	0.8254	0.8959	0.8187	0.9025	0.8108	0.9104	0.8055	0.9157	0.7946	0.9266
July, 12, 1996	0.8439	0.9063	0.8381	0.9121	0.8311	0.9191	0.8263	0.9240	0.8167	0.9335
August, 1, 1996	0.8142	0.8791	0.7581	0.9352	0.8008	0.8925	0.7959	0.8974	0.7859	0.9074
August, 3, 1996	0.8444	0.09061	0.8386	0.9119	0.8317	0.9188	0.8268	0.8937	0.8175	0.9330
August, 4, 1996	0.8049	0.9274	0.7934	0.9389	0.7797	0.9526	0.7714	0.9609	0.7514	0.9808

Table 3.8: Confidence Levels for days without rain.

The effect of having a lower correlation coefficient can also be seen in the size of the confidence intervals. Having a lower correlation coefficient corresponds with a larger confidence interval. The dotted lines in Figure 3.9 represent the regression lines that would have been found when using the upper and lower bounds of β with confidence level $\gamma = 95\%$.

3.5.2 Rain Involved

Linearity Check by Correlation

For days with rain the following correlation coefficients are found (Table 3.9):

Day	Correlation Coefficient
May, 16, 1996	0.986
May, 21, 1996	0.956
May, 22, 1996	0.913
June, 8, 1996	0.983
June, 28, 1996	0.983
June, 29, 1996	0.867
July, 2, 1996	0.966
July, 3, 1996	0.971
July, 4, 1996	0.898

Table 3.9: Correlation Coefficients for days with rain.

In contrary to the days without rain, the correlation coefficients of all days except for June, 29 and July, 4 are very high. The correlation coefficients vary from 0.913 to 0.986 for the days except for June, 29 and July, 4. The mean of the correlation coefficients is 0.947 with a standard deviation of 0.0409.

Month	$\mu_{corr.coeff.}$	$\sigma_{corr.coeff.}$
May	0.9517	0.0300
June	0.9443	0.0548
July	0.9450	0.0.0333

Table 3.10: Mean and standard deviation per month of correlation coefficients for days with rain.

Table 3.10 shows the means and standard deviations per month for days with rain.

Synchronisation

The correlation coefficients are again used to check whether a time shift (or drift) has occurred between the data of both radiometers. Again positive and negative shift are checked. This check is done for May, 16, 1996. Figure 3.10 shows the effect of the time shift on the correlation coefficient.

A time shift of +2 to +6 seconds will increase the correlation coefficient but this increasement only takes place in the fourth decimal. Other time shifts decrease the correlation coefficient.

We may conclude that it is not necessary to shift one of the data files relative each other, because it only results in a slight increasement of the correlation coefficient. For the other days with rain it is also not necessary to shift the data files.

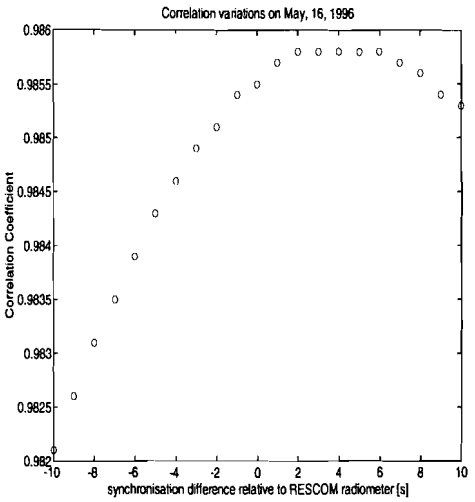

Figure 3.10: Correlation coefficient variations on 16 May 1996

Regression Lines for Brightness Temperature Translations

By the least squares method of Gauss the following regression lines have been found (Table 3.11) The slopes of the regression lines found for days with rain show more variation than

Day	Regression Lines
May, 16, 1996	$T_{TUE} = -4.9116 + 0.9592 \cdot T_{RESCOM_{ref}}$
May, 21, 1996	$T_{TUE} = 2.5358 + 0.7599 \cdot T_{RESCOM_{ref}}$
May, 22, 1996	$T_{TUE} = 2.1287 + 0.8070 \cdot T_{RESCOM_{ref}}$
June, 8, 1996	$T_{TUE} = -4.5878 + 0.9151 \cdot T_{RESCOM_{ref}}$
June, 28, 1996	$T_{TUE} = 0.0701 + 0.8401 \cdot T_{RESCOM_{ref}}$
June, 29, 1996	$T_{TUE} = 8.4693 + 0.9136 \cdot T_{RESCOM_{ref}}$
July, 2, 1996	$T_{TUE} = 0.2567 + 0.8923 \cdot T_{RESCOM_{ref}}$
July, 3, 1996	$T_{TUE} = -4.7468 + 1.0534 \cdot T_{RESCOM_{ref}}$
July, 4, 1996	$T_{TUE} = 1.3554 + 1.0896 \cdot T_{RESCOM_{ref}}$

Table 3.11: Regression lines for days with rain.

for the days without rain. They vary from 0.7599 to 1.0896. The mean of the slope is 0.9145, with a standard deviation of 0.1019. The constant factor varies from -4.9116 to 8.4693 (a mean of 0.0633 and standard deviation of 4.1132), except for June, 29 where the value for the constant factor is 8.4693.

The slope of the regression line for that day, however, lies inside the range of the other slopes. For July, 4, both the constant factor and the slope in the regression line are high compared to the other days. This is also caused by the lower correlation coefficient.

Table 3.12 shows the means and standard deviations for both constant factor and slope per month for days with rain.

Figure 3.11 shows the regression lines together with the average of one minute data for May, 16, 1996 and May, 21, 1996.

Month	$\mu_{constant}$	$\sigma_{constant}$	μ_{slope}	σ_{slope}
May	-0.0824	3.4188	0.8420	0.0851
June	1.3172	5.4030	0.8896	0.0350
July	-1.0449	2.6558	1.0118	0.0858

Table 3.12: Mean and standard deviation per month for constant factor and slope for days with rain.

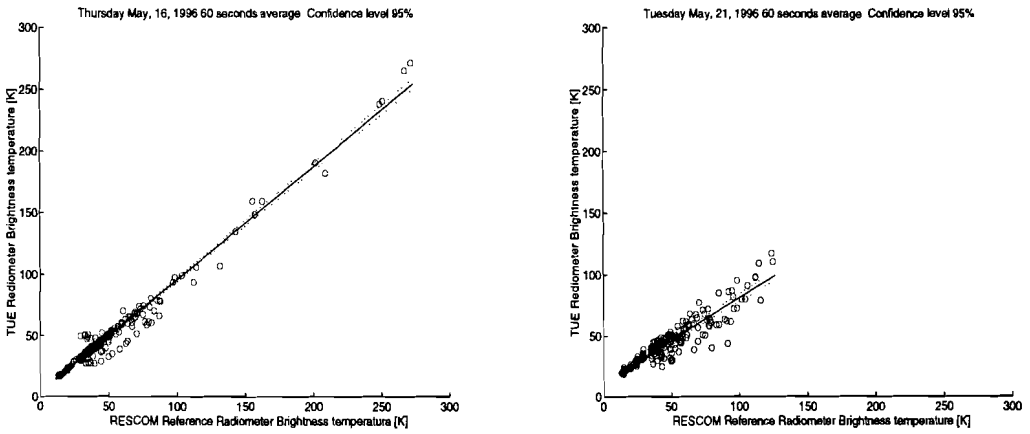

(a) (b)

Figure 3.11: Regression Lines together with one minute average data: (a) May, 16, 1996; (b) May, 21, 1996.

Confidence Levels

Table 3.13 shows the upper and lower bounds of the confidence intervals for several confidence levels.

Day	$\gamma = 0.9$		$\gamma = 0.95$		$\gamma = 0.98$		$\gamma = 0.99$		$\gamma = 0.999$	
	$b-k$	$b+k$	$b-k$	$b+k$	$b-k$	$b+k$	$b-k$	$b+k$	$b-k$	$b+k$
May, 16, 1996	0.9524	0.9666	0.9511	0.9673	0.9496	0.96886	0.9485	0.9699	0.9464	0.9720
May, 21, 1996	0.7503	0.7695	0.7484	0.7714	0.7463	0.7735	0.7448	0.7750	0.7419	0.7779
May, 22, 1996	0.7921	0.8219	0.7893	0.8247	0.7860	0.8280	0.7837	0.8303	0.7791	0.8349
June, 8, 1996	0.8994	0.9308	0.8965	0.9337	0.8929	0.9373	0.8906	0.9396	0.8857	0.9445
June, 28, 1996	0.8251	0.8551	0.8223	0.8579	0.8190	0.8612	0.8167	0.8635	0.8116	0.8686
June, 29, 1996	0.8796	0.9476	0.8732	0.9540	0.8656	0.9616	0.8605	0.9667	0.8500	0.9772
July, 2, 1996	0.8803	0.9043	0.8780	0.9066	0.8753	0.9093	0.8735	0.9111	0.8698	0.9148
July, 3, 1996	1.0410	1.0658	1.0387	1.0681	1.0359	1.0709	1.0341	1.0727	1.0303	1.0765
July, 4, 1996	1.0382	1.1410	1.0286	1.1506	1.0171	1.1621	1.0093	1.1699	0.9934	1.1858

Table 3.13: Confidence Levels for days with rain.

Again it can be seen that a lower correlation coefficient results in a larger confidence interval compared to the days with a higher correlation coefficients.

The dotted lines in Figure 3.11 represent the regression lines that would have been found when using the upper and lower bounds of β with confidence level $\gamma = 95\%$.

3.6 Conclusions

3.6.1 Linearity

For days without rain the correlation coefficients vary from 0.756 to 0.998. The mean of all these correlation coefficients is 0.902, while their standard deviation is 0.0827. For days with rain correlation coefficients varying between 0.867 and 0.986 have been found. Their mean is 0.947, their standard deviation 0.0409.

Perfect linearity would have been achieved when the correlation coefficients were exactly 1. We see that the linearity is better and more stable for days with rain than without rain. Days with high rainrates have a better linearity. The maximum rainrates during the days with rain can be found in appendix C. In our situation there were four days with a low rainrate and five days with a high rainrate, thus high rainrates and low rainrates are almost equally distributed. The real distribution of rainrates occuring in the Netherlands has not been taken into account. When this is done, the linearity probably will be a little lower.

When the regression lines for days with and without rain are compared, we see that the means of the slopes are almost equal. There is however a larger difference in the mean of the constant factor. This larger difference is partly caused by the constant factor of June, 29, 1996. From this we may conclude that the behaviour of the TUE radiometer is linear over its complete range. When all constant factors and slopes for days with and without rain are combined, the means and standard deviations are calculated for the constant factor and slope. The mean of the constant factor is -1.2107 K, with a standard deviation of 3.5657 K. The mean of the slope is 0.9187, with a standard deviation of 0.0776. Together with equation 3.1 we can calculate a conversion equation:

$$T_{TUE} = -12.3231 + 0.9518 \cdot T_{RESCOM} \tag{3.30}$$

3.6.2 Short Term Evaluations

- For days without rain, there is only a slight variation within each month, when the regression lines are considered. The constant factor has a standard deviation varying from 0.9764 to 2.8222. The slope has a standard deviation varying from 0.0119 to 0.0574.

- For days with rain, a great variation within a month occurs, in the constant factor as well as in the slope of the regression lines. The standard deviation of the constant factor varies from 2.6558 to 5.4030, while the standard deviation of the slope varies from 0.0350 to 0.0858. An explanation of this variation is given in the section dealing with the longterm variations.

- The last two days of July and all three days of August have a structural lower correlation coefficient, which results in a higher constant factor for the regression line, as well as a lower value for the slope of the regression line. Together with a low correlation coefficient also the convergence intervals will increase.

3.6.3 Long Term Evaluations

- In the beginning of this chapter a $T_{RESCOM_{ref}}$ has been introduced, in order to compensate the difference in measurement frequency between the RESCOM Radiometer and the TUE Radiometer. One of our goals was to find a translation of TUE brightness temperatures to $RESCOM_{ref}$ brightness temperatures (derived from RESCOM brightness temperature). The regression lines give a good indication, whether a standard translation can be found from TUE brightness temperature to $RESCOM_{ref}$ brightness temperature. For days without rain, the constant factor of the regression lines has a mean of -2.1662 K with a standard deviation of 2.7259 K, over all analysed measurement days. The slope has a mean of 0.9203, with a standard deviation of 0.0522.

- Days of rain give a lot of variations in the regression lines. A mean of 0.0633 K and a standard deviation of 4.1132 K for the constant factor, have been found. The slope has a mean of 0.9145 and a standard deviation of 0.1019. These variations are caused by variations in the rainrate. A high rainrate results in a high brightness temperature. This temperature will be upto and above 200 K, for heavy rain. May, 16, 1996, June, 8, 1996, June, 29, 1996, July, 2, 1996 and July, 3, 1996 are days with heavy rain. When these days are compared with the other days on which rain occured, we see a difference. For days with a high rainrate, the constant factor in the regression line is low, whereas the slope of the regression line is high. For days with light rain the constant factor on the other hand is high, while the slope of the regression line is low. June, 29, 1996 and July, 4, 1996 are an exception of this rule, but this exception can be explained by the lower correlation coefficient.

- As we can see,the means of the slopes of the regression lines are almost the same for days with and without rain. The standard deviation for days with rain, however, is almost twice the standard deviation for days without rain. For the constant factor the standard deviation for days with rain is also almost twice the standard deviation for days without rain. From this may be concluded that the regression lines for days

without rain are the most stable and therefore the translation function from T_{TUE} to $T_{RESCOM_{ref}}$ is the most stable for days without rain.

- There is a tendency in the correlation coefficient, especially during days without rain, that the correlation coefficient decreases in July and August. For days with rain, data from August are unfortunately not available, but the last day analysed in July, also has a lower correlation coefficient.

- For days with high rainrates we see that there are more data points located above the regression line, than for days with low rainrates. This can be explained as follows: The feed of the TUE radiometer has no equipment for the removal of rain droplets on the feed. The RESCOM radiometer has a blower inside that removes raindrops from the feed. The rain drops that are not removed from the TUE radiometer, therefore cause a higher brightness temperature. This effect of more data points being above the regression line is much stronger for days with low rain rates. When we define the angle of arrival of a raindrop as the angle relative to zenith, then we see that a low rain rate goes together with a larger angle of arrival. A high rainrate results in an angle of arrival close to zenith. Rain drops with a large angle of arrival wet the feed of radiometer more easily than drops with a small angle of arrival.

- Another reason for the location of more data points above the regression lines is the larger beamwidth of the TUE Radiometer antenna, as a result of which more radiation from the ground is measured, resulting in a higher brightness temperature.

- A time shift of the data files was not necessary. Besides the exclusion of synchronisation differences,thereby is excluded that there was a difference in the elevation angle of the radiometers. If there was any difference is elevation angles, a difference between days with and without clouds would have been noticed. For days with clouds it would have been necessary to shift the data files, while for days without clouds it would not have been necessary.

3.6.4 General Conclusions Calibration

- The best linearity has been obtained from days with rain. One thing, however, should be considered. For days with rain, the rainrate has not been criterium for selection. Days with high rainrates have a better linearity. In our situation there were four days with a low rainrate and five days with a high rainrate, thus high rainrates and low rainrates are almost equally distributed. The real distribution of rainrates occurring in the Netherlands has not been taken into account. When this is done, the linearity probably will be a little lower.

- In the ideal situation a regression line should have been found with a slope of 1, which means that the brightness temperature of the TUE radiometer and the reference temperature obtained from the RESCOM radiometer, differ only a constant. This situation, however will never be reached. Based on the standard deviations the regression lines for days without rain are the most stable, so they also result in most stable translation function. We may conclude that the behaviour of the TUE radiometer is linear over its complete range. A linear conversion equation from T_{RESCOM} to T_{TUE} has been calculated (Equation 3.30).

- The decreasement of the correlation coefficient in July and August occurs in both the days with and without rain. Within the framework of this graduation work it was not possible to investigate whether this decreasement persists September, October, etc. Possibly it could even be a periodic variation with a period of a year. This, however, cannot be concluded from the data that has been analysed. Further research in that direction could be a subject for future traineeship.

- When the radiometer is placed at a location where man-made or natural external influences are excluded as much as possible, the TUE radiometer is suitable for atmospheric measurements as they have been carried out with the RESCOM radiometer. A disadvantage however is that the TUE radiometer is not transportable, because it uses the ground for its cooling. Besides this cooling problem, also the registration equipment is not transportable.

Chapter 4

Matched Atmosphere Algorithm

4.1 Principles of Radiometry

The atmosphere is an absorbing medium. Liquid water, water vapor and oxygen are the main constituents of the atmosphere that cause absorption in the frequency range from 20 GHz up to 50 GHz. In Kirchhoff's law is stated that all energy absorbed in the atmosphere is emitted again. This property of the atmosphere gives us the opportunity to measure characteristics related to the energy absorption of the atmosphere with a radiometer.

Black bodies are objects that absorb all incident radiation. Planck stated that for all black bodies, the spectral brightness B_f, that is the radiated power per unit area, solid angle and bandwidth, is given by

$$B_f = \frac{2h_p f^3}{c^2} \frac{1}{\exp\left(\frac{h_p f}{kT}\right) - 1} \quad \left[\frac{W}{m^2 sr Hz}\right] \tag{4.1}$$

with

h_p is Planck's constant, $6.626 \cdot 10^{-34}$ Js
f is the frequency in Hz
k is Boltzmann's constant, $1.38 \cdot 10^{-23}$ J/K
T is the absolute temperature in K
c is the speed of light in m/s

As shown in [4] for frequencies in the microwave range (up to 100 GHz) it is justified to use the Rayleigh-Jeans approximation. It introduces a deviation of not more than 5% on power density.

$$B_f = \frac{2f^2 kT}{c^2} \quad \left[\frac{W}{m^2 sr Hz}\right] \tag{4.2}$$

Furthermore, the power received by the antenna is equal to

$$P_r = \frac{1}{2} \iint B_f d\Omega dA \quad \left[\frac{W}{Hz}\right] \tag{4.3}$$

A black body only exists in theory. In practice objects only absorb part of the incident radiation and therefore they are called grey bodies. The brightness temperature of a grey

body is defined as the physical temperature T of a black body emitting the same amount of power.

Thus for a real grey object the spectral brightness becomes

$$B_f = \frac{2f^2kT_b}{c^2} \quad \left[\frac{W}{m^2srHz}\right] \tag{4.4}$$

The atmosphere can be considered as a grey body. In general the atmosphere is inhomogeneous. In the model that will be used, this inhomogeneous atmosphere is divided in a large number of horizontal layers, with a certain thickness. Each of these layers is assumed to be homogeneous and has a constant temperature. In this model the troposphere is therefore divided in layers with constant absorption. Figure 4.1 shows a graphical interpretation of this model.

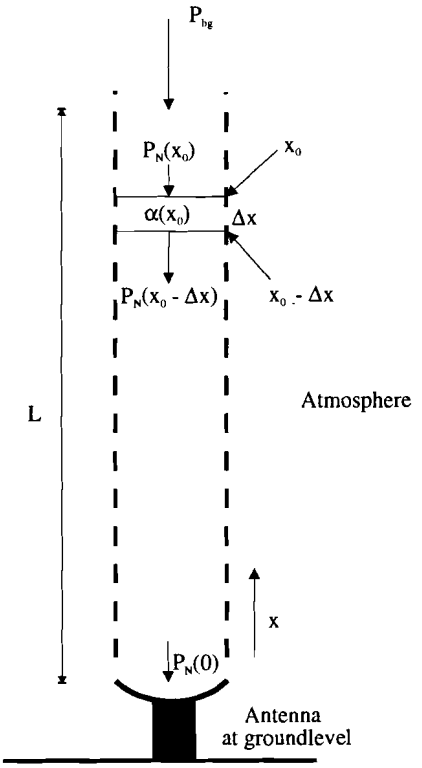

Figure 4.1: Transfer Model of the Atmosphere.

The symbols in this figure represent:

P_{bg}	the cosmic background noise power entering the atmosphere, $P_{bg} = P_N(L)$
L	total thickness of the atmosphere (taken to be 12 km in our calculations)
$P_N(0)$	the resulting noise power at the antenna
$P_N x$	the noise power at distance x
$\alpha(x)$	the absorption coefficient
	$\alpha_{Np}(x) = \ln(\alpha(x))$ is the absorption in Np/m
Δx	the thickness of one layer

In each layer, an amount of radiation is transmitted, and an amount of radiation is emitted by the layer. The amount of radiation transmitted in a layer is $(1 - \alpha(x))\Delta x P(x)$, where $\alpha(x)$ is

the absorption coefficient of the layer. In the next section (discussing MPM) we will calculate this absorption coefficient from the spectra of water vapor, liquid water and oxygen. The amount of radiation emitted by the layer is $\alpha(x)\Delta x P_r(x)$, because the atmosphere behaves like a grey body. Therefore the power $P(x - \Delta x)$ is equal to

$$P(x - \Delta x) = (1 - \alpha(x)\Delta x)P(x) + \alpha(x)\Delta x P_r(x) \tag{4.5}$$

or

$$\frac{P(x) - P(x - \Delta x)}{\Delta x} - \alpha(x)P(x) = \alpha(x)P_r(x) \tag{4.6}$$

By applying the Raleigh -Jeans approximation and with $\Delta x \longrightarrow 0$

$$\frac{dT_b(x)}{dx} - \alpha(x)T_b(x) = \alpha(x)T(x) \tag{4.7}$$

Solving this equation leads to an expression for the radiative transfer equation. It is only valid for non-scattering atmospheres

$$T_b = T_{bg}e^{-\tau(0,L)} + \int_0^L \alpha_{Np}(x')T(x')e^{-\tau(0,x')}dx' \tag{4.8}$$

where

T_b	is the brightness temperature at the antenna in K ; $T_B = T_N(0)$
T_{bg}	is the cosmic background noise temperature in K
τ	is the optical thickness, defined as $\tau(a,b) = \int_a^b \alpha_{Np}(s)ds$
$T(x')$	is the physical temperature at a height x' in K

As one can see, T_b is composed of a cosmic background (absorption) and an atmospheric emission contribution.

According to [4], section 2.1, the assumption that the atmosphere is non-scattering is only legimate when there is no precipitation or only low rain rates. Equation (4.8) consists of two parts. The first part contains the cosmic background brightness and is the solution of the homogeneous differential equation. The second part contains the atmospheric emission and is the solution of the nonhomogeneous differential equation. T_b depends on the vertical temperature and absorption profiles. From relevant atmospheric profiles, it is possible to calculate the brightness temperature of the atmosphere. This problem is Referred to as the direct problem. On the other hand, in remote sensing, the aim is to derive atmospheric characteristics (liquid water content and water vapor in our case) from the measured brightness temperature. This is called the inverse problem.

4.2 Millimeter-wave Propagation Model

In 1985 H.J. Liebe [11] published a broadband model for complex refractivity to predict propagation effects of loss and delay for the neutral atmosphere at frequencies up to 1000 GHz. In 1989 this model was updated [6], and this updated model will be used in this report. In the remaining part of this report this Millimeter-wave Propagation Model will be called MPM. In our application MPM will be used to determine brightness temperatures and attenuation of the atmosphere.

Contributions from dry air, water vapor, suspended water droplets (haze, fog and clouds) and rain are taken into account. For clear air situations the local line database (44 O_2 + 30 H_2O lines) is supplemented by an empirical water vapor continuum.

4.2.1 Calculation of internal parameters

As input variables barometric pressure, temperature, relative huidity, suspended water droplet concentration, rainfall rate and frequency are used. Barometric pressure $P(h)$, temperature $T(h)$ and relative humidity $RH(h)$ are given as height profiles (from 0 to 10 km) obtained from radiosonde data or standard profiles, based on for instance groundlevel values of P,T and RH. For all these input variables validity ranges are specified (Tabel4.1).

name	symbol	validity range	unit
frequency	f	1 - 1000	GHz
barometric pressure	P	$120 - 10^{-5}$	kPa
temperature	T	$-50 - +50$	$°C$
relative humidity	RH	0 - 100	% RH
hygroscopic aerosol reference concentration growing for 80% to 99.9%RH into suspended droplets	w_0(80% RH)	0 - 1	mg/m^3
suspended water droplet concentration	W(100% RH)	0 - 5	g/m^3
rainfall rate	R	0 - 200	mm/h

Table 4.1: Validity ranges for the input variables.

These input variables are used to calculate internal parameters.

Air conditions are measured by barometric pressure, temperature and partial water vapor pressure. The barometric pressure is given by

$$P = p + e \quad [kPa] \tag{4.9}$$

where p and e are partial pressures for dry air and water vapor, respectively. The temperature T given in $°C$ is converted into a relative inverse temperature

$$\theta = \frac{300}{T + 273.15} \quad [K^{-1}]. \tag{4.10}$$

The partial water vapor pressure, finally is given by

$$e = e_s \cdot \frac{RH}{100} \quad [kPa] \tag{4.11}$$

with e_s, the water vapor saturation pressure in kPa and RH the relative humidity in %.

Liebe used empirical methods to find an expression for the water vapor density (v)

$$v = 7.223 \cdot e \cdot \theta \quad [g/m^3] \tag{4.12}$$

For the temperature range from -40°C up to +40°C also an approximation is made for the temperature dependence of the water vapor saturation pressure e_s, with an error smaller than 0.2%.

$$v = 1.739 \cdot 10^9 \cdot RH \cdot \theta^5 \exp(-22.64 \cdot \theta) \quad [g/m^3] \tag{4.13}$$

The liquid water density (w) is found to be composed of contributions from three phenomena:

$$w = w_C + w_A + w_R \tag{4.14}$$

w_C is the liquid water density contribution of clouds in g/m^3. According to Liebe the relative humidity inside a cloud is 100%. When no drop size spectra or other methods are available to determine the contribution of clouds to the liquid water density, the model by Slobin is used, which results in the following liquid water density profile

$$w_C(h) = C \cdot (\rho_{base} - \rho_{top}) \cdot \left(\frac{h - H_{base}}{H_{top} - H_{base}} \right) \quad [g/m^3] \tag{4.15}$$

where ρ_{base} is the saturated water vapor density at the base of the cloud, ρ_{top} the saturated water vapor density at the top of the cloud, both in g/m^3;

$$\rho(h) = 1.739 \cdot 10^{11} \cdot \theta^5 \exp(-22.64 \cdot \theta(h))$$

h the height in m; C a tuning parameter depending on the type of the cloud, typical between 0.1 and 0.75.

In the algorithm H_{top}, H_{base} and C have to be chosen in such a way that they match to actual values as close as possible. H_{base} and H_{top} could eventually, when data are available, be determined by radar and/or lidar,

w_A is the liquid water density contribution of hydroscopic aerosols in g/m^3. The concentration of hygroscopic aerosols in the atmosphere is related to the relative humidity. Solution droplets appear for $80\% \leq RH \leq 99.9\%$ and can reach concentrations up to 0.1 g/m^3. The suspended water droplet concentration due to aerosols (w_A) is modelled by Liebe as:

$$w_A = \begin{cases} 0 & \text{for } 0\% \leq RH < 80\% \\ w_0 \cdot \frac{20 \cdot (C_1 + 4) - RH}{C_1 \cdot (100 - RH)} & \text{for } 80\% \leq RH \leq 99.9\% \end{cases} \quad [g/m^3] \tag{4.16}$$

where w_0 is the dry mass concentration of hygroscopic aerosols in g/m^3 and C_1 a parameter that depends on the particular location

The liquid water density contribution due to rain w_R is given by

$$w_R(h) = R \cdot mR \quad \text{for } 0 \leq h \leq H_{top} \quad [g/m^3] \tag{4.17}$$

mR is an empirical determined constant only usable for rainrates up to 200 mm/h.

$$mR = \begin{cases} 0.1 & \text{for } 0 \leq R \leq 2.5\ mm/h \\ 0.07 & \text{for } 2.5 < R \leq 12.5\ mm/h \\ 0.05 & \text{for } 12.5 < R \leq 110\ mm/h \\ 0.04 & \text{for } 110 < R \leq 200\ mm/h \end{cases} \tag{4.18}$$

location	parameter
Rural environment	$C_1 = 1.87$
Urban environment	$C_1 = 2.41$
Maritime environment	$C_1 = 5.31$
Maritime and strong wind	$C_1 = 5.83$

Table 4.2: Location specific parameter for hydroscopic aerosols.

Now both the integrated water vapor (V) as well as the integrated liquid water content (L) can be calculated by integrating respectivily v and w over the path s through the atmopsphere

$$V = \frac{100}{\rho_w} \int_0^\infty v(s)ds \tag{4.19}$$

$$L = \frac{100}{\rho_w} \int_0^\infty w(s)ds \tag{4.20}$$

with ρ_w the specific weight of water, $10^6 g/m^3$.

4.2.2 Attenuation

According to MPM the attenuation can be calculated from the complex dispersive refractivity $N_t(f)$:

$$N_t(f) = N_0 + N(f) = N_0 + N'(f) - j \cdot N''(f) \tag{4.21}$$

where N_0, the nondispersive part is real and positive and N is a function of the frequency. Refractivity is easily converted into path-specific propagation parameters: The imaginary part of (4.21) leads to power attenuation

$$\alpha = 0.1820 f N''(f) \quad [dB/km] \tag{4.22}$$

and the real part to phase dispersion

$$\beta = 1.2008 f N'(f) \quad [deg/km] \tag{4.23}$$

or group delay

$$\tau = 3.336 N'(f) \quad [ps/km] \tag{4.24}$$

where f is in GHz throughout this report.

Because we are interested in the attenuation part of the complex dispersive refractivity, only the imaginary part will be considered.

This imaginary part is a sum of five contributing terms:

$$N''(f) = N''_L(f) + N''_d(f) + N''_c(f) + N''_w(f) + N''_R(f) \tag{4.25}$$

with

$N''_L(f)$: moist air resonance contributions
$N''_d(f)$: dry air nonresonance spectra
$N''_c(f)$: water vapor continuum spectrum
$N''_w(f)$: suspended water-droplet refactivity
$N''_R(f)$: rain approximation

Moist air resonance contributions $N''_L(f)$

In the considered frequency range from 1 to 1000 GHz, water vapor and oxygen play an important role in the absorption of millimeter waves. In MPM the absorption coefficient for water vapor and oxygen are separately calculated for each layer in the atmosphere. For each layer $N''_L(f)$ is given by a summation of oxygen resonance contributions at 44 frequencies and water vapor contributions at 30 different frequencies.

$$N_L(f) = \sum_{i=1}^{44} S_i F_i(f) + \sum_{k=1}^{30} S_k F_k(f) \tag{4.26}$$

Where S_i is a line strength in kHz; $F(f) = F'(f) - jF''(f)$, a complex shape function in GHz^{-1}.

The Van Vleck-Wiesskopf shape function is used to describe the resonance contributions. Again we are only interested in the imaginary part of F, because that part determines the absorption line spectrum

$$\begin{cases} F''_i(f) = \frac{f}{f_i}\left(\frac{\Delta f_i - \delta_i\cdot(f_i+f)}{(f_i-f)^2+\Delta f_i^2} + \frac{\Delta f_i - \delta_i\cdot(f_i+f)}{(f_i+f)^2+\Delta f_i^2}\right) \\ F''_k(f) = \frac{f}{f_k}\left(\frac{\Delta f_k - \delta_k\cdot(f_k+f)}{(f_k-f)^2+\Delta f_k^2} + \frac{\Delta f_k - \delta_k\cdot(f_k+f)}{(f_k+f)^2+\Delta f_k^2}\right) \end{cases} \tag{4.27}$$

Within this shape function the following line parameters are used:

	Oxygen	**Water vapor**	
Δf	$\Delta f_i = a_3 \cdot \left(p \cdot \theta^{(0.8-a_4)} + 1.1 \cdot e \cdot \theta\right)$	$\Delta f_k = b_3 \cdot \left(p \cdot \theta^{b_4} + b_5 \cdot e \cdot \theta^{b_6}\right)$	(4.28)
δ	$\delta_i = (a_5 + a_6\theta) \cdot 10^{-3} \cdot p \cdot \theta^{0.8}$	$\delta_k = 0$	(4.29)
S	$S_i = a_1 \cdot 10^{-6} \cdot p \cdot \theta^3 \exp\left(a_2(1-\theta)\right)$	$S_k = b_1 \cdot e \cdot \theta^{3.5} \exp\left(b_2(1-\theta)\right)$	(4.30)

$N''_L(f)$ can be calculated using the resonance line frequencies f_i and f_k and the so-called spectroscopic parameters a_{1-6} and b_{1-6}, which can be found in table 1 in [6]. From (4.27) to (4.30) can be seen that the moist air resonance contributions and therefore also the attenuation depends on the inverse temperature $\theta(h)$, the pressure profile $p(h)$ and the partial water vapor pressure $e(h)$.

Nonresonant dry air spectrum $N''_d(f)$

Nonresonant refractivity terms of dry air make a small contribution at groundlevel pressures due to the Debye spectrum of oxygen below 10 GHz and pressure-induced nitrogen absorption that becomes effective above 100 GHz. Calculations of these effects can be found in [6].

Water vapor continuum spectrum $N_c''(f)$

The water vapor continuum contribution $N_c''(f)$ supplements the H_2O line contributions in (4.26).

$$N_c''(f) = f \cdot \left(3.57 \cdot \theta^{7.5} \cdot e + 0.113 \cdot \right) \cdot 10^{-5} \cdot e \cdot \theta^3 \tag{4.31}$$

This continuum spectrum was determined by a series of accurate laboratory experiments in the 140 GHz window range.

The moist air part of $N(f)$ is now completed. Molecular resonance absorption can be recognized in the 60 GHz band, at 119 GHz and higher due to O_2, as well as around 22, 183 GHz, and higher due to H_2O. Across the spectrum one notices more or less transparent window ranges separated by molecular resonance peaks. Relative humidity is a key value to describe the dominating (> 125 GHz) water vapor effects of absorption.

Suspended water droplet refraction $N_w''(f)$

Suspended water droplets in haze, fog, or clouds are efficient millimeter-wave absorbers. Their size range of radii below 50 μm, which allows the Rayleigh approximation of Mie scattering theory to be applied to formulate refractivity contributions $N_w''(f)$ [12]. This refractivity contributions are given by

$$N_w''(f) = \frac{4.5 \cdot w}{\varepsilon''(f) \cdot (1 + \eta^2)} \tag{4.32}$$

where w is the liquid water density profile

$$\eta = \frac{2 + \varepsilon'(f)}{\varepsilon''(f)} \tag{4.33}$$

$\varepsilon''(f)$ is the imaginary part of the permittivity for liquid water

$$\varepsilon''(f) = (\varepsilon_0 - \varepsilon_1) \cdot \frac{f}{f_p} \cdot \frac{1}{\left(1 + \left(\frac{f}{f_p}\right)^2\right)} + (\varepsilon_1 - \varepsilon_2) \cdot \frac{f}{f_s} \cdot \frac{1}{\left(1 + \left(\frac{f}{f_s}\right)^2\right)} \tag{4.34}$$

ε' is the real part of the permittivity for liquid water

$$\varepsilon'(f) = \frac{\varepsilon_0 - \varepsilon_1}{1 + \left(\frac{f}{f_p}\right)^2} + \frac{\varepsilon_1 - \varepsilon_2}{1 + \left(\frac{f}{f_s}\right)^2} + \varepsilon_2 \tag{4.35}$$

$$\varepsilon_0 = 77.666 + 103.3 \cdot (\theta - 1) \tag{4.36}$$

$$\varepsilon_1 = 5.48 \tag{4.37}$$

$$\varepsilon_2 = 3.51 \tag{4.38}$$

$$f_p = 20.09 - 142 \cdot (\theta - 1) + 294 \cdot (\theta - 1)^2 \quad [GHz] \tag{4.39}$$

$$f_s = 590 - 1500 \cdot (\theta - 1) \quad [GHz]. \tag{4.40}$$

Rain approximation $N_R''(f)$

Refractivity of rain, N_R, is governed by absorption and scattering effects. Substantial interactions take place when drop diameters (0.1 to 55 mm) and radio wavelengths become comparable. By-passing elaborate, lengthy Mie calculations that require drop shape and size distributions as well as the dielectric pemittivity of water (4.34) and (4.35), the following approximation is used

$$N_R''(f) \approx C_R R^z \tag{4.41}$$

A regressional fit to individual (C_R, z)-pairs over the frequency range from 1 to 1000 GHz resulted in the calculation scheme

$$C_R = x_1 f^{y1} \qquad z = x_2 f^{y_2} \tag{4.42}$$

f [GHz]	x_1	y_1	f [GHz]	x_2	y_2
1 to 2.9	$3.51 \cdot 10^{-4}$	1.03	1 to 8.5	0.851	0.158
2.9 to 54	$2.31 \cdot 10^{-4}$	1.42	8.5 to 25	1.41	-0.0779
54 to 180	0.225	-0.301	25 to 1664	2.63	-0.272
180 to 1000	18.6	-1.151	164 to 1000	0.616	0.0126

Table 4.3: Rain approximation parameters.

A major concern for all telecommunication systems operating at frequencies above 10 GHz is their performance in rain. The MPM rain model (4.41) provides estimates on propagation effects by such event. Predictions are made by adding to the known state of moist air (P,T,RH) only one additional parameter, namely the point rainfall rate R. Rain exists from the top of the cloud to the ground level, and the rain rate is constant over the complete rain path. Above 10 GHz, rain attenuation rates increase rapidly; actually they can be excessive above 20 GHz for a small fraction of time ($t_R < 0.01$, $R > 50mm/h$).

In equation (4.22) an expression for the absorption coefficient α is given. Integrating over the total number of layers in the atmosphere results in the total attenuation A in dB, which can be written as

$$A_{dB} = \int_0^s \alpha(h')dh' \quad [dB] \tag{4.43}$$

with h' a path through the atmosphere [km].

A quantity that is often used to express the attenuation is the optical thickness or opacity (τ), which is nothing more than A_{Np}:

$$\tau = 0.23025 \cdot A_{dB} \quad [Np] \tag{4.44}$$

The radiometer measures brightness temperatures. Therefore, it is necessary to calculate T_b for the test frequencies from the atmospheric profiles. The following relation between brightness temperature T_b and attenuation will be used:

$$A_{dB} = 10 \cdot \log \frac{T_{eff} - T_{bg}}{T_{eff} - T_b} \quad [dB] \qquad \tau = \ln \frac{T_{eff} - T_{bg}}{T_{eff} - T_b} \quad [Np] \tag{4.45}$$

where T_{eff} is the effective temperature of the atmosphere in Kelvin and T_{bg} is the cosmic background temperature in Kelvin.

The effective temperature T_{eff} is defined as:

$$T_{eff} = \frac{\int_0^\infty T(h)\alpha_{Np}(h)\exp(-\tau_{(0,h)})ds}{1-\exp(-\tau_{(0,h)})} \tag{4.46}$$

Usually an estimated value for T_{eff} is determined, based on climatological parameters, which is used in further calculations.

MPM is a model that is suitable for the determination of attenuation, brightness temperatures, water vapor and liquid water content from atmospheric profiles within the validity ranges as mentioned in table 4.1.

4.3 Matched Atmosphere Algorithm

The Matched Atmosphere Algorithm is based on the 'profile algorithm' developed by Peter and Kämpfer [13]. This algorithm uses the absorption model of Liebe (MPM). Parametric representations of both water vapor and liquid water are adjusted until measured and calculated brightness temperatures do agree, within a tolerated margin. H.J. Hollander described several implementations of the Matched Atmosphere Algorithm. One of these uses linear interpolation to calculate V and L from a beforehand determined look-up table. This implementation was called MALU (Matched Atmosphere look-up) and is the basis for the Matched Atmosphere Algorithm as it is implemented now. Wherever Matched Atmosphere Algorithm is mentioned in the remaining part of this report, the MALU implementation is meant.

The brightness temperatures are calculated with MPM. Therefore the troposphere is divided in horizontal homogeneous layers with a thickness of 100 m. For each layer the absorption coefficient is calculated, using the input parameters of MPM: temperature, relative humidity and pressure. These parameters are derived from a tropospheric model, consisting of vertical profiles (with a altitude resolution of 100 m) of temperature, pressure, relative humidity and droplet concentration and the rain rate. The most accurate results will be obtained by using radiosonde profiles, however, they are only available 3 times a day (during CLARA campaigns). The profile of droplet concentration and the rainrate have already been described in the section discussing MPM, so the profiles for temperature, pressure and relative humidity remain.

The standard temperature profile is produced by first creating a nominal temperature profile from standard U.S. Standard Atmosphere Supplements (1966). In order to match the groundlevel temperature, an exponential fit of the nominal profile to the surface value is used:

$$T(h) = T_{nom}(h) + [T_s - T_{nom}(0)]\exp(-h/H) \quad [K] \tag{4.47}$$

where

T_s = measured surface temperature in Kelvin
H = scale height, 3 km

The pressure profile is not critical and can be approximated by a standard exponential profile, matched to the pressure at ground level. The pressure up to 10 km is determined by the ITU-R standard conditions:

$$P(h) = P_0\left(\frac{T_0}{T_0 - 6.5h}\right)^{\frac{34.163h}{-6.5}} \quad [kPa] \tag{4.48}$$

where

h = height [km]
P_0 = standard pressure of 101.325 kPa
T_0 = standard ground temperature of 288.15 K

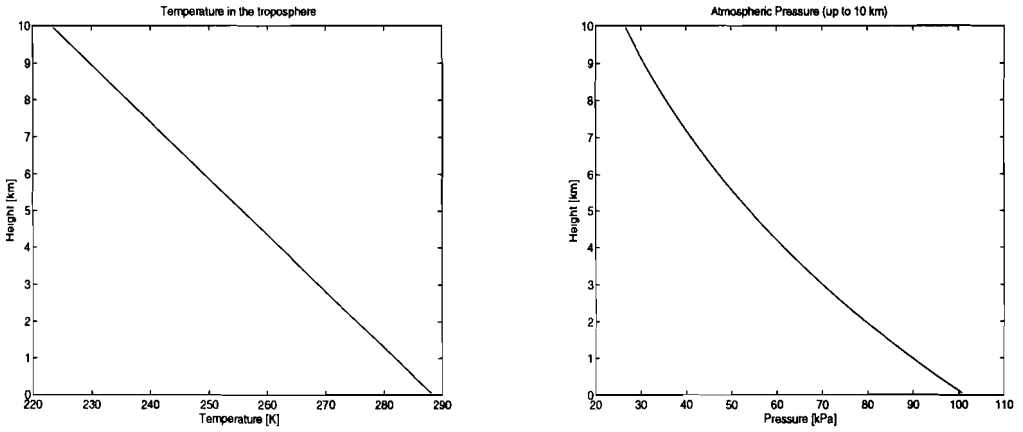

Figure 4.2: Temperature and Pressure Profiles: (a) Temperature Profile ; (b) Pressure Profile.

Temperature and pressure profiles are completely determined by their ground data.

For the relative humidity Peter and Kämpfer developed a piecewise linear profile. For the creation of a relative humidity profile, information with regard to ground data, cloud base, cloud top and reference relative humidity is necessary.

In a cloud layer the relative humidity will be 100% and at ground level $RH(0)$ will be the measured relative humidity. At 10 km altitude, where very little water vapor is present the relative humidity is set to 0%. The thickness of a cloud layer is specified by two parameters, H_{base}, the base height of the cloud and H_{top}, the height of the top of the cloud. When no cloud is around, $H_{top} = H_{base}$. Furthermore, a tuning parameter for water vapor RH_{ref} is introduced in such a manner, that the relative humidity in the altitude range from 1.5 km above observing site to H_{base} and from H_{top} of the assumed cloud level to 1.5 km above H_{top} of the cloud is equal to RH_{ref}. from ground level to 1.5 km above ground level as well as from 1.5 km above H_{top} to 10 km the relative humidity is found by linear interpolation.

In formula this becomes

$$RH(h) = \begin{cases} RH(0) + \frac{RH_{ref} - RH(0)}{1.5} \cdot h & \text{for } 0 \leq h \leq 1.5 \\ RH_{ref} & \text{for } 1.5 \leq h < H_{base} \\ 100 & \text{for } H_{base} \leq h < H_{top} \\ RH_{ref} & \text{for } H_{top} \leq h < H_{top} + 1.5 \\ -\frac{RH_{ref}}{10-(H_{top}+1.5)} \cdot h + \frac{10RH_{ref}}{10-(H_{top}+1.5)} & \text{for } H_{top} + 1.5 \leq h \leq 10 \end{cases} \quad [\%] \tag{4.49}$$

with h in km.

The choice of the altitude range where $RH(h)$ is equal to the tuning parameter RH_{ref} is not critical for V and L retrieval and is therefore done intuitively. Moreover, it is evident

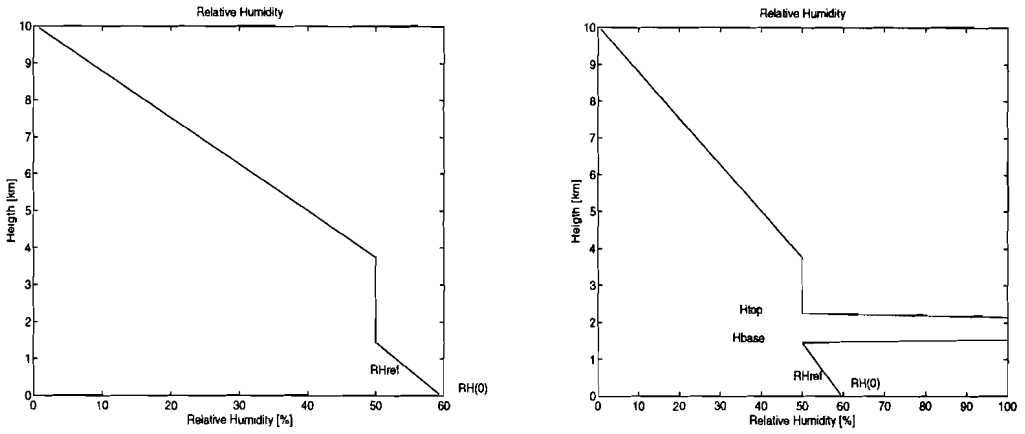

Figure 4.3: Relative Humidity Profiles: (a) Profile for situation without a cloud; (b) Profile for situation with a cloud.

that meteorological phenomena near the surface as low-level clouds, fog, or inversion layers cannot be adequately described by such a parameterization.

The RH–profile is converted into a water vapor density from which the water vapor is calculated by equation (4.13) as empirically found by Liebe.

In contrast to the temperature and pressure profile, both relative humidity and droplet concentration profiles are tunable using the tuning parameters RH_{ref}, H_{base}, H_{top} and C. The original objective was to use two of these variables as tuning parameters, so that both T_{20} and T_{30} can be matched.

H_{base} and C are used for the characterisation of the cloud. H_{base} and H_{top} specify the cloud thickness, whereas C is a parameter for the fine tuning of the total liquid water content. The parameter RH_{ref} tunes the amount of water vapor, and H_{base} tunes both water vapor and liquid water.

In [7] H.J. Hollander showed that both RH_{ref} and H_{base} are more important for the retrieval of V and L, than C. Therefore C is set to a fixed value of 0.4, that is the middle of the range from 0.1 to 0.75 in which it may vary. RH_{ref} and H_{base} are used as tuning parameters.

Peter and Kämpfer suggested to set H_{top}, the top of the cloud, to the level where the droplets begin to freeze. Above this level no water vapor or liquid water exists. The ice crystals that are present do not contribute significantly in the frequency region we consider. For simplicity Peter and Kämpfer took the height where the temperature is $0°C$ as H_{top}, although the temperature at which ice crystals start growing varies from $-3°C$ to $-10°C$. H_{top} therefore can be determined from the temperature profile, and is therefore related to the temperature at ground level. In order to prevent unrealistic low cloud top heights to occur, a minimum value for H_{top} is set to 2 km. There are now two tuning parameters left, H_{base} and RH_{ref}.

For each combination of ground level temperature, pressure and relative humidity all possible atmospheres can be constructed by varying RH_{ref} and H_{base} over their full range.

For RH_{ref} this range is from 0% till 100% in steps of 10% , for H_{base} this is from 100m above groundlevel to H_{top} in steps of 100m. From all atmospheres constructed this way, the brightness temperatures at 21.3 GHz and 31.7 GHz can be calculated using Liebe's MPM. Also the corresponding V and L values can be calculated. By storing the T_{20}, T_{30} together with the V and L values the look–up tables are obtained. These look–up tables contain all combinations of T_{20} and T_{30} that, according to the atmosphere model, can be realized with the particular ground level values of T, P, and RH; the so-called convergence area.

The amount of water vapor and liquid water are a function of the brightness temperatures defined with the convergence area as domain. In the implementation of Hollander the indices for the matrix elements are the brightness temperatures T_{20} and T_{30}. Thus when both T_{20},T_{30} are varied from 1 to 100 K with a step size of 1K, a $100x100$–matrix called interpolation set is generated. The matrix elements $V(T_{20}, T_{30})$ and $L(T_{20}, T_{30})$ are calculated from the look up tables using linear interpolation when inside the convergence area and linear extrapolation when outside the convergence area. When MALU is used to calculate the integrated water vapor and liquid water with the measured brightness temperatures, this is done by choosing the right interpolation set, corresponding to the actual ground level meteorological values, and determining V and L from this set by bi-linear interpolation (Figure 4.4).

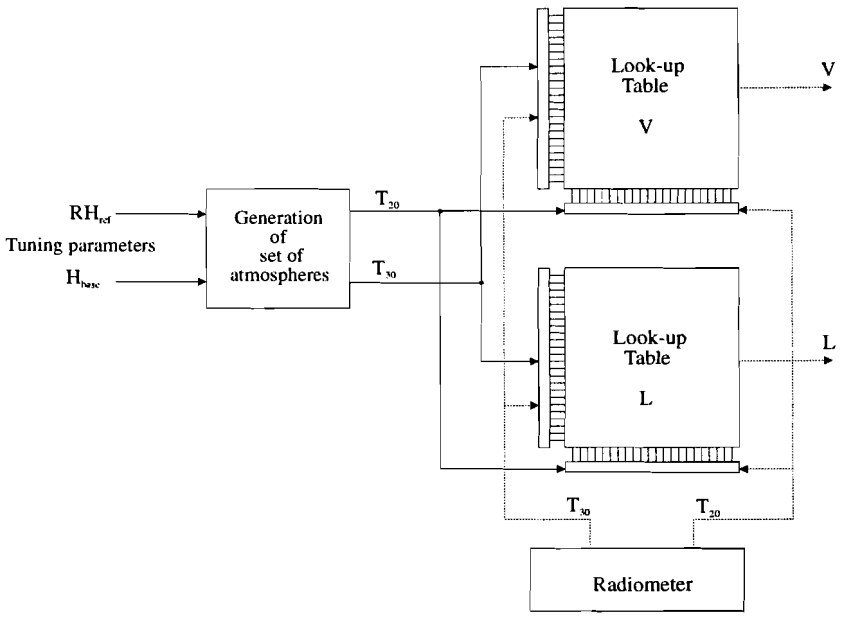

Figure 4.4: Malu algorithm in functional blocks.

The solid lines represent the creation of the look–up tables, while the dotted lines represent the retrieval of the V and L value from a measured T_{20},T_{30} combination.

This implementation suggested by Hollander, however, leads to practical problems, like lack of calculation speed and disc space. In his graduation work P. Trommelen [14] introduced some methods to solve both problems:

- For each fixed value of H_{base}, both T_{20}, T_{30} as well as V increase linear with RH_{ref}. This means that the brightness temperatures and water vapor valuesa only have to be calculated for the points in the look–up table that correspond to $RH_{ref} = 0\%$ in combination with all values of H_{base} and $RH_{ref} = 100\%$ in combination with all valuesa

of H_{base}. All intermediate points can be found by linear interpolation, which can be carried out considerably faster than calculating each individual point in the look-up table using MPM.

- The amount of liquid water does not depend on the tuning parameter RH_{ref}, but only on the thickness of the cloud, and thus H_{base}. Therefore also for the amount of liquid water values only have to be calculated for the points in the look-up table that correspond to $RH_{ref} = 0\%$ in combination with all values of H_{base} and $RH_{ref} = 100\%$ in combination with all values of H_{base}, and the intermediate points can be found by means of linear interpolation.

- The calculation of the interpolation set becomes superfluous when for the measured brightness temperature combinations the corresponding V and L values are directly calculated from the look-up tables. This is done with a special interpolation procedure. The V and L values are calculated from the three nearest points in the look-up table, which are not on a straight line, by linear interpolation in two dimensions. Outside the convergence area this procedure is used for extrapolation.

- Besides the brightness temperatures, V and L also the corresponding values for RH_{ref}, H_{base} and H_{top} are stored, which makes it possible to reconstruct a Modelled atmosphere that resulted in these values.

- In the real implementation of the Matched Atmosphere Algorithm the convergence area is defined by the area in-between the 4 corner points which correspond to the following RH_{ref}, H_{base} combinations: $(RH_{ref} = 0\%, H_{base} = 0.1)$, $(RH_{ref} = 0\%, H_{base} = H_{top})$, $(RH_{ref} = 100\%, H_{base} = h_{top})$, and $(RH_{ref} = 100\%, H_{base} = 0.1km)$.

In chapter 6 some refinements of the implementation of MPM and the Matched Atmosphere Algorithm are presented.

Chapter 5

Possible Causes of Negative L–Values: RESCOM Radiometer

5.1 Introduction

During the three CLARA measurement campaigns in 1996, the RESCOM radiometer was used for the measurement of the brightness temperatures at 21.3, 23.8, 31.7, 51.25, 53.85 and 54.85 GHz. The brightness at 21.3 (T_{20}) and 31.7 GHz (T_{30}) are used in MALU to determine both the integrated precipitable water vapor (V) and integrated liquid water (L).

While Analysing these data, a strange phenomenon has been noticed. During periods with clear sky conditions, that is without any clouds, the integrated liquid water L, retrieved from T_{20} and T_{30}, appeared to be negative. This is, however, physically impossible. Physically an atmosphere can be only in one of two possible states: The atmosphere contains no amount of liquid water, or the atmosphere contains an amount of liquid water (this amount is positive). An accompanying effect of this negative L–value is, that the matched atmosphere algorithm increases the value of V above its real value, in order to compensate for the negative L–value and to find a match, for a given T_{20}, T_{30} combination.

There are various possible causes for the occurrence of negative L–values during clear sky periods.

According to the specifications of the RESCOM Radiometer, all channels have an overall accuracy of $\pm$ 1 K. This means that the real brightness temperature may differ $\pm$ 1 K from the measured brightness temperature. This difference might cause the negative L–values.

Another possible cause is the Matched Atmosphere Algorithm itself. The Malu implementation of the Matched Atmosphere Algorithm uses an interpolation and extrapolation technique for the retrieval of both vapor and liquid. In cases of clear sky periods the measured brightness temperatures are located outside the convergence area, so extrapolation is necessary. This extrapolation procedure however might not be accurate enough.

In this chapter is investigated whether the negative L–values can be explained by variations of the brightness temperatures T_{20} and T_{30} within the range of the accuracy.

A new procedure for extrapolation will be discussed in chapter 6.

5.2 Analysis Methods

5.2.1 Relationship between T_{20}, T_{30}, V and L

The relationship between T_{20}, T_{30}, V and L is given by the matched atmosphere algorithm. This algorithm is rather complex, but there are some basic properties.

- T_{20} and T_{30} both have influence on V and L.
- V is more sensitive for T_{20} variations than for T_{30} variations.
- L is more sensitive for T_{30} variations than for T_{20} variations.
- When T_{20} is increased, V will increase and L will decrease.
- When T_{30} is increased, L will decrease and V will decrease.

These properties will be used for the elimination of the negative values of L. Together with the elimination of negative L–values the V–values will be reduced. This can be done by changing both T_{20} and T_{30}. Increasing T_{20} and increasing T_{30} is the quickest method to eliminate negative L–values. Furthermore, an decreasement of T_{20} results in a decreasement of the V–values.

5.2.2 Calibration and Accuracy of the RESCOM radiometer

Calibration of the radiometer is performed by RESCOM prior to delivery of the equipment. This basic calibration is to adjust the level of the noise pulses to be injected via the coupler into the input waveguide of the receiver front end at the two measurement frequencies. For this calibration high-precision cryogenic loads are used.

On-site calibration is done by tip-curve calibration, as described in Chapter 2. When this tip-curve calibration has been carried out, the specification of the RESCOM radiometer guarantee an absolute accuracy in the 10—150 K range of 1 K.

In his graduation report Peter Trommelen [14] showed that an increasement of T_{30} by 1 K and a simultaneous decreasement of T_{20} by 1 K, does not eliminate negative L–values. This means that the negative L values Cannot be explained by the accuracy of the RESCOM radiometer. His analysis however showed that the only possibility to eliminate negative L–values is to increase T_{30} and decrease T_{20}.

5.2.3 Strategy

For each measurement campaign the worst case situation will be used. When the problem is solved for the worst case it is also solved for all other situations. In order to find the worst case situation, for each day within a campaign, the minimum of the L–values is calculated. The day with the lowest minimum (which means the most negative L–value) is the worst case situation in a campaign period. Only the first and the second CLARA campaigns have been analysed, because the received groundlevel data of the third campaign is not complete yet. The worst case situation in the first campaign occurred on April 22, 1996. The worst case situation in the second campaign occurred on August 22, 1996. These days will be used in the analysis.

Two methods for the calculation of the amounts by which T_{20} and T_{30} have changed, in order to obtain only positive L–values, will be used. In both cases T_{20} will be decreased, while T_{30} will be increased. As we saw in chapter 2 correction with a tip–curve calibration is not a translation but a rotation. This means that the correction for points near the rotation point is less than the correction for points further away from the rotation point. Because we are dealing, in case of clear sky periods, with low brightness temperatures far away from the rotation point, in that range we may assume that this correction is almost a translation instead of a rotation. Therefore the amounts by which T_{20} and T_{30} are changed in both methods will be independent of the brightness temperatures themselves.

Simultaneous Variation

In the first method the amount by which T_{20} is decreased, Δ, is the same as the amount by which T_{30} is increased. With a given stepsize Δ will be increased.

$$\begin{cases} T_{20,new} = T_{20,measured} - \Delta \\ T_{30,new} = T_{30,measured} + \Delta \end{cases} \tag{5.1}$$

It is possible to make an initial guess for the amount by which both brightness temperatures are changed. This procedure will continue until the minimum of the L–values becomes positive. Then the procedure is stopped.

Independent Variation

In this method two parameters are running, the first, Δ_{20}, is the amount by which T_{20} is decreased. This Δ_{20} varies in a given range with a given stepsize. The second parameter, Δ_{30} is the amount by which T_{30} is increased. This parameter varies in the same range as Δ_{20} with the same stepsize.

$$\begin{cases} T_{20,new} = T_{20,measured} - \Delta_{20} \\ T_{30,new} = T_{30,measured} + \Delta_{30} \end{cases} \tag{5.2}$$

In contrary to the first method all combinations of Δ_{20} and Δ_{30} within the given range are possible. For all the combinations of Δ_{20} and Δ_{30} the minimum of L is calculated. The combination of the lowest Δ_{20} and Δ_{30} that results in a positive minimum for L, is the combination we are looking for.

5.3 Results

5.3.1 Simultaneous Variation

During his graduation work Peter Trommelen [14] showed that an increasement of T_{30} by 1 K and a simultaneous decreasement of T_{20} by 1 K was not enough to eliminate negative L–values. This situation will be used as an initial guess. The procedure is repeated for various stepsizes (table 5.1).

Table 5.1 shows that T_{20} should be de creased with an amount between 2.2 K and 2.3 K, in order to make the minimum of L exactly zero in the worst case situation during the first CLARA campaign. T_{30} should be increased with the same value. When T_{20} is decreased

Campaign	Stepsize [K]	Initial Guess [K]	Δ	min(L) [cm]
First CLARA Campaign 960422	1	1.0	2.0	-8.3854E-4
			3.0	+0.0028
	0.5	2.0	2.0	-8.3854E-4
			2.5	+0.0010
	0.1	2.0	2.2	-1.1096E-4
			2.3	+2.4717E-4
Second CLARA Campaign 960822	1	3.0	3.0	-0.0012
			4.0	+0.0023
	0.1	3.0	3.3	-1.6448E-4
			3.4	+1.9243E-4

Table 5.1: Results of the elimination with simultaneous variation.

with 2.3 K and T_{30} is increased with 2.3 K, the minimum value of L retrieved during the first CLARA campaign will $+2.4717 \cdot 10^{-4}$ cm.

For the second CLARA campaign T_{20} should be decreased somewhere between 3.3 K and 3.4 K, while T_{30} should be decreased with the same amount to make the minimum of L exactly zero in the worst case situation. When T_{20} is decreased with 3.4 K and T_{30} is increased with 3.4 K then the resulting minimum retrieved L–value will be $+1.9243 \cdot 10^{-4}$ cm.

5.3.2 Independent Variation

For the first campaign the parameters Δ_{20} and Δ_{30} varied from 2.0 K to 2.3 K with a stepsize of 0.1 K. This means that 16 iterations, inwhich a complete day is analysed, were carried out. Each iteration takes about 15 minutes calculation time on a Pentium 166 MHz with 16 Mb internal RAM. This means that the analysis took up 4 hours.

During these iterations the following minimum values for L have been found (table 5.2).

The best combination of Δ_{20} and Δ_{30}, is the combination with the lowest values for Δ_{20} and Δ_{30}, for which min(L) is positive (table 5.2). This combination is $\Delta_{20} = 2.1\ K$ and $\Delta_{30} = 2.3\ K$. The minimum of L then becomes $4.2327 \cdot 10^{-5}$ cm.

For the second CLARA campaign Δ_{20} and Δ_{30} were varied from 3.1 K to 3.5 K with a stepsize of 0.1 K. That will be 36 iterations, taking about 9 hours calculation time on the same Pentium 166 MHz with 16 Mb RAM. The following results have been found (table 5.3).

Table 5.3 showes that in order to eliminate negative L–values, T_{20} should be decreased with 3.1 K, and T_{30} should be increased by 3.5 K. The minimum retrieved L-value then becomes $1.5511863 \cdot 10^{-4}$. There is another combination of Δ_{20} and Δ_{30} for which L is positive and lesser than $1.5511863 \cdot 10^{-4}$, but that results in a higher Δ_{20}, Δ_{30}.

Δ_{20}	Δ_{30}	min(L)
2.0	2.0	-8.3854398e-004
2.0	2.1	-5.8944545e-004
2.0	2.2	-3.2476970e-004
2.0	2.3	-6.0093953e-005
2.1	2.0	-7.3640584e-004
2.1	2.1	-4.7450093e-004
2.1	2.2	-2.2234919e-004
2.1	2.3	4.2326564e-005
2.2	2.0	-6.3426769e-004
2.2	2.1	-3.7236278e-004
2.2	2.2	-1.1045788e-004
2.2	2.3	1.4474708e-004
2.3	2.0	-5.3212955e-004
2.3	2.1	-2.7022464e-004
2.3	2.2	-8.3197327e-006
2.3	2.3	2.4716760e-004

Table 5.2: Results of the elimination with independent variation for the first CLARA campaign.

5.3.3 New Retrievals

With both strategies new V– and L–values have been retrieved. The result of the vapor retrieval for the worst case situation of the first CLARA measurement campaign is showed in figure 5.1 We see that the V retrieval is decreased for both independent and simultaneous elimination of negative L–values. There is also less difference between the retrieval with the two strategies. Furthermore, the vapor values retrieved from the corrected brightness temperatures of the radiometer are located closer to the vapor values retrieved with the radiosondes.

Figure 5.2 shows that both strategies indeed eliminate negative L–values. Again there is less difference between simultaneous and independent elimination.

For the second CLARA measurement the following retrievals are found:

The vapor values again are decreased after using both strategies (figure 5.3). Only for one radiosonde retrieval (12 hours UTC) the new vapor retrieval by the radiometer is better. For the other (18 hours UTC) it is worse.

Figure 5.4 shows that both strategies indeed eliminate negative L–values. Again there is less difference between simultaneous and independent elimination.

Δ_{20}	Δ_{30}	$\min(L)$
3.1	3.1	-8.7829778e-004
3.1	3.2	-6.1994367e-004
3.1	3.3	-3.6158957e-004
3.1	3.4	-1.0323547e-004
3.1	3.5	1.5511863e-004
3.2	3.1	-7.7974337e-004
3.2	3.2	-5.2138927e-004
3.2	3.3	-2.6303517e-004
3.2	3.4	-4.6810696e-006
3.2	3.5	2.5367303e-004
3.3	3.1	-6.8118897e-004
3.3	3.2	-4.2283487e-004
3.3	3.3	-1.6448077e-004
3.3	3.4	9.3873334e-005
3.3	3.5	3.5222743e-004
3.4	3.1	-5.8263457e-004
3.4	3.2	-3.2428046e-004
3.4	3.3	-6.5926364e-005
3.4	3.4	1.9242774e-004
3.4	3.5	4.5078184e-004
3.5	3.1	-4.8408016e-004
3.5	3.2	-2.2572606e-004
3.5	3.3	3.2628039e-005
3.5	3.4	2.9098214e-004
3.5	3.5	5.4933624e-004

Table 5.3: Results of the elimination with independent variation for the first CLARA campaign.

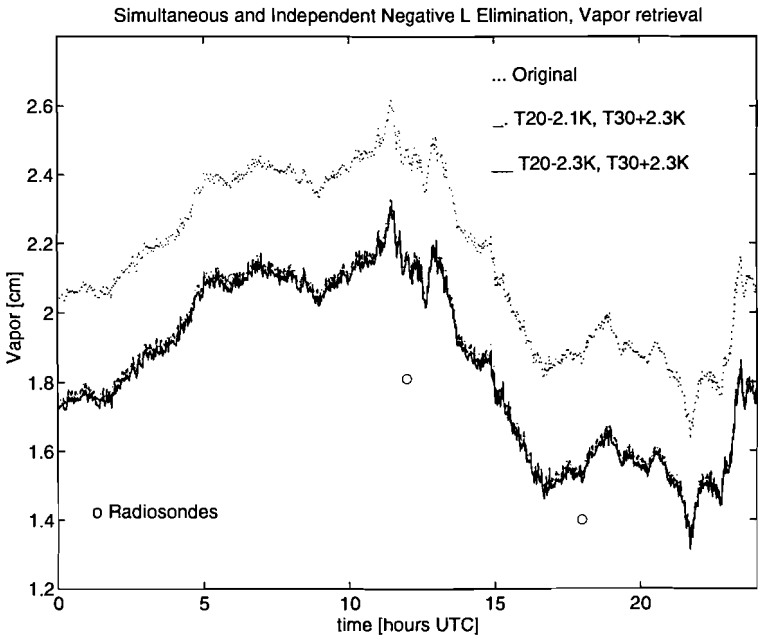

Figure 5.1: Vapor retrieval for simultaneous and independent negative L–value elimination. $\cdots$ = original retrieved vapor, -. = retrieval with independent elimination, – = retrieval with simultaneous elimination; o = radiosonde retrieval.

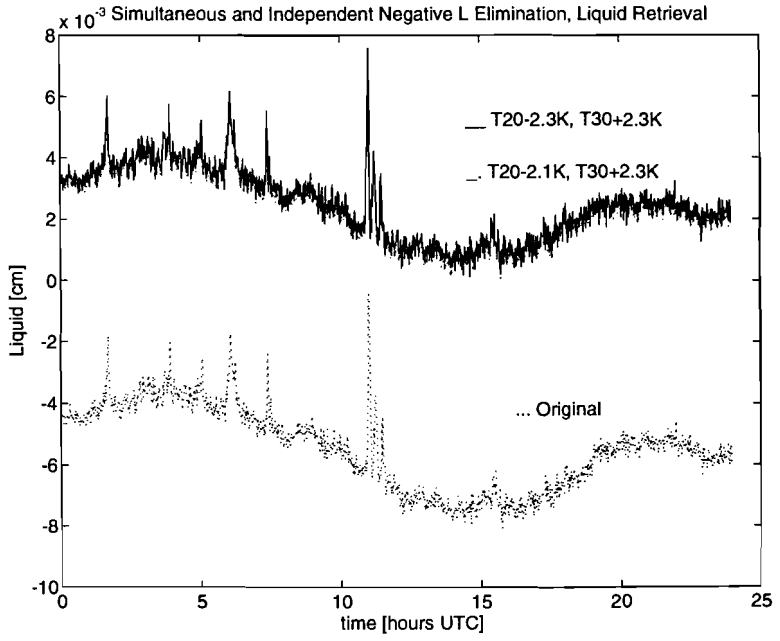

Figure 5.2: Liquid retrieval for simultaneous and independent negative L–value elimination. $\cdots$ = original retrieved vapor, -. = retrieval with independent elimination, – = retrieval with simultaneous elimination; o = radiosonde retrieval.

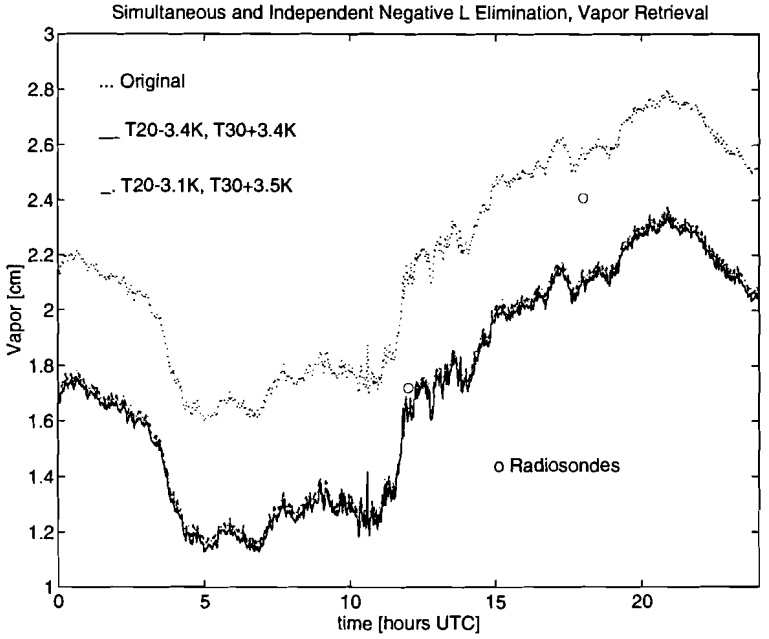

Figure 5.3: Vapor retrieval for simultaneous and independent negative L–value elimination. $\cdots$ = original retrieved vapor, -. = retrieval with independent elimination, – = retrieval with simultaneous elimination; o = radiosonde retrieval.

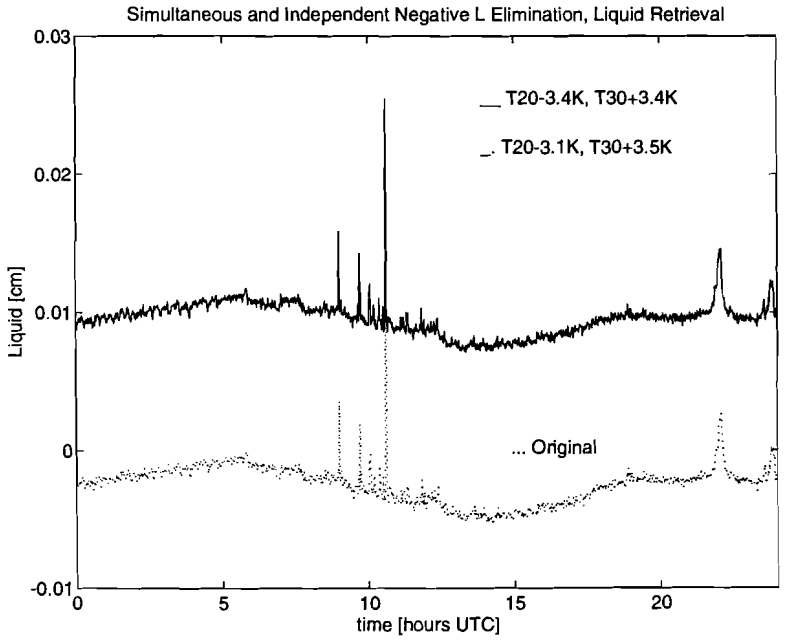

Figure 5.4: Liquid retrieval for simultaneous and independent negative L–value elimination. $\cdots$ = original retrieved vapor, -. = retrieval with independent elimination, – = retrieval with simultaneous elimination.

5.4 Conclusions and Recommendations

5.4.1 Conclusions

- With both strategies the negative liquid values are eliminated.
- The amounts by which T_{20} and T_{30} have to be changed are larger than the accuracy of ± 1 K, as specified in the manual of the RESCOM radiometer. This means that the occurence of negative L–values cannot solely be explained by the accuracy of the RESCOM radiometer.
- The amounts by which T_{20} and T_{30} have to be corrected in order to eliminate negative liquid values, are different for the two CLARA periods. This difference is almost 1 K.
- Although both strategies result in other combinations by which T_{20} and T_{30} have to be corrected in order to retrieve only positive liquid values, there is less difference between the two strategies in the retrieval of both vapor and liquid.
- The retrieval of vapor after the correction of T_{20} and T_{30} corresponds better with the vapor retrieval obtained from radiosonde measurements.

5.4.2 Recommendations

- The tip–curve procedure is very well suited for the detection of changes in the calibration of the RESCOM radiometer. Regular tip–curve calibrations, without changing the factor L_h can give an indication of fluctuations in the calibration.
- The effect of radiation picked up by the sidelobes of the antenna of the radiometer, generated by elements in the neighbourhood of the radiometer, could easily be detected by a simple test. Carry out a tip–curve calibration. Then repeat that tip–curve calibration after the neigbourhood of the radiometer has been covered with metal plates. If this results in a real different tip–curve calibration, the radiation picked up from the environment is not neglectable.
- Tip–curve calibrations should be carried out during clear sky periods. When after such a tip–curve control also normal measurements, also under clear sky conditions, are carried out, together with measurements of groundlevel conditions, then negative L–values should be retrieved. Calculations of the amounts by with T_{20} and T_{30} have to be changed in order to retrieve only positive L–values, could give information of reason why there is a variation in these amounts. An annual variation should not be excluded, because weather changes with an annual variation, specified by the seasons.

Chapter 6

Extensions and Refinements in MPM and Matched Atmosphere Algorithm

6.1 Introduction of Rain Attenuation in MPM

In the original implementation [7] rain attenuation was included as a part of the liquid water content w. The attenuation is included in the liquid water density profile using the following relation:

$$w_R(h) = R \cdot mR \quad \text{for } 0 \leq h \leq H_{top} \quad [g/m^3] \tag{6.1}$$

mR is an empirical determined constant only valuable for rainrates up to 200 mm/h.

$$mR = \begin{cases} 0.1 & \text{for } 0 \leq R \leq 2.5\ mm/h \\ 0.07 & \text{for } 2.5 < R \leq 12.5\ mm/h \\ 0.05 & \text{for } 12.5 < R \leq 110\ mm/h \\ 0.04 & \text{for } 110 < R \leq 200\ mm/h \end{cases} \tag{6.2}$$

This is, however, not the correct contribution of rain in the total attenuation. As we saw in Figure 3.4 the attenuation contribution due to rain could be very dominant depending on the rain rate and frequency. This effect cannot only be explained with the contribution of rain in the liquid water density. In section 4.2 we saw that another contribution of rain attenuation, rain approximation $N''_R(f)$, is described in MPM. This contribution however was not yet implemented in the MPM version of H.J. Hollander.The following approximation was used:

$$N''_R(f) \approx C_R R^z \tag{6.3}$$

A regressional fit to individual (C_R, z)-pairs over the frequency range from 1 to 1000 GHz resulted in the calculation scheme

$$C_R = x_1 f^{y1} \qquad z = x_2 f^{y2} \tag{6.4}$$

f [GHz]	x_1	y_1	f [GHz]	x_2	y_2
1 to 2.9	$3.51 \cdot 10^{-4}$	1.03	1 to 8.5	0.851	0.158
2.9 to 54	$2.31 \cdot 10^{-4}$	1.42	8.5 to 25	1.41	-0.0779
54 to 180	0.225	-0.301	25 to 1664	2.63	-0.272
180 to 1000	18.6	-1.151	164 to 1000	0.616	0.0126

Table 6.1: Rain approximation parameters.

The contribution of rain is also represented as a profile, although the rain attenuation remains constant over the total rain path, with the same resolution as the other profiles, where rain is defined from the top of the cloud to the ground. Above H_{top} this profile is zero. For this representation has been chosen, because this simplifies the inclusion of the rain attenuation in the MATLAB version of MPM, where all input parameters are given as a profile. The summation over all layers of the rain profile results in the total rain attenuation.

This attenuation contribution now has been implemented in an updated MPM program. The source code of the new MPM procedure in MATLAB language can be found in appendix B.

6.2 Possible Causes of negative L–values: Extrapolation Improvements

6.2.1 Introduction

In chapter 4 we saw that Malu, a version of the Matched Atmosphere Algorithm, using look-up tables for the retrieval of both liquid and vapor was introduced. For a given T_{20}, T_{30} combination the V and L values are calculated by interpolation (inside the convergence area) and extrapolation (outside the convergence area), using the three nearest points in the convergence area.

Chapter 5 showed that there are two possible causes for the retrieval of negative L–values. The first one, the accuracy of the RESCOM radiometer was dealt with in that chapter. We saw that it was not possible to explain the negative L–values by variations of the measured T_{20} and T_{30} within their accuracy range.

The other possible cause is the Matched Atmosphere Algorithm itself (the Malu implementation). The problems with negative L–values arise during clear sky periods. The T_{20}, T_{30} combinations corresponding with these periods are all located outside the convergence area (below the convergence area), which implies that in order to remove the negative L–values, the extrapolation procedure should be improved. In this section two extrapolation methods will be discussed.

6.2.2 The Original Method using the Three Nearest Points

The original method for interpolation and extrapolation uses the three nearest points of the convergence area for the determination of the V and L values. When these three points are not located on a straight line, a plane can be determined with these three points. This is done both in the V and L look-up tables. This plane makes a certain angle with the ground

plane. The V and L values corresponding with the measured T_{20} and T_{30} combination are calculated with the expression found for the plane.

If these three points are located on a straight line, one of these points is eliminated (making the distance to the measured point infinite) and the next closest point is detected and used. This procedure will be repeated untill not all three points are located on a straight line.

For measurement points inside the convergence area this causes no problems, because the three nearest points will never lie on a straight line and a plane can be found with these three points.

For measurement points outside the convergence area the detection of the three nearest points, not located on a straight line, is the main problem. In his implementation of Malu P. Trommelen describes the convergence area with four corner points and the borders with straight lines between those corner points. The three nearest points of a measurement point located outside the convergence area are three points on the border of the convergence area. These points are located on a straight line, so one new point has to be found. This point automatically lies inside the convergence area. The other two points still lie on the border of the convergence area. The L value of this point is higher than those of the points on the border, because the L values increase inside the convergence area. This results in an increasement of the angle the plane makes with the ground plane. Whenever the measurement point lies farther away from the border of the convergence area, this will result in a lower L-value, eventually becoming negative. Figure 6.1 shows this effect, with a view perpendicular to the lowest border of the convergence area.

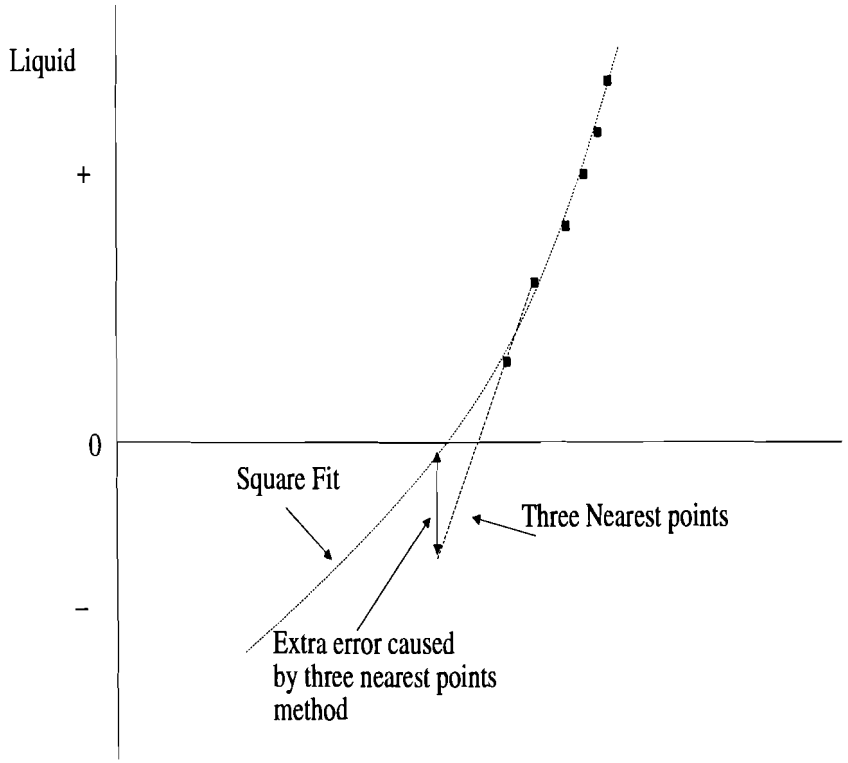

Figure 6.1: Extrapolation error of the three nearest points method, with a view perpendicular to lowest border of the convergence area.

6.2.3 Strategy

Because the problems are located in and around the lower part of the convergence area, it is useful to deal with this part in another way. The convergence area is divided into two parts. The first part is the part containing thin clouds, which means the lower part of the convergence area. The other part is the part for thick clouds. Thin clouds are clouds with a maximum thickness of 500 m. For the part with thin clouds, new extrapolation procedures are used, based on a reduced look-up table for thin clouds. These procedures will be compared with the original three nearest points method.

In many articles about the retrieval of water vapor and liquid water in the atmosphere, linear retrieval algorithms are used. Therefore, a linear fit is made on the values of the reduced look-up tables of V and L. We will go one step further in the accuracy and will also calculate a square fit on the values of the look-up tables.

How these fits are calculated, will be described in the next subsection.

6.2.4 Extrapolation Tools

With a given groundlevel configuration, Malu generates the look-up tables specifying the convergence area for both V and L. From these look-up tables the reduced look-up tables are calculated. The new extrapolation methods are based on the least squares method of Gauss. With this method the best linear fits in two dimensions and the best square fits in two dimensions are determined. In contrast of chapter 3 now the representation with vector spaces [15] will be used.

Two-dimensional Linear Fit

The basic function for a two-dimensional linear fit (with standard variables x, y and z) is

$$z = ax + by + c \tag{6.5}$$

Our goal is to determine a, b, c so that

$$\sum_{i=1}^{n} (z - ax - by - c)^2 \tag{6.6}$$

is minimized.

When the convergence area is built with n points, we can interpret this in $\mathbb{R}^n$ as

$$\left|\underline{z} - a\underline{x} - b\underline{y} - c\underline{e}\right| \tag{6.7}$$

with

$$\begin{aligned} \underline{x} &= (x_1, x_2, \ldots, x_n) \\ \underline{y} &= (y_1, y_2, \ldots, y_n) \\ \underline{z} &= (z_1, z_2, \ldots, z_n) \\ \underline{e} &= (1, 1, \ldots, 1) \quad \text{also length } n \end{aligned}$$

Minimizing equation 6.7 means

$$\underline{z} - a\underline{x} - b\underline{y} - c\underline{e} \in \langle \underline{x}, \underline{y}, \underline{e} \rangle^{\perp} \tag{6.8}$$

or

$$\underline{z} - a\underline{x} - b\underline{y} - c\underline{e} \perp \underline{x} \tag{6.9}$$
$$\underline{z} - a\underline{x} - b\underline{y} - c\underline{e} \perp \underline{y} \tag{6.10}$$
$$\underline{z} - a\underline{x} - b\underline{y} - c\underline{e} \perp \underline{e} \tag{6.11}$$
$$\tag{6.12}$$

This results in a system of linear equations,

$$\begin{array}{llll} (\underline{x},\underline{x}) \cdot a & +(\underline{x},\underline{y}) \cdot b & +(\underline{x},\underline{e}) \cdot c & = (\underline{x},\underline{z}) \\ (\underline{y},\underline{x}) \cdot a & +(\underline{y},\underline{y}) \cdot b & +(\underline{y},\underline{e}) \cdot c & = (\underline{y},\underline{z}) \\ (\underline{e},\underline{x}) \cdot a & +(\underline{e},\underline{y}) \cdot b & +(\underline{e},\underline{e}) \cdot c & = (\underline{e},\underline{z}) \end{array}$$

where $(\underline{x}, \underline{y})$ etc. are inner products. This system of linear equations can be written in a matrix structure

$$\begin{pmatrix} (\underline{x},\underline{x}) & (\underline{x},\underline{y}) & (\underline{x},\underline{e}) \\ (\underline{y},\underline{x}) & (\underline{y},\underline{y}) & (\underline{y},\underline{e}) \\ (\underline{e},\underline{x}) & (\underline{e},\underline{y}) & (\underline{e},\underline{e}) \end{pmatrix} \cdot \begin{pmatrix} a \\ b \\ c \end{pmatrix} = \begin{pmatrix} (\underline{x},\underline{z}) \\ (\underline{y},\underline{z}) \\ (\underline{e},\underline{z}) \end{pmatrix} \tag{6.13}$$

This results in exactly one solution for a, b, c, and thus exactly one linear fit in two dimensions.

Two-dimensional Square Fit

The basic function for a two-dimensional square fit (with standard variables x, y and z) is

$$z = ax^2 + bx + cxy + dy + fy^2 + g \tag{6.14}$$

Our goal is to determine a, b, c, d, f, g, so that

$$\sum_{i=1}^{n} \left(z - ax^2 - bx - cxy - dy - fy^2 - g\right)^2 \tag{6.15}$$

is minimized.

When the convergence area is built with n points,we can interpret this in $\mathbb{R}^n$ as

$$\left|\underline{z} - a\underline{x}^2 - b\underline{x} - c\underline{xy} - d\underline{y} - f\underline{y}^2 - g\underline{e}\right| \tag{6.16}$$

with

$$\begin{array}{rcl} \underline{x} & = & (x_1, x_2, \ldots, x_n) \\ \underline{y} & = & (y_1, y_2, \ldots, y_n) \\ \underline{z} & = & (z_1, z_2, \ldots, z_n) \\ \underline{x}^2 & = & (x_1^2, x_2^2, \ldots, x_n^2) \\ \underline{y}^2 & = & (y_1^2, y_2^2, \ldots, y_n^2) \\ \underline{xy} & = & (x_1 y_1, x_2 y_2, \ldots, x_n y_n) \\ \underline{e} & = & (1, 1, \ldots, 1) \quad \text{also length } n \end{array}$$

Minimizing equation 6.16 means

$$\underline{z} - a\underline{x}^2 - b\underline{x} - c\underline{xy} - d\underline{y} - f\underline{y}^2 - g\underline{e} \in \langle \underline{x}^2, \underline{x}, \underline{xx}, \underline{y}, \underline{y}^2, \underline{e} \rangle^{\perp} \tag{6.17}$$

or

$$\underline{z} - a\underline{x}^2 - b\underline{x} - c\underline{xy} - d\underline{y} - f\underline{y}^2 - g\underline{e} \perp \underline{x}^2 \tag{6.18}$$

$$\underline{z} - a\underline{x}^2 - b\underline{x} - c\underline{xy} - d\underline{y} - f\underline{y}^2 - g\underline{e} \perp \underline{x} \tag{6.19}$$

$$\underline{z} - a\underline{x}^2 - b\underline{x} - c\underline{xy} - d\underline{y} - f\underline{y}^2 - g\underline{e} \perp \underline{xy} \tag{6.20}$$

$$\underline{z} - a\underline{x}^2 - b\underline{x} - c\underline{xy} - d\underline{y} - f\underline{y}^2 - g\underline{e} \perp \underline{y} \tag{6.21}$$

$$\underline{z} - a\underline{x}^2 - b\underline{x} - c\underline{xy} - d\underline{y} - f\underline{y}^2 - g\underline{e} \perp \underline{y}^2 \tag{6.22}$$

$$\underline{z} - a\underline{x}^2 - b\underline{x} - c\underline{xy} - d\underline{y} - f\underline{y}^2 - g\underline{e} \perp \underline{e} \tag{6.23}$$

This results in a system of linear equations,

$$\begin{array}{lllllll}
(\underline{x}^2, \underline{x}^2) \cdot a & +(\underline{x}^2, \underline{x}) \cdot b & +(\underline{x}^2, \underline{xy}) \cdot c & +(\underline{x}^2, \underline{y}) \cdot d & +(\underline{x}^2, \underline{y}^2) \cdot f + (\underline{x}^2, \underline{e}) \cdot g & = (\underline{x}^2, \underline{z}) \\
(\underline{x}, \underline{x}^2) \cdot a & +(\underline{x}, \underline{x}) \cdot b & +(\underline{x}, \underline{xy}) \cdot c & +(\underline{x}, \underline{y}) \cdot d & +(\underline{x}, \underline{y}^2) \cdot f + (\underline{x}, \underline{e}) \cdot g & = (\underline{x}, \underline{z}) \\
(\underline{xy}, \underline{x}^2) \cdot a & +(\underline{xy}, \underline{x}) \cdot b & +(\underline{xy}, \underline{xy}) \cdot c & +(\underline{xy}, \underline{y}) \cdot d & +(\underline{xy}, \underline{y}^2) \cdot f + (\underline{xy}, \underline{e}) \cdot g & = (\underline{xy}, \underline{z}) \\
(\underline{y}, \underline{x}^2) \cdot a & +(\underline{y}, \underline{x}) \cdot b & +(\underline{y}, \underline{xy}) \cdot c & +(\underline{y}, \underline{y}) \cdot d & +(\underline{y}, \underline{y}^2) \cdot f + (\underline{y}, \underline{e}) \cdot g & = (\underline{y}, \underline{z}) \\
(\underline{y}^2, \underline{x}^2) \cdot a & +(\underline{y}^2, \underline{x}) \cdot b & +(\underline{y}^2, \underline{xy}) \cdot c & +(\underline{y}^2, \underline{y}) \cdot d & +(\underline{y}^2, \underline{y}^2) \cdot f + (\underline{y}^2, \underline{e}) \cdot g & = (\underline{y}^2, \underline{z}) \\
(\underline{e}, \underline{x}^2) \cdot a & +(\underline{e}, \underline{x}) \cdot b & +(\underline{e}, \underline{xy}) \cdot c & +(\underline{e}, \underline{y}) \cdot d & +(\underline{e}, \underline{y}^2) \cdot f + (\underline{e}, \underline{e}) \cdot g & = (\underline{e}, \underline{z})
\end{array}$$

where $(\underline{x}, \underline{y})$ etc. are inner products.

This system of linear equations can be written in a matrix structure

$$\begin{pmatrix}
(\underline{x}^2, \underline{x}^2) & (\underline{x}^2, \underline{x}) & (\underline{x}^2, \underline{xy}) & (\underline{x}^2, \underline{y}) & (\underline{x}^2, \underline{y}^2) & (\underline{x}^2, \underline{e}) \\
(\underline{x}, \underline{x}^2) & (\underline{x}, \underline{x}) & (\underline{x}, \underline{xy}) & (\underline{x}, \underline{y}) & (\underline{x}, \underline{y}^2) & (\underline{x}, \underline{e}) \\
(\underline{xy}, \underline{x}^2) & (\underline{xy}, \underline{x}) & (\underline{xy}, \underline{xy}) & (\underline{xy}, \underline{y}) & (\underline{xy}, \underline{y}^2) & (\underline{xy}, \underline{e}) \\
(\underline{y}, \underline{x}^2) & (\underline{y}, \underline{x}) & (\underline{y}, \underline{xy}) & (\underline{y}, \underline{y}) & (\underline{y}, \underline{y}^2) & (\underline{y}, \underline{e}) \\
(\underline{y}^2, \underline{x}^2) & (\underline{y}^2, \underline{x}) & (\underline{y}^2, \underline{xy}) & (\underline{y}^2, \underline{y}) & (\underline{y}^2, \underline{y}^2) & (\underline{y}^2, \underline{e}) \\
(\underline{e}, \underline{x}^2) & (\underline{e}, \underline{x}) & (\underline{e}, \underline{xy}) & (\underline{e}, \underline{y}) & (\underline{e}, \underline{y}^2) & (\underline{e}, \underline{e})
\end{pmatrix} \cdot \begin{pmatrix} a \\ b \\ c \\ d \\ f \\ g \end{pmatrix} = \begin{pmatrix}
(\underline{x}^2, \underline{z}) \\ (\underline{x}, \underline{z}) \\ (\underline{xy}, \underline{z}) \\ (\underline{y}, \underline{z}) \\ (\underline{y}^2, \underline{z}) \\ (\underline{e}, \underline{z})
\end{pmatrix} \tag{6.24}$$

This results in exactly one solution for a, b, c, d, f, g, and thus also one square fit in two dimensions.

In the analysis, the standard variables will be changed in $x = T_{20}$, $y = T_{30}$ and $z = V$or L. resulting in:

$$V = a_{1l}T_{20} + b_{1l}T_{30} + c_{1l} \tag{6.25}$$

$$L = a_{2l}T_{20} + b_{2l}T_{30} + c_{2l} \tag{6.26}$$

for linear extrapolation, and

$$V = a_{1s}T_{20}^2 + b_{1s}T_{20} + c_{1s}T_{20}T_{30} + d_{1s}T_{30} + f_{1s}T_{30}^2 + g_{1s} \tag{6.27}$$

$$L = a_{2s}T_{2}20^2 + b_{2s}T_{20} + c_{2s}T_{20}T_{30} + d_{2s}T_{30} + f_{2s}T_{30}^2 + g_{2s} \tag{6.28}$$

for square extrapolation.

As we can see the linear fit is included inside the square fit, which means that the square fit will always be more accurate than the linear fit.

6.2.5 Comparison of the Fits

Before the fits are used for the retrieval of vapor and liquid, first is evaluated how much the linear fit and square fit differ from the values in the look-up table. This is done for one groundlevel combination

The set of atmospheres is generated for a groundlevel configuration with $T_s = 15°C$, $P_s = 101.3\ kPa$, $RH_s = 60\%$ and $R_s = 0\ mm/h$. As a result of this configuration, the altitude of H_{top} ($T = 0°C$) is 2.3 km.

Linear as well as square fits are made for both V and L. The linear fits are

$$V_{lin} = 0.0931 \cdot T_{20} - 0.0523 \cdot T_{30} - 0.2055 \quad (6.29)$$

$$L_{lin} = -0.0009 \cdot T_{20} + 0.0026 \cdot T_{30} - 0.0170. \quad (6.30)$$

The square fits are

$$V_{sqr} = 0.0003 \cdot (T_{20})^2 + 0.0815 \cdot T_{20} - 0.0002 \cdot T_{20} \cdot T_{30} - 0.0480 \cdot T_{30} + 1.2834 \cdot 10^{-5} \cdot (T_{30})^2 - 01020 \quad (6.31)$$

$$L_{sqr} = -1.0237 \cdot 10^{-5} \cdot (T_{20})^2 - 0.0005 \cdot T_{20} + 9.4081 \cdot 10^{-6} \cdot T_{20} \cdot T_{30} + 0.0020 \cdot T_{30} + 7.68 \cdot 10^{-6} \cdot (T_{30})^2 - 0.0169 \quad (6.32)$$

For the T_{20},T_{30} combinations in the data set for thin clouds, the results of the linear fit and the square fit are compared with the V and L values calculated by Malu.

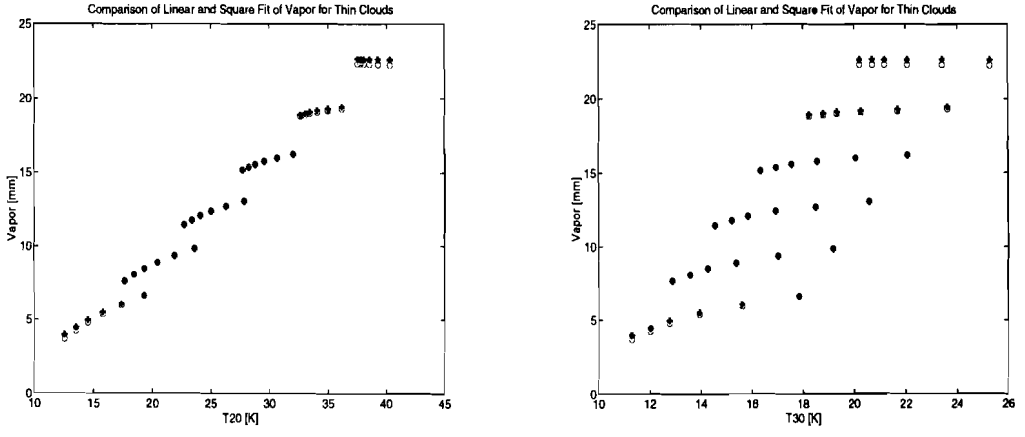

(a) (b)

Figure 6.2: Comparison of linear and square fit of vapor for thin clouds, + = square fit, o = linear fit and · = calculated by Malu; (a) Vapor, T_{20} relation, (b) Vapor, T_{30} relation.

Figure 6.2 shows that for $V(T_{20})$ as well as for $V(T_{30})$ both fits are nearly the same. This means that for this groundlevel for the retrieval of V both linear and square fit can be used.

In contrary to the fits for vapor, the fits for liquid show quite a difference between the linear and square fit. The square fit is much better than the linear fit (figure 6.3). This means that for the retrieval of liquid for this groundlevel situation, the square fit is the best option.

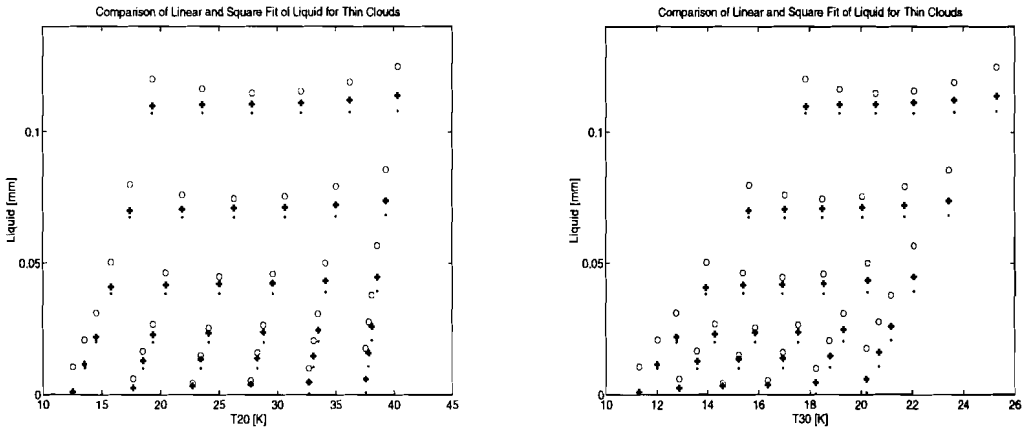

(a) (b)

Figure 6.3: Comparison of linear and square fit of liquid for thin clouds, + = square fit, o = linear fit and · = calculated by Malu; (a) Liquid, T_{20} relation, (b) Liquid, T_{30} relation.

In the comparison of the method of the three nearest points with the new extrapolation method, this last method is going to be used for measurement points outside the reduced look-up table. Measurement points inside the reduced look-up table are calculated with the method of the three nearest points.

6.2.6 Determination of the Location of a Measurement Point

Before the V and L values of a measured T_{20}, T_{30} combination can be determined, first has to be decided whether this point is located in the part describing thin clouds or the part describing thick clouds. The upper bound of the part describing the thin clouds, are the points in the look-up table with a cloud thickness of 500m. When the points of the reduced look-up table are projected on the T_{20},T_{30}–plane, we can describe this upper bound with a straight line through the (T_{20}, T_{30})–point with $RH_{ref} = 0\%$ and a cloud thickness of 500 m, and the (T_{20}, T_{30})–point with $RH_{ref}= 100\%$ and a cloud thickness of 500 m. A measured T_{20}, T_{30} point is located in the thin cloud part if this point is located on or below the line through the two points of the upper bound (figure 6.4).

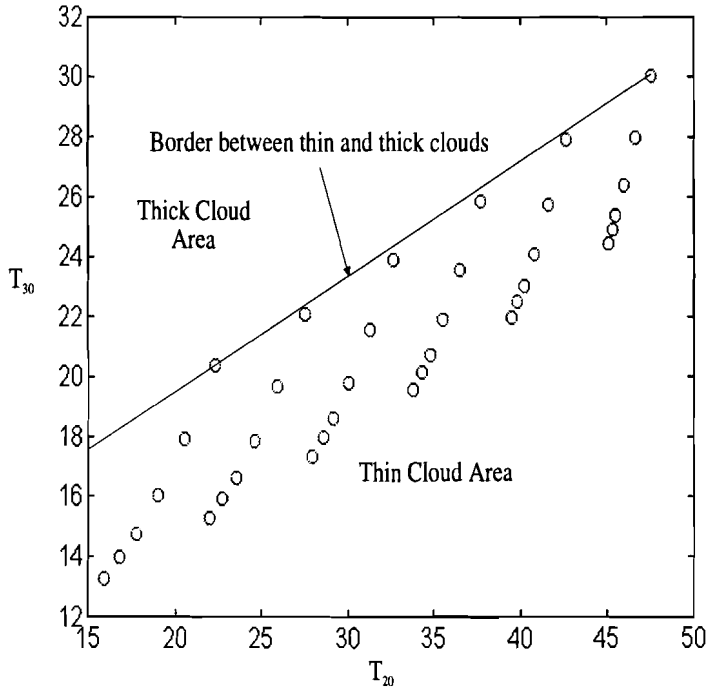

Figure 6.4: Detection of points inside the thin cloud part of the convergence area.

6.3 Results Retrieval

With the new extrapolation method again the data of the worst case days of the first and second CLARA campaign are analysed. This gives the following results for the first campaign:

Figure 6.5 showes that the retrieval of vapor decreases with the new extrapolation procedure and matches the radiosonde retrievals much better.

Figure 6.6 showes that the retrieval of liquid with the new extrapolation method is better than with the original three nearest points method. The new method however does not eliminate the problem of the negative L–values, completely. The retrieved L-values are still negative, but less negative than the values retrieved with the three nearest points method.

For the second CLARA period the following results have been found:

Figure 6.7 showes the results of the retrieval of vapor for the worst case of the second CLARA campaign. Except for the first radiosonde retrieval, the new extrapolation matches much better than the original three nearest points method. The match is almost perfect.

Figure 6.8 showes again that the retrieval with the new extrapolation procedure is better than the retrieval with the three nearest points method. Again the problem of negative L–values is not solved completely. The values are still negative but less negative than with the three nearest points method.

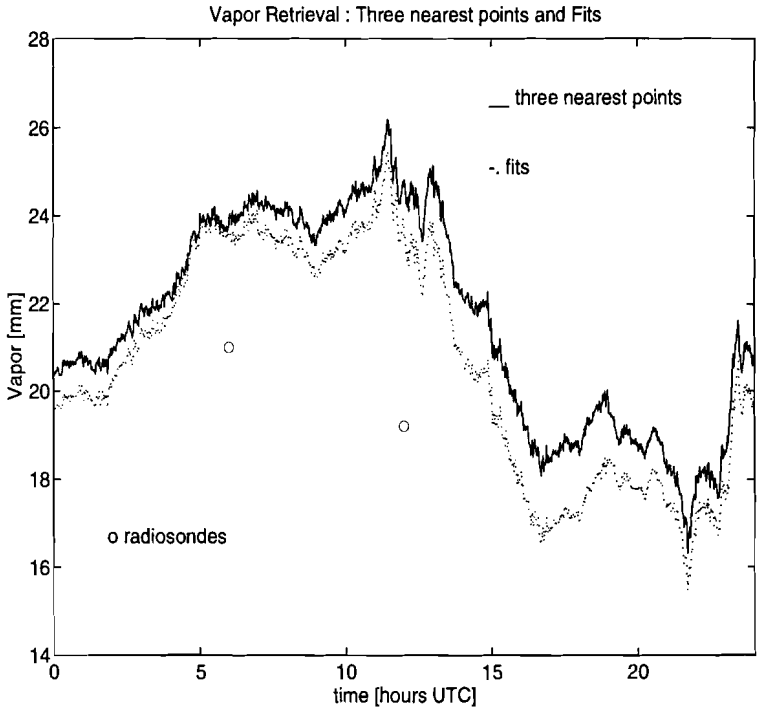

Figure 6.5: Comparison of the retrieval of vapor using the method of the three nearest points and the new extrapolation procedure; – = method of the three nearest points, $\cdots$ = new extrapolation procedure, o = radiosonde measurements

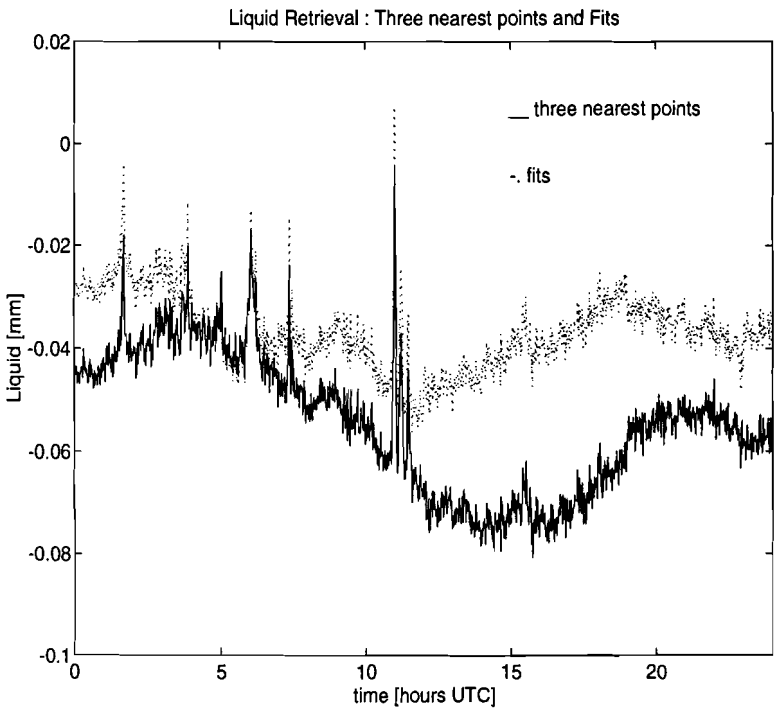

Figure 6.6: Comparison of the retrieval of liquid using the method of the three nearest points and the new extrapolation procedure; – = method of the three nearest points, ··· = new extrapolation procedure, o = radiosonde measurements

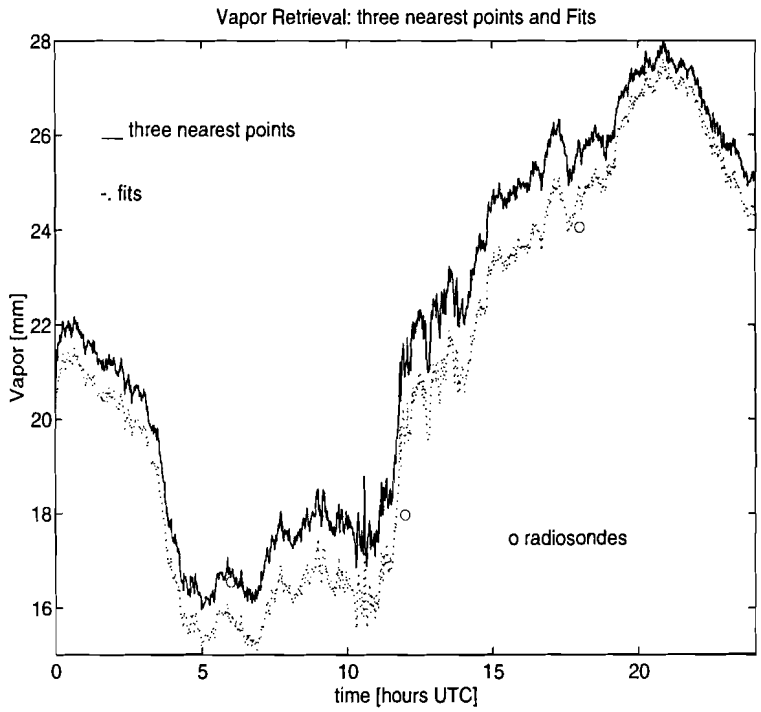

Figure 6.7: Comparison of the retrieval of vapor using the method of the three nearest points and the new extrapolation procedure; – = method of the three nearest points, ··· = new extrapolation procedure, o = radiosonde measurements

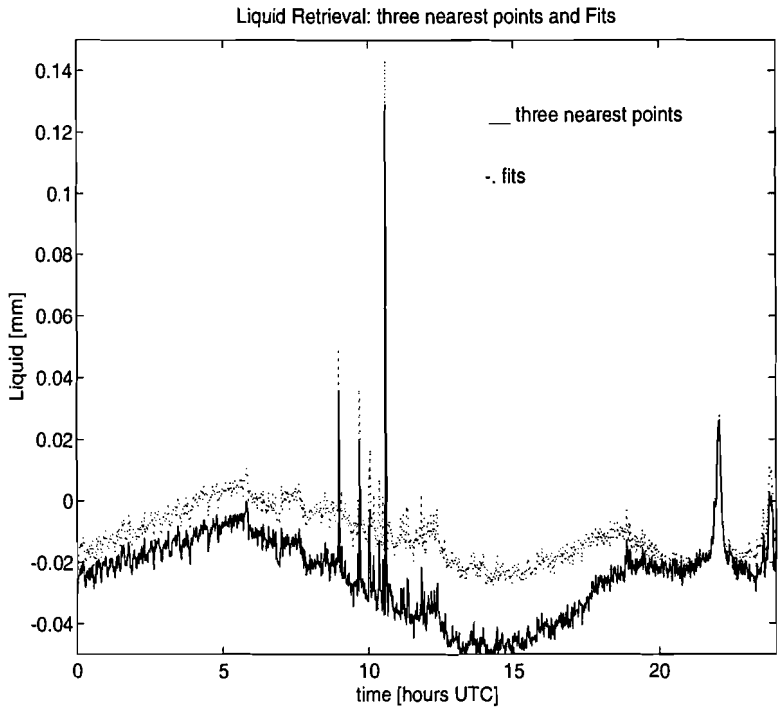

Figure 6.8: Comparison of the retrieval of liquid using the method of the three nearest points and the new extrapolation procedure; – = method of the three nearest points, ··· = new extrapolation procedure, o = radiosonde measurements

6.4 Conclusions

- The negative L–values are not completely eliminated by the new extrapolation technique for the worst case situations in the first and second measurement campaign. The values, however become less negative.
- The retrieved vapor values match better with the values retrieved with radiosondes
- The only criterion used for the calculation of the amounts by which T_{20} and T_{30} have to be changed is that the minimum of all L–values on a day should be positive. This means that there will always be a dependency between the amounts by which T_{20} and T_{30} have to be changed. This dependency can be removed by introducing more criteria. The purpose of the analysis in this chapter was to find an indication of the amounts by which T_{20} and T_{30} have to be changed, and compare these amounts by the accuracy of the radiometer. Therefore, it was not necessary to completely eliminate the dependency between the amounts.

Chapter 7

General Conclusions and Recommendations

7.1 Conclusions

- The TUE radiometer 29.8 GHz channel has a linear behaviour on his total range, therefore the TUE radiometer 29.8 GHz channel is suitable for atmospheric measurements as they have been carried out with the RECOM radiometer. The TUE radiometer, however has one major disadvantage. The radiometer uses a ground cooling system, which means that the radiometer has a fixed location. The data storage takes place on a Unix system that is also not transportable. This means that only measurements at the satellite groundstation of Eindhoven University of Technology can be carried out with the 29.8 GHz channel.

- The amounts by which T_{20} and T_{30} have to be changed in order to eliminate negative L–values are larger than the accuracy of the RESCOM Radiometer. This means that the occurrence of negative L–values cannot be explained solely by the accuracy of the radiometer.

- The original extrapolation using the method of the three nearest points was not accurate enough for clear sky periods. The new extrapolation procedure based on a square fit of a reduced look–up table for thin cloud situations, does not completely eliminate negative L–values. This method, however, is better than the originally used method of three nearest points.

7.2 Recommendations

- The tip–curve calibration of the RESCOM radiometer is very well suited for the detection of changes in the calibration of the RESCOM radiometer. When tip–curve calibrations are carried out on a regular base, without changing the correction factor, fluctuations in the calibration of the radiometer can be detected.

- Tip–curve calibrations should be carried out during clear sky conditions. These conditions are exactly those for which negative L–values occur. When after such a tip–curve calibration normal measurements and measurements of groundlevel data are carried

out, again negative L–values should be retrieved. Calculation of the amounts by which T_{20} and T_{30} have to be changed in order to retrieve only positive L–values, could give information about the reason why there is a variation in these amounts, although the calibration parameter has not been changed.

- Further research is necessary in order to investigate whether the new extrapolation method in combination with a variation of T_{20} and T_{30} within the accuracy range of the radiometer, eliminates the negative L–values completely.

References

[1] Arnout Feijt. CLARA www pages. Pages on the World Wide Web URL: http://www.knmi.nl/PROJECTS/CLARA, 1996. Last update 9 May 1997.

[2] Michael E. Janssen, editor. *Atmospheric Remote Sensing by Microwave Radiometry.* John Wiley & Sons, Inc., New York, United States of America, 1993.

[3] P.J.I. de Maagt. *The Microwave Radiometer as a Remote Sensing Device: Design and Application.* PhD thesis, Eindhoven University of Technology, Faculty of Electrical Engineering, Telecommunication Division, Radiocommunication Group, December 1992.

[4] J.M.W.M. Janssen. Design of a Radiometer System for Remote Sensing Applications. Technical report, Stan Ackermans Institute, Information- and Communication Technology, December 1995.

[5] Lars D. Kristensen. *20/30 GHz Radiometer system KA-1 User's Manual.* Rescom A/S, Vedbaek, Denmark, 1996.

[6] Hans J. Liebe. MPM-An Atmospheric Millimeter-Wave Propagation Model. *International Journal of Infrared and Millimeter Waves*, 10(6), 1989.

[7] H.J. Hollander. Radiometric Water Retrieval from the Atmosphere using a Matched Atmosphere Algorithm. Master's thesis, Eindhoven University of Technology, Faculty of Electrical Engineering, Telecommunication Division, Radiocommunication Group, April 1995.

[8] Erwin Kreyzig. *Advanced Engineering Mathemathics*, chapter 24. John Wiley & Sons, Inc., New York, United States of America, sixth edition, 1988.

[9] The MathWorks, Inc., Natick, NA, United States of America. *Using MATLAB*, fourth edition.

[10] E. Cohen. *Programming in the 1990s, An Introduction to the Calculation of Programs.* Springer-Verlag, Berlin, New York, 1990.

[11] Hans J. Liebe. An Updated Model for Millimeter wave Propagation in Moist Air. *Radio Science*, 20:1069–1089, September 1985.

[12] G.A. Hufford H.J. Liebe, T. Manabe. Millimeter-Wave Attenuation and Delay Rates due to Fog/Cloud Conditions. *IEEE Transactions on Antennas and Propagation*, 37, December 1989.

[13] R.Peter and N. Kämpfer. Radiometric Determination of Water Vapor and Liquid Water and its Validation with Other Techniques. *Journal of Geophysical Research*, 97(16):18,173–18,183, November 1992.

[14] Peter Trommelen. Algorithms for Determining Water Vapour and Liquid Water Contents of the Atmosphere using Radiometer and Meteorological Data. Master's thesis, Eindhoven University of Technology, Faculty of Electrical Engineering, Telecommunication Division, Radiocommunication Group, 1997.

[15] van der Meijden. Syllabus en vraagstukken bij het college Lineaire Algebra en Lineaire Analyse 1. Collegedictaat number 2299, course number 2Y510, Eindhoven University of Technology, Eindhoven.

Appendix A

t–Distribution

F(c)	Number of degrees of freedom									
	22	24	26	28	30	40	50	100	200	∞
0.5	0.00	0.00	0.00	0.00	0.00	0.00	0.00	0.00	0.00	0.00
0.6	0.26	0.26	0.26	0.26	0.26	0.26	0.26	0.25	0.25	0.25
0.7	0.53	0.53	0.53	0.53	0.53	0.53	0.53	0.53	0.53	0.52
0.8	0.86	0.86	0.86	0.86	0.85	0.85	0.85	0.85	0.84	0.84
0.9	1.32	1.32	1.32	1.31	1.31	1.30	1.30	1.29	1.29	1.28
0.95	1.72	1.71	1.71	1.70	1.70	1.68	1.68	1.66	1.65	1.65
0.975	2.07	2.06	2.06	2.05	2.04	2.02	2.01	1.98	1.97	1.96
0.99	2.51	2.49	2.48	2.47	2.46	2.42	2.40	2.37	2.35	2.33
0.995	2.82	2.80	2.78	2.76	2.75	2.70	2.68	2.63	2.60	2.58
0.999	3.51	3.47	3.44	3.41	3.39	3.31	3.26	3.17	3.13	3.09

Table A.1: t-Distribution.

Appendix B

Source Codes

B.1 MPM including Rain Attenuation

```
        function out=mpm(Htop,groundlev,f,prof,elev);

% This function is used to calculate the brightness temperature for
% one test frequency.
% Input variables are:
% 'Htop' height of the top of the cloud, needed for the determination of
% the rainpath length,
% 'groundlev' vector containing groundlevel data, including rain rate,
% 'f' the test frequency in GHz,
% 'prof' an atmosphere profile which is a matrix containing the relative
% inverse temperature theta [1/T], the partial water vapour pressure
% e [kPa] ,
% the dry air pressure p [kPa]
% the liquid water contence w [g/m3] for different height h [km]
% (see profcl.m),
%
% Output are brightness temperature (Tb [K]), total attenuation (At [dB]),
% attenuation due to oxygen (Oxi [dB]), attenuation due to water vapor
% (Vap [dB]).
% and attenuation due to rain (Rain [dB])
%
%         FUNCTION [Oxi,Vap,Liq,Tb,At,Rain]=MPM(Htop,groundlev,f,prof,elev)
%
% H.J. Hollander nov 1994.
%
% Update of the MPM procedure
%
% The minimum frequency is 1 GHz.
% A frequency check is included  for testing the lower frequency bound
% The effects of Rain are also included in the updated version.
% Rain occurs from Htop to the ground, and although its attenuation is not
```

```
%specified in layers it will be presented in a layer structure.
%
% M.J.H. Pleijers jun 1997



% Initialisation



% mpmdata
if ~exist('ox'),%load ox and wv the mpm89 line coefficients
  load ox;
  load wv;
 % disp('loading Liebe data');
end;%if ~exist('ox'),



h=prof(:,1); theta=prof(:,2); e=prof(:,3); p=prof(:,4); w=prof(:,5);
Tbg=2.75; %background temperature


if elev==0,
disp('elevation of zero degrees is not allowed');
disp('elevation is set to 90 degrees ( pointing towards zenith)');
elev=90;
end; %if elev

delta=(h(2)-h(1))/sin(elev*pi/180); %thickness of a layer in the atmospere

lp=length(p); lox=length(ox(:,1)); lwv=length(wv(:,1));

% Frequency validation

while ((f<1)|(f>300))
if (f<1)
disp('   ');
disp('------WARNING---------')
disp(' Minimum frequency for MPM is 1 GHz ');
f=input(' Please give another frequency between [1..300 GHz]: ');
end % if f<1

if (f>300)
disp('    ');
disp('------WARNING---------')
disp(' This a reduced MPM model with only absorption lines ');
```

```
disp(' up to  300 GHz ');
f=input(' Please give another frequency between [1..300 GHz]: ');
end % if f>300
end % while


% N" due to ox
  fi=ox(:,1); a1=ox(:,2); a2=ox(:,3); a3=ox(:,4);
  a4=ox(:,5); a5=ox(:,6); a6=ox(:,7);


  dumm1=theta*a6';
  dumm2=p.*(theta.^0.8);
  dumm3=(ones(lp,1)*a5')+dumm1;
  d=1e-3*((dumm2*ones(1,lox)).*dumm3);

   clear dumm1 dumm2 dumm3



  % Width of resonance line
  dumm1=exp(log(theta)*(0.8-a4)');
  dumm2=(p*ones(1,lox)).*dumm1;
  dumm3=1.1*e.*theta;
  dumm4=dumm2+(dumm3*ones(1,lox));
  df=(dumm4.*(ones(lp,1)*a3'))*1e-3;
  clear dumm1 dumm2 dumm3 dumm4;
   % strenght of resonance line
  dumm1=(p.*(theta.^3))*a1';
  dumm2=exp((1-theta)*a2');
  sox=1e-6*(dumm1.*dumm2);
  clear dumm1 dumm2;
   % van vleck-weiskoppf
  dumm1=fi-f;
  dummy1=df - d.*(ones(lp,1)*dumm1');
  dummy2=(ones(lp,1)*((fi-f).^2)') + (df.^2);
  dumm2=fi+f;
  dummy3=df - d.*(ones(lp,1)*dumm2');
  dummy4=(ones(lp,1)*((fi+f).^2)') + (df.^2);
   % line-shape
  ls=(ones(lp,1)*((f./fi)')).*((dummy1./dummy2) + (dummy3./dummy4));
  clear dummy1 dummy2 dummy3 dummy4 dumm1 dumm2;



  Oxd=(sum((ls.*sox)'))';
```

```
   % Oxygen continuum
  ap=(1-1.2*(f^1.5)*1e-5)*1.4e-10;
  go=5.6e-3*(p+1.1*e).*theta;
  sd=6.14e-4*p.*(theta.^2);
  dummy=go.*(1+((f./go).^2));
  ocx=((sd*f)./dummy)+(ap*f).*(p.^2).*(theta.^3.5);


  Oxd=Oxd+ocx;
  clear ap go sd dummy oxc ls sox d df;
  O=size(Oxd)

% N" due to water vapor
  fi=wv(:,1); b1=wv(:,2); b2=wv(:,3); b3=wv(:,4); b4=wv(:,5);
  b5=wv(:,6); b6=wv(:,7);
   % width of resonance line
  dumm1=exp(log(theta)*b4');
  dumm2=(p*ones(1,lwv)).*dumm1;
  dumm3=e*b5';
  dumm4=exp(log(theta)*b6');
  dumm5=dumm3.*dumm4;
  df=((dumm2+dumm5).*(ones(lp,1)*b3'))*1e-3;
  clear dumm1 dumm2 dumm3 dumm4 dumm5;
   % strength of resonance line
  dumm1=(e.*(theta.^3.5))*b1';
  dumm2=exp((1-theta)*b2');
  swv=dumm1.*dumm2;
   % van vleck-weiskoppf
  dummy2=(ones(lp,1)*((fi-f).^2)') + (df.^2);
  dummy4=(ones(lp,1)*((fi+f).^2)') + (df.^2);
   % line-shape
  ls=(ones(lp,1)*((f./fi)')).*((df./dummy2) + (df./dummy4));
  clear dummy2 dummy4 dumm1 dumm2 dumm3 dumm4;

  Vapd=(sum((ls.*swv)'))';

  W=ls.*swv;


   % water vapor continuum
  bf=0.113;
  bs=3.57*(theta.^7.5);
  wvc=((f*((bs.*e)+(bf*p))*1e-5).*e).*(theta.^3);

  Vapd=Vapd+wvc;
  V=size(Vapd)
```

```
clear d df swv bf bs wvc

% N" due to liquid water
Liqd=0; e1=5.48; e2=3.51;
 % than clouds are present
e0=77.66+103.3*(theta-1);
fp=20.09-142*(theta-1) + 294*((theta-1).^2);
fs=590-1500*(theta-1);
dumm1=e0-e1;
dumm2=1 + ((f ./fp).^2);
dumm3=e1-e2;
dumm4=1 + ((f ./fs).^2);
ei=(dumm1./dumm2) + (dumm3./dumm4) + e2;
eii=((dumm1*f)./(dumm2.*fp)) + ((dumm3*f)./(dumm4.*fs));
n=(2+ei)./eii;
Liqd=(4.5./(eii.*(1+(n.^2)))).*w;
L=size(Liqd)
save liquid.txt Liqd -ascii
clear dumm1 dumm2 dumm3 dumm4 e0 fp fs ei eii n lh ;

% N" due to rain,  Rain Rate Rs [mm/h]
 % initialisation frequency dependent rain parameters
if ((f<=2.9)&(f>=1))
   x1=3.51E-4;
   y1=1.03;
end
if ((f<=54)&(f>2.9))
   x1=2.31E-4;
   y1=1.42;
end
if ((f>54)&(f<=180))
   x1=0.225;
   y1=-0.301;
end
if ((f<=300)&(f>180))
   x1=18.6;
   y1=-1.151;
end

if ((f<=8.5)&(f>=1))
   x2=0.851;
   y2=0.158;
end
if ((f<=25)&(f>8.5))
   x2=1.42;
   y2=-0.0779;
end
```

```
  if ((f<=164)&(f>25))
     x2=2.63;
     y2=-0.272;
  end
  if((f<=300)&(f>164))
     x2=0.616;
     y2=0.0126;
  end
wrain=zeros(100,1); % rain profile
  dumm1=1/delta;
  for i=1:1:(Htop)
wrain(i)=1;
  end % for

  clear i ;

  % end initialisation
Rs=groundlev(4);
cr=x1*(f^(y1));
z=x2*(f^(y2));
dumm2=cr*Rs^(z);
Raind=(dumm2).*wrain;
Rn=size(Raind)
clear dumm1 dumm2 x1 x2 y1 y2 ;


% Attenuation coefficient [Np/km]
  Atc=(Oxd+Vapd+Liqd+Raind)*0.1820*f*0.2302585093;


% Contribution of layer k to brightness temperature
  Atccum=cumsum(Atc);
  Atccum=[0;Atccum];
  Atccum(lp+1)=[];
  dumm1=300 ./theta;
  dumm2=exp(-delta*Atccum);
  dumm3=Atc;
  Tbr=dumm1.*dumm2.*dumm3;
  Tb=sum(Tbr*delta)+Tbg*exp(-Atccum(lp)*delta);

  clear dumm1 dumm2 dumm3;

% Total N" due to oxygen and water vapor
  SumOx=sum(Oxd);
  SumVap=sum(Vapd);
  SumLiq=sum(Liqd);
  SumRain=sum(Raind);
```

```
clear theta e p Atc Tbr Atccum;

% Total attenuation [dB], in NP
  Oxi=0.1820*f*delta*SumOx;
  Vap=0.1820*f*delta*SumVap;
  Liq=0.1820*f*delta*SumLiq;
  Rain=0.1820*f*delta*SumRain;
  At=(Oxi+Vap+Liq+Rain); %in dB
  clear SumOx SumVap SumLiq
  out=[Oxi Vap Liq Tb At Rain];
```

B.2 New Extrapolation Procedures

B.2.1 Total Procedure

```
function [out]= maluplt(matrixin,delta)

n=size(matrixin);
m=1;

T=matrixin(m,5);
RH=matrixin(m,6);
for m=1:n(1),
  P=101.77;
     groundlv=[matrixin(m,5) P matrixin(m,6) 0];
     if m == 1
[lookup,convar]=genset1w(groundlv,delta,90);
     [fittot,Vtot,Ltot,fitdun,Vdun,Ldun,lookupdn]=fitsel(lookup);
     else
       if (abs(matrixin(m,5)-T) > 2) | (abs(matrixin(m,6)-RH) > 5)
 [lookup,convar]=genset1w(groundlv,delta,90);
 [fittot,Vtot,Ltot,fitdun,Vdun,Ldun,lookupdn]=fitsel(lookup);
T=matrixin(m,5);
 RH=matrixin(m,6);
       end % if
     end

  if round(m/100)*100==m
      m
  end;

%[fittot,Vtot,Ltot,fitdun,Vdun,Ldun,lookupdn]=fitsel(lookup);
isdn = isdun(lookupdn,matrixin(m,3),matrixin(m,2));

if isdn == 0 % in dik gebied
if fittot(1)==1
```

```
         V=vlin(Vtot,matrixin(m,3),matrixin(m,2));
else
        V=vsqr(Vtot,matrixin(m,3),matrixin(m,2));
end % fittot(1)==1

if fittot(3)==1
        L=llin(Ltot,matrixin(m,3),matrixin(m,2));
else
        L=lsqr(Ltot,matrixin(m,3),matrixin(m,2));
end % fittot(3)==1

else          % in dun gebied
if fitdun(1)==1
           V=vlin(Vdun,matrixin(m,3),matrixin(m,2));
else
        V=vsqr(Vdun,matrixin(m,3),matrixin(m,2));
end % fitdun(1)==1

if fitdun(3)==1
L=llin(Ldun,matrixin(m,3),matrixin(m,2));
else
        L=lsqr(Ldun,matrixin(m,3),matrixin(m,2));
end % fitdun(3)==1

end % end if isdn ==0
out=[out;matrixin(m,1),matrixin(m,3),matrixin(m,2),V,L];
end % for
```

B.2.2 Generation of Look–Up Tables

```
function [data,convar]=genset1w(groundlev,delta,elev)

% this function generates the dataset used by Malu

C=0.4;
f20=21.3;
f30=31.7;

convar=zeros(4,2);
[prof,Htop]=profma(groundlev,delta,delta,0,C);
out20 = mpm(Htop,groundlev,f20,prof,elev);
out30 = mpm(Htop,groundlev,f30,prof,elev);
convar(1,:)=[out20(4),out30(4)];

[prof,Htop]=profma(groundlev,delta,Htop,0,C);
out20 = mpm(Htop,groundlev,f20,prof,elev);
```

```
out30 = mpm(Htop,groundlev,f30,prof,elev);
convar(2,:)=[out20(4),out30(4)];

[prof,Htop]=profma(groundlev,delta,Htop,100,C);
out20 = mpm(Htop,groundlev,f20,prof,elev);
out30 = mpm(Htop,groundlev,f30,prof,elev);
convar(3,:)=[out20(4),out30(4)];


[prof,Htop]=profma(groundlev,delta,delta,100,C);
out20 = mpm(Htop,groundlev,f20,prof,elev);
out30 = mpm(Htop,groundlev,f30,prof,elev);
convar(4,:)=[out20(4),out30(4)];


data=[];
for RHref=0:20:100,
%RHref
for Hbasedum= 0.1:0.1:Htop,
%Hbasedum
[prof,Htop]=profma(groundlev,delta,Hbasedum,RHref,C);
out20= mpm(Htop,groundlev,f20,prof,elev);
out30= mpm(Htop,groundlev,f30,prof,elev);
[V,L]= genvl2(prof);
data=[data; out20(4),out30(4),V,L,Hbasedum,Htop,RHref];
end;
end;

        function [V,L]=genvl(prof);

%generates the integrated V [cm] and L [cm] out of a profile (see profma.m)

%  delta=prof(2,1)-prof(1,1);
  h=prof(:,1);
  w=prof(:,5);
  e=prof(:,3);
  theta=prof(:,2);
  v=7.223*e.*theta; %g/m3

  V=trapz(h,1000*v)*1E-4; %cm
  L=trapz(h, w*1000)*1E-4; %cm
```

B.2.3 Selection Thin or Thick Clouds

```
function [isdn] = isdun(lookpdn,T20m,T30m)
```

```
left=lookpdn(1,:);
right=lookpdn(31,:);
dumm1=right(1)-left(1);
dumm2=(T20m-left(1))*right(2)+left(2)*(right(1)-T20m);
T30g=dumm2/dumm1;
isdn=0;
if T30m<=T30g,
isdn=1;
else
isdn=0;
end %if
```

B.2.4 Calculation of Fit Parameters

Square Fit

```
function [r]=convfit(data1,data2,data3)

% Fitten van een functie z= ax^2+bx+cxy+dy+fy^2+g
% Marc Pleijers
% Juli 1997



% de datafile heeft nu de volgende structuur:
% [ xwaarde  ywaarde  zwaarde] van elk punt van het convergentie gebied.

% introductie aantal hulp variabelen
x=data1;
y=data2;
z=data3;
t=size(x);
e=ones([t(1,1) 1]);
minx=min(x);
maxx=max(x);
miny=min(y);
maxy=max(y);
x2=x.*x;
y2=y.*y;
xy=x.*y;

%initialisatie matrix A en vector B
A=zeros(6);
B=zeros([6 1]);
%eind initialisatie
```

```
% vullen vector B
B(1,1)=sum(x2.*z);
B(2,1)=sum(x.*z);
B(3,1)=sum(xy.*z);
B(4,1)=sum(y.*z);
B(5,1)=sum(y2.*z);
B(6,1)=sum(z);
% einde vullen B

% vullen matrix A
% eerste kolom
A(1,1)=sum(x2.*x2);
A(2,1)=sum(x2.*x);
A(3,1)=sum(x2.*xy);
A(4,1)=sum(x2.*y);
A(5,1)=sum(x2.*y2);
A(6,1)=sum(x2);

%tweede kolom
A(1,2)=sum(x2.*x);
A(2,2)=sum(x2);
A(3,2)=sum(x2.*y);
A(4,2)=sum(xy);
A(5,2)=sum(x.*y2);
A(6,2)=sum(x);

%derde kolom
A(1,3)=sum(x2.*xy);
A(2,3)=sum(x.*xy);
A(3,3)=sum(xy.*xy);
A(4,3)=sum(x.*y2);
A(5,3)=sum(xy.*y2);
A(6,3)=sum(xy);

%vierde kolom
A(1,4)=sum(x2.*y);
A(2,4)=sum(xy);
A(3,4)=sum(x.*y2);
A(4,4)=sum(y2);
A(5,4)=sum(y.*y2);
A(6,4)=sum(y);

%vijfde kolom
A(1,5)=sum(x2.*y2);
A(2,5)=sum(x.*y2);
A(3,5)=sum(xy.*y2);
A(4,5)=sum(y.*y2);
```

```
A(5,5)=sum(y2.*y2);
A(6,5)=sum(y2);

%zesde kolom
A(1,6)=sum(x2);
A(2,6)=sum(x);
A(3,6)=sum(xy);
A(4,6)=sum(y);
A(5,6)=sum(y2);
A(6,6)=sum(e);

r= A\B;
```

Linear Fit

```
function [r]=convfit1(data1,data2,data3)

% Fitten van een functie z= ax+by+c
% Marc Pleijers
% Juli 1997



% de datafile heeft nu de volgende structuur:
% [ xwaarde  ywaarde  zwaarde] van elk punt van het convergentie gebied.

% introductie aantal hulp variabelen
x=data1;
y=data2;
z=data3;
t=size(x);
e=ones([t(1,1) 1]);
minx=min(x);
maxx=max(x);
miny=min(y);
maxy=max(y);
x2=x.*x;
y2=y.*y;
xy=x.*y;

%initialisatie matrix A en vector B
A=zeros(3);
B=zeros([3 1]);
%eind initialisatie


% vullen vector B
```

```
B(1,1)=sum(x.*z);
B(2,1)=sum(y.*z);
B(3,1)=sum(z);
% einde vullen B

% vullen matrix A
% eerste kolom
A(1,1)=sum(x.*x);
A(2,1)=sum(x.*y);
A(3,1)=sum(x);

%tweede kolom
A(1,2)=sum(x.*y);
A(2,2)=sum(y.*y);
A(3,2)=sum(y);

%derde kolom
A(1,3)=sum(x);
A(2,3)=sum(y);
A(3,3)=sum(e);

r= A\B;
```

B.2.5 Calculation of Linear and Square Fits of V and L

Linear Vapor Retrieval

```
function [V]= vlin(param,T20val,T30val)
Vs=[];
n=size(T20val);
for i=1:n(1),
V2=param(1)*T20val(i)+param(2)*T30val(i)+param(3);
Vs=[Vs;V2];
end
V=Vs;
```

Square Vapor Retrieval

```
function [V]=vsqr(param,T20val,T30val)
Vs=[];
n=size(T20val);
for i=1:n(1),
V2=param(1)*(T20val(i))^2+param(2)*T20val(i)+param(3)*T20val(i)*T30val(i)
+param(4)*T30val(i)+param(5)*(T30val(i))^2 + param(6);
Vs=[Vs;V2];
end
V=Vs;
```

Linear Liquid Retrieval

```
function [L]= llin(param,T20val,T30val)
Ls=[];
n=size(T20val);
for i=1:n(1)
L2=param(1)*T20val(i)+param(2)*T30val(i)+param(3);
Ls=[Ls;L2];
end
L=Ls;
```

Square Liquid Retrieval

```
function [L]=lsqr(param,T20val,T30val)
Ls=[];
n=size(T20val);
for i=1:n(1),
L2=param(1)*(T20val(i))^2+param(2)*T20val(i)+param(3)*T20val(i)*T30val(i)
+param(4)*T30val(i)+param(5)*(T30val(i)).^2 + param(6);
Ls=[Ls;L2];
end
L=Ls;
```

Appendix C

Maximum Rainrates of Days with Rain

For the days with rain the maximum rainrate per day is:

Day	**Maximum Rainrate** [mm/h]
May, 16, 1996	45
May, 21, 1996	4
May, 22, 1996	1
June, 8, 1996	20
June, 28, 1996	5
June, 29, 1996	25
July, 2, 1996	8
July, 3, 1996	14
July, 4, 1996	5

Table C.1: Maximum rainrate per day for day with rain.

Appendix D

Example of Doubles and Gaps in a RESCOM Data file

The examples in this appendix are obtained from the data file from June, 11, 1996.

D.1 Double time periods

The following data set is the file er960611.txt and shows the times on which a double occurs. The times marked with an *, show that there are hours in which two doubles occur.

```
8.4027778e-001
1.8466667e+000
2.8286111e+000*
2.8752778e+000*
3.8102778e+000*
3.8569444e+000*
4.7919444e+000*
4.8386111e+000*
5.8200000e+000*
5.8669444e+000*
6.8516667e+000
7.8394444e+000*
7.8863889e+000*
8.8255556e+000*
8.8722222e+000*
9.8597222e+000*
9.9069444e+000*
1.0918611e+001
1.1881667e+001*
1.1952222e+001*
1.2938056e+001*
1.2985000e+001*
1.3995000e+001
1.4983889e+001
1.5030833e+001*
```

1.5994722e+001*
1.7051111e+001
1.8035556e+001*
1.8082222e+001*
1.9113056e+001
2.0096944e+001
2.1103611e+001
2.2085833e+001
2.3138333e+001

D.2 Gap time periods

The following data set is the file gp960611.txt and shows the locations of the gaps.
2.8522222e+000
3.8338889e+000
4.8155556e+000
5.8436111e+000
7.8630556e+000
8.8491667e+000
9.8836111e+000
1.1905556e+001
1.2961667e+001
1.5007500e+001
1.8059167e+001